Design and Synthesis of Bilayer Nanocomposite Hydrogels for Minimally Invasive Cartilage Replacement

Mohammad Mostakhdemin

A thesis submitted to

Auckland University of Technology

In fulfilment of the requirements for the degree of

Doctor of Philosophy (PhD)

2021

School of Engineering, Computer and Mechanical Sciences

I hereby declare that this submission is my own work and that, to the best of my knowledge and belief, it contains no material previously published or written by another person (except where explicitly defined in the acknowledgements), nor material which to a substantial extent has been submitted for award of any other degree or diploma of a university or other institution of higher learning.

Signed_____ Date 25 April 2021

ABSTRACT

The complex structure of healthy articular cartilage facilitates the joint withstanding the imposed pressures and retaining interstitial fluid to lessen stresses on its soft tissue, while easing the locomotion and minimizing friction between cartilage mates. Avascular nature of this tissue results in unrecoverable damaged lesions and severe pain over time. Polymeric hydrogels are promising candidate materials for the replacement of the damaged cartilage. Recently, bilayer hydrogels have been developed with distinct techniques as artificial cartilage due to their resemblance to the native cartilage structure. Bilayer hydrogels contain bulk and lubricious layers that enhance water retention in their lubricious layer and improve tribological properties such as wear resistance and coefficient of friction (CoF). However, design and manufacturing bilayer hydrogels with desirable mechanical and tribological performance is challenging, because promoting mechanical properties results in mitigation of tribological properties and vice versa. Specifically, the lubricious layer of the bilayer hydrogels was found susceptible to wear under sliding motions. Therefore, the current study focused on design and manufacturing of bilayer hydrogels strengthened with nanoparticles to overcome this problem and achieve enhanced mechanical and tribological performances.

In the first phase of this research, the formation of the lubricious and bulk layers was conducted with appropriate synthesis processes. The second phase was focused on optimizing the mechanical properties by variations in monomers and crosslinkers amounts. In the third phase, tribological properties were evaluated; and finally in the fourth phase, mathematical approaches were applied to determine mechanical surface energy, viscoelastic or poroelastic relaxation and define effective parameters in the design of artificial soft tissue with respect to both mechanical and tribological properties.

In this study, two common types of nanoparticles in orthopaedic research, titania nanoparticles (TiO_2 NPs) and Silica nanoparticles (SNPs), were utilized to strengthen both bulk and lubricious layers for the sake of mechanical and tribological improvements. Wide ranges of

experiments on monomers and nanoparticles were conducted to assess mechanical properties such as elastic modulus, hardness, compressive strength, compressive moduli, tangent modulus, and relaxation parameters. Also, wide ranges of tribological tests were performed to evaluate CoF, wear-loss volume, surface topography, wear mechanisms, and lubrication regimes. All mechanical and tribological experiments were conducted according to the required tests for the native and artificial cartilage according to U.S. Food and Drug Administration (FDA) and the International Cartilage Repair Society (ICRS).

Hydrogel formulation with 0.2wt% TiO_2 NPs was found to have superior mechanical properties compared to other NPs-loaded samples and non-reinforced hydrogels (NRHs). Tribological test results showed a low mean coefficient of friction values of 0.007 and 0.014 for NRHs and nanocomposite hydrogels (NCHs), respectively, and wear resistance of NCHs improved significantly. SEM images showed that wear mechanisms are a combination of adhesive wear and fatigue wear. Silica NCHs, however, showed optimum results by topping 0.6wt% SNPs into the designed bilayer hydrogels. It is shown that poroelastic relaxation occurred before viscoelastic relaxation according to diffusion rate theory. Interfacial surface energy was also analyzed, and NCHs showed superior surface energy compared to NRHs. Lubrication regimes models were developed, and CoF results were addressed in the elastoviscous transition regime based on the Stribeck curve framework. SEM images showed a strengthened lubricious layer after sliding tests and an increased wear resistance compared to NRHs.

The outcomes of the research presented in this thesis creates a framework for designing, deficiencies-free synthesizing, testing, and analyzing essential elements of bilayer hydrogels for cartilage replacement.

LIST OF PUBLICATIONS FROM THIS RESEARCH

1. M Mostakhdemin, A Nand, M Arjmandi, M Ramezani (2020). Mechanical and microscopical characterisation of bilayer hydrogels strengthened by TiO_2 nanoparticles as a cartilage replacement candidate. Materials Today Communications, 25, 101279.

2. Mohammad Mostakhdemin, Ashveen Nand, Maziar Ramezani (2021). A novel assessment of microstructural and mechanical behaviour of bilayer silica-reinforced nanocomposite hydrogels as a candidate for artificial cartilage. Journal of the Mechanical Behavior of Biomedical Materials, 16, 104333.

3. Mohammad Mostakhdemin, Ashveen Nand, Maziar Ramezani (2021). Tribological assessments of bilayer titanium nanocomposite hydrogels for cartilage replacement in articular joints. Wear, 484, 204017.

4. Mohammad Mostakhdemin, Ashveen Nand, Maziar Ramezani (2021). Articular and artificial cartilage, characteristics, properties, and testing approaches-A review. Polymers, 13, 2000.

TABLE OF CONTENTS

ACKNOWLEDGMENTS

I would first like to thank my main research supervisor, Associate Professor Maziar Ramezani of the Department of Mechanical Engineering, Faculty of Design & Creative Technology at Auckland University of Technology. Prof. Ramezani was always open to my ideas and relentlessly supported me anytime I needed his advice. He consistently motivated me with his constructive comments and professional advice.

I would also like to thank the experts and technicians in engineering workshops and laboratories involved in the validation survey for this research project. Especial thanks to My dear friend Dr. Mohammadreza Arjmandi from the University of Auckland. Without their passionate participation and input, the validation survey could not have been successfully conducted.

I am also delighted to acknowledge Dr. Ashveen Nand of the Faculty of Engineering, at the University of Auckland. I am gratefully indebted to his very valuable technical supports and professional advice.

Finally, I must express my very profound gratitude to my lovely family who provided me with unfailing support and continuous encouragement during my years of study. I also like to take this opportunity to appreciate my grandfather, Abbas Mostakhdemin, who had brightened up the education road map for us. This accomplishment would not have been possible without them. Thank you.

Mohammad Mostakhdemin

LIST OF FIGURES

LIST OF TABLES

NOMENCLATURE

a	*Contact radius*
A_P	projected contact area
D	Diffusion rate
E	Elastic modulus
F	Amonton's law
f	Frequency
f_p	Pressure function
f_v	Speed function
H	Hardness
h	Film thickness
h_{max}	indentation depth
K	Wear coefficient
L	Hydrogel geometric scale
P	Normal load [N]
P_{max}	Maximum load
R	Radius of indenter
r	Pore radius
R_q	Surface roughness
s	Sliding distance
S	Contact stiffness
S_c	Shear strength
U_E	Elastic energy
U_M	Mechanical energy
U_S	Surface energy
U_T	Total energy
W	Wear/ Total volume loss [mm^3]
w	Wear rate

Greek Symbols:

μ	Coefficient of friction
ν	Poisson's ratio
γ	Energy per unit contact area
δ	Elastic displacement
η	Dynamic viscosity [Pa.s]
Λ	Lubrication regimes
$\dot{\varepsilon}(t)$	Strain rate with respect to time
τ_v	Time of viscoelastic relaxation
τ_p	Time of poroelastic relaxation

σ	Compressive stress
σ_f	Maximum stress value

LIST of Abbreviations

3D	Three Dimensional
AAc	Acrylic Acid
AAm	Acrylamide
ACL	Anterior Cruciate Ligament
AFM	Atomic Force Microscopy
Alg	Alginate
APS	Ammonium Persulfate
ASTM	American Society for Testing and Materials
$CaCl_2$	Calcium Chloride
CoF	Coefficient of Friction
DI	Deionized Water
DMAA	N,N-di-methyl-acrylamide
DN	Double Networks
DNA	Deoxyribonucleic Acid
ECM	Extracellular Matrix
EDS	Electro Discharge Scanning
EHL	Elasto-hydrodynamic
EVT	Elastoviscous Transition
FCL	Fluid confined lubrication
FDA	Food and Drug Administration
FRP	Free Radical Polymerization
GAGs	Glycos-amino-glycans
HA	Hyaluronic Acid
HAp	hydroxyapatite
ICRS	International Cartilage Repair Society
IPN	Interpenetrating Network
IS	Ionic Strength
MBAA	Methylene-bis-acrylamide
METAC	Methacryloyloxy-ethyl-trimethyl-ammonium-chloride
MMHs	Micromolecular Microsphere Hydrogels
MRI	Magnetic Resonance Imaging
MW	Molecular Weight
NCHs	Nanocomposite Hydrogels
NPs	Nanoparticles
NRHs	Non-Reinforced Hydrogels
OA	Osteoarthritis
OA-POSS	Octa-aminopropyl polyhedral oligomeric silsesquioxane hydrochloride salt
PAMPS	poly-(2-Acrylamido-2-methylpropane sulfonic acid)/

PCA	Principle Component Analysis
PCL	Poly-capro-lactone
PDMAAm	poly-(N,N'-dimethyl acrylamide)
PDMS	Poly-di-methyl-siloxane
PEG	Polyethylene-Glycol
PG	Proteoglycan
PGA	Polyglycolic Acids
PVA	Polyvinyl Alcohol
SA	Sodium Alginate
SAL	Surface Amorphous Layer
SEM	Scanning Electron Microscopy
Silica NCHs	Silica Nanocomposite Hydrogels
SN	Single Network
SNPs	SiO_2 Nanoparticles
TEM	Transmission Electron Microscopy
TEMED	Tetra-methyl-ethylene-diamine
THR	Total Hip Replacement
TKR	Total Knee Replacement
TPHs	Topology Hydrogels
UHMWPE	Ultra-High Molecular Weight Polyethylene

CHAPTER 1

INTRODUCTION

1.1 BACKGROUND

Articular cartilage (AC), coupled with viscous synovial fluid, dissipates imposed stresses at diarrheal joints [1]. The biphasic cartilage incorporated with chondrocytes and collagen fibers mitigates overstressing on the tissue [2, 3]. Cartilage is avascular; thus, deprived migration of chondrocytes slows down the process of self-recovery and causes severe pain on the damaged lesions [4, 5]. Research on replacing damaged cartilage lesions rather than the entire joint is gaining recognition and has been extensively investigated [6-8]. Total knee/hip replacement (TKR/THR) is the standard procedures that has been applied to treat patients with damaged or degenerated cartilage. However, arthroplasty is a maximally invasive procedure and the limited service life of the implant usually results in revision surgery for patients undergoing TKR/THR. Other procedures that have been developed for damaged cartilage are microfracture [9, 10], autologous-matrix induced chondrogenesis [11], autologous chondrocyte implantation, autologous cultured chondrocytes on porcine collagen membrane [12]. However, long-term clinical follow-ups have revealed durability issues with all the above mentioned procedures and treatments [13]. All mentioned treatments are temporary and have a short service life. The worse scenario is when younger patients are entailed with degenerated tissue and any treatments mentioned above would introduce the risk of revision surgery, which is complicated, expensive and usually could only be done once in patient's lifetime. Thus, a minimally invasive implant with longer service life would save cost, and significantly improve the quality of life for younger patients with osteoarthritis (OA). Therefore, developing an alternative material that simulates the

articular cartilage's mechanical and tribological responses, along with its biocompatibility in a bioactive environment is desirable for OA treatment [14].

To this end, polymeric hydrogels have been studied vastly due to their resemblance to AC in mechanical and tribological properties [6-8]. Hydrogels are biologically favored materials because of their biocompatibility [15] and no toxic effects or stimuli of the immune system [16]. With the aid of customizable hydrogels, only degenerated or damaged lesions would be reamed and replaced. Due to its minimally invasive feature, it is expected that the implantation could be conducted multiple times to treat damaged lesions until joint arthroplasty becomes inevitable. Thus, in the next section, the design and structural performance of the implant will be proposed.

1.2 CONCEPT DESIGN OF A MINIMALLY-INVASIVE JOINT IMPLANT

A bilayer hydrogel integrated with a porous scaffold and its base could replace the deteriorated regions of the AC. In this solution, the damaged region is reamed as shown in Fig. 1.1 and polymeric hydrogel could be implanted into the specified lesion. The implant was conceptualized as a plug roughly 3-4mm in thickness. The schematic of the implant, as shown in Fig. 1.1, demonstrates multiple components as follows:

1. A major part of the implant is the bilayer hydrogel, consisting of a thin porous lubricious layer and a thicker bulk layer; both layers are capable of retaining interstitial fluid within its networks. Different pore sizes result in fluid diffusion rate variations, which maintain contact pressure from the joint and minimize stresses. The lubricious layer maintains low friction and lubrication, while the bulk layer could sustain mechanical loading and transmit impact energy and stresses smoothly to the porous scaffold. The hydrogel can be further strengthened by loading nanoparticles.

2. Porous scaffold which can be fabricated with a high strength biomaterial (such as UHMWPE) with greater hardness compared to the proposed hydrogel and absorb imposing energy and reduce the transfer of stress to the next layer.

3. UHMWPE mesh is embedded in this design that performs similar to truss in structural engineering that plays two roles in this regard. First, it dissipated all energy that has been transferred through previous layers like a flexible spring. Second, it connects the implant plug to the subchondral bone and allows the trabecular bone to grow into the mesh regions.

By this concept design, if any failure or damage occurs in the implant, only the hydrogel part could get replaced, and the rest of the plug remains intact. Therefore, in the revision surgery for this implant, another customized hydrogel can be inserted into the porous scaffold, and by considering the swelling ratio of the proposed hydrogel, it fits into the scaffold and merges with the scaffold's mesh. The advantage of this approach is its minimally invasive procedure and repeatable implantation as revision surgeries which is desirable, especially for younger patients. Although the whole implant design is shown here, the scope of the current study is to focus on the design, synthesis, and assessment of bilayer hydrogels which is the most important part of the implant plug. The rest of the components can be developed in future research studies.

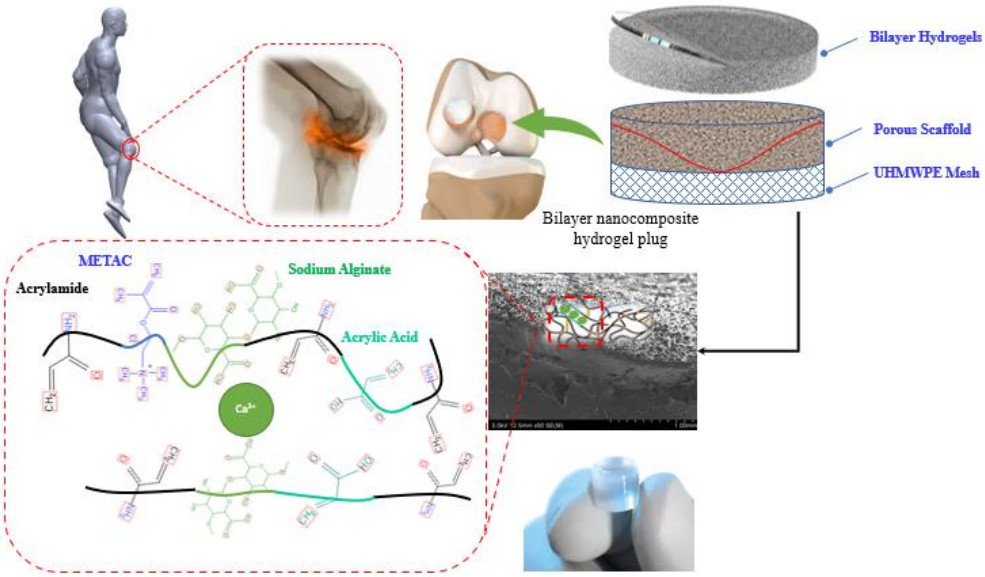

Figure 1. 1 Schematic of implant plug and its components for local treatment of damaged cartilage.

1.3 SYNTHESISE PROCESS OF NANO COMPOSITE BILAYER HYDROGELS

The proposed implant concept is based on the natural cartilage structure with stiffness gradient through the thickness and a full interpenetrating network (full-IPN) system strengthened by titania (TiO_2) and Silica (SiO_2) nanoparticles (NPs) with two layers to support both lubricating functioning and load-bearing capacity. The strengthening of hydrogels by Silica and Titania nanoparticles (NPs) is attracting considerable attention because of their interactions with polymer functional groups and have been devoted mainly to biomedical applications. Titania NPs have contributed to improved hydrogel properties such as swelling [17], porosity [18], strength [19], low toxicity, excellent biocompatibility, and low cost [18]. Unlike other NPs, silica nanoparticles (SNPs) showed a significant impact on initial shear modulus and viscoelastic properties, since it could immobilize the polymer chains and form NPs-polymer interphases [20]. SNPs reported increasing the number of tie points in each entanglement, which results in the improvement of the compressive strength [21]. SNPs also enhance slower chain kinetics and relaxation due to tough NPs-polymer bonds [22]. Polymer bonds relax promptly when NPs are located far from chains [23]. Viscoelasticity of the SNP loaded nanocomposite hydrogels (NCHs) was studied extensively and found to be similar to that of AC [23-25].

NPs will be used at the step of the free radical polymerization process to react with polymer chains. Hydrogel implant would be synthesized by chemical (covalent) crosslinking approach to form a high-density network, followed by ionic crosslinking to form the second network to enhance mechanical and tribological properties.

To synthesize the bilayer hydrogels, FDA approved monomers were used in this study, including acrylamide (AAm), acrylic acid (AAc), N,N′-methylenebis (acrylamide) (MBAA), 2-(Methacryloyloxy)ethyl]trimethyl ammonium chloride (METAC), alginic acid sodium salt from brown algae (Alg), SiO_2 nanoparticles (SNPs), ammonium persulfate (APS), N,N,N′,N′ tetramethyl ethylenediamine (TEMED), and calcium chloride ($CaCl_2$).

1.4 AIMS OF THE STUDY

This research aims to address the gaps that have been identified (based on the literature review presented in the next chapter) in manufacturing bilayer hydrogels suitable for cartilage replacement. Most of the required mechanical assessments were conducted on the proposed hydrogels. Alongside mechanical evaluation, tribological properties were also investigated to find the wear mechanisms and coefficient of friction (CoF) of the synthesized hydrogels. Lubrication regimes were also defined as a function of contact pressure and sliding speed, and different regimes were discussed by combining the Stribeck curve parameters and surface topography of the treated surfaces. In addition, diffusion rate theory and mechanical surface energy of the developed bilayer hydrogels were investigated. These methods can be considered for hydrogel evaluation for both mechanical and tribological aspects. The aims of the current study are as follows:

- To select proper hydrogel materials that effectively promote both mechanical and tribological properties.
- To optimize the synthesizing process of the hydrogel layer by designing the right material mixture, polymerization, and deficiencies-free solution.
- To utilize optimum amounts of titania and silica NPs to strengthen the hydrogels in terms of both mechanical and tribological performances.
- To apply mathematical models to better assess the features and properties of the proposed hydrogels.
- To find out the lubrication regimes and dominant wear mechanisms of the developed hydrogel samples.

1.5 RATIONALE AND SIGNIFICANT OF THE STUDY

Osteoarthritis (OA) is a common disease that is ranked 18th by the World Health Organization (WHO) among all injuries/diseases in the pacific region, imposing substantial costs on the healthcare section. There is no cure for OA and the last solution for patients with OA is total knee/hip replacement (TKR/THR), which is a complicated and expensive surgery. Between 2006 and 2011, a total number of 31260 and 31958 operations were performed in New Zealand for

THR and TKR, respectively, while by 2026, the demand for those surgeries will be increased by 84% and 183% for THR and TKR, respectively [26]. According to Roos report [27], 41% to 51% of people with joint injuries will show signs of OA, on average, fifteen years after injury [28]. According to a survey, nearly 17% of New Zealanders reported chronic pain in joints [29]. Ministry of social development data indicates that in 2009, over one-fifth of all sickness and benefit payments are provided for bone and joint disorders costing $320 million for NZ companies [30]. Sport-wise, an analysis of eight-year injury claims data of the Accident Compensation Corporation (ACC) for rugby league injury in NZ reported that knee joint injuries were the highest common ones [31]. The aforementioned data shows the need for the design and development of a new class of implants that can be used for younger patients with OA, to postpone or eliminate the need for total joint replacement.

Thus, a polymeric hydrogel implant was designed in this study that can be used as artificial cartilage, closely resembling the native cartilage in terms of load-bearing, fluid retention and wear resistance. Moreover, it is necessary to develop a research framework to study the mechanical and tribological properties of the proposed implant.

1.6 OVERVIEW OF THE RESEARCH

In this research, the bilayer hydrogel material will be synthesized with AAc, AAm, Alg and METAC monomers, covalently crosslinked with MBAA and ionically crosslinked with $CaCl_2$. It will be strengthened with titania NPs and silica NPs and results will be compared with non-reinforced hydrogels (NRHs). The proposed bilayer hydrogels will be assessed under sliding tests similar to the conditions experienced by articular cartilage during daily activities. The thesis outline is briefly as follows:

In chapter 2, a comprehensive literature survey is conducted to detail recent advances in the development of nano-composite hydrogels (NCHs) and critical design considerations. The main focus is to address both mechanical and tribological aspects, synthesis methods and standard tests.

At the end of the chapter, potential research gaps are defined, and research questions will be identified.

Chapter 3 describes materials and methods implemented in this study for synthesizing, mechanical and tribological experiments, methods of results interpretation, and equipment used during evaluation processes.

Chapter 4, 5, 6 and 7 are dedicated to all associated results for NCHs with both TiO_2 and SiO_2 NPs. Different results associated with the assessment of load bearing orthopedic implants will be presented in these chapters, including mechanical strength and structural performance, CoF, wear mechanisms and lubrication regimes of the developed NCHs.

And chapter 8 includes the conclusions from this research and recommendations for future studies.

CHAPTER 2

LITERATURE REVIEW

An overview of recent research on structural, mechanical, and tribological properties of both articular and artificial cartilage is presented in this chapter. Recent findings on material selection criteria, critical parameters in design, manufacturing methods, as well as standard and essential tests are discussed extensively.

2.1 SYNOVIAL JOINTS

Synovial joints, being the most common joints in mammals, are characterized by allowing movement in multiple planes, as is illustrated in Fig. 2.1. They allow for the articulation of long bones, ends of which are covered with articular cartilage (AC) within a fluid-filled cavity. AC, incorporated with a viscous synovial fluid, is a biphasic tissue that provides extremely low friction [32]. It mitigates overstressing on the tissue's solid phase while dissipating energy and enabling smooth joints movements. The synovial fluid consists of hyaluronic acid (HA), glycosaminoglycans (GAGs) containing chondroitin-4-sulfate, chondroitin-6-sulfate, keratan sulfate and mobile ions and is a dialysate of blood plasma without haemoglobin [33]. The synovial fluid is contained mainly within the molecular pore spaces of the cartilage cells [34]. AC incorporates the viscous synovial fluid to mitigate shock-loadings initiated by physiological activities and body weight [35]. Hence, AC supports smooth joint movements at an extremely low coefficient of friction (CoF) [36].

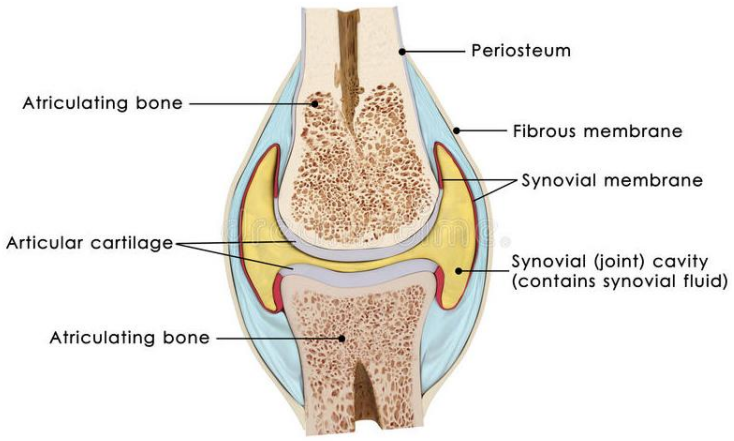

Figure 2. 1 Synovial joint and its components [37]

2.2 ARTICULAR CARTILAGE

2.2.1 The Structure of Articular Cartilage

The AC structure is complex, as the compositions of GAGs, chondrocytes, and collagen are in random orientations and densities; with the main components of this composition contains water (60-85%), collagen type II (15-22%), and Proteoglycan (PG) (4-7%) [2]. Its deep zone includes hydroxyapatite (HAp) combined with collagen and chondrocyte in the vertical orientation [38], as illustrated in Fig. 2.2. AC is a biphasic substrate categorized as a nonlinear, anisotropic, viscoelastic, and inhomogeneous material [2, 3].

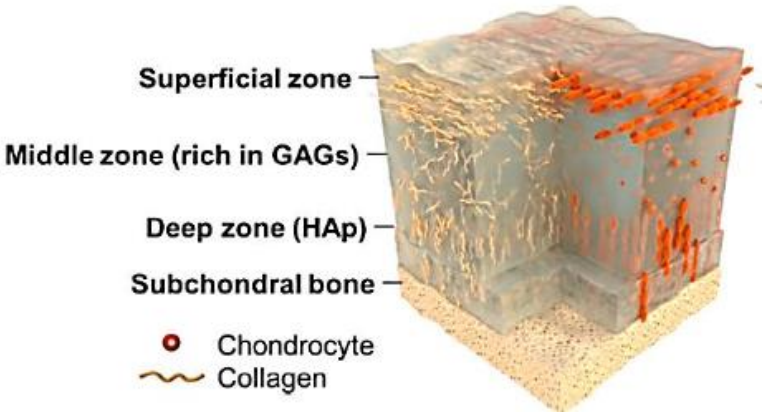

Figure 2. 2 Illustration of the AC structure: superficial, transition and deep zones [39]

2.2.2 Zonal Categories of Articular Cartilage

AC is a soft avascular tissue with a 3-4mm thickness and integrates three depth-dependent layers of superficial, transition, and deep zones. Each layer is responsible for minimizing either the imposing load or friction of the sliding movement as described below:

The top layer (superficial zone) contains collagen fibrils cells in the horizontal orientation, which confers high tensile stiffness and strength. This layer is just 10-20% of the tissue's thickness [40]; both fibrils and chondrocytes are stretched along their length and surrounded at the surface with the finest size compared to the other layers' chondrocytes [41]. This feature also custodies the tissue against high tensile stresses and prevents interstitial fluid permeation, which plays a vital role in sliding on cartilage surface mates [42]. While this layer has high water content, it has the lowest PG [43]. The superficial zone is also called the surface amorphous layer (SAL) that is acellular with no fibril content [2]. Its thickness is a few micrometres, containing proteins, glycoproteins, PGs, hyaluronic acid-protein complexes, chondroitin/keratin sulfates, and lipids [44]. In summary, the superficial zone is shear resistant because of the low content of PGs and low permeability [45, 46]. This layer plays a crucial role in attaining smooth sliding contact while controlling the synovial fluid diffusion rate. The transition zone is the thickest part of the tissue; contributing to 40-60% of the total thickness of the AC [47]. Collagen fibrils and chondrocytes are both ringed by an extracellular matrix (ECM) that includes GAGs [48]. Moreover, compared to the superficial zone, the transition zone has a higher PG content. The deep zone consists of orthogonally oriented collagen fibres in hydroxyapatite content and has the lowest water content. Its collagen structure is bundled together with fibres in the perpendicular direction to the articular surface. The deep zone forms an interface with the subchondral bone. The stiffness of the whole structure varies gradually through the thickness. The PG, water content, and cell density are the lowest in the deep zone [47].

2.3 OSTEOARTHRITIS

Osteoarthritis (OA) is the result of AC degeneration, as illustrated in Fig. 2.3. The recovery process of the damaged lesions is prolonged because of tissue avascularity [2]. Therefore, degenerated tissue experiences high pressure upon sliding of bones at the joints, which results in severe pain as well as movement disorders [4]. Factors that lead to OA are ageing, musculoskeletal disordering, and over-pressuring due to either physiological activities or obesity [5]. It is worth mentioning that joint immobilization yields to PG loss, contributing to AC thinning [49, 50].

OA is categorized into two types, namely primary and secondary. Primary OA occurs in healthy AC without any abnormality of ligaments and menisci. The reason for primary OA in the elderly is repetitive loadings on thinned AC [4]. Secondary OA, however, is due to injury, trauma, or inflammatory factors [51]. In the last decade, studies showed that OA does not result only from AC disease but from defects in the ligament, menisci, periarticular muscles, and bone [52]. AC engrossed with any of the mentioned factors instigate knee instability and alteration in joint kinematics and consequently nonuniformly distributed stresses, which initiate OA [32].

Figure 2. 3 Osteoarthritis in knee-joint [20]

2.3.1 Treatment Methods for the Damaged Cartilage

The gold standard treatments for patients with OA are total knee/hip replacement (TKR/THR) or hemiarthroplasty. In hemiarthroplasty, only half of the joint in which cartilage deteriorated would be reamed, and either metallic or ceramic components are implanted. In case of hip joint damage, the acetabular cup is left intact, and damaged lesions of the femoral head cartilage would be reamed, and a metallic or ceramic cup is replaced. However, TKR or THR is not the practical solution at mid-adulthood ages due to the limitation of arthroplasty prostheses' life span [53]. Due to the short implant service life (15-20 years), THR/TKR procedures are only suitable for elderly patients [54].

Moreover, any failure after primary surgery yields a revision surgery. The revision surgery can be implemented for patients just once in their treatment life since the second revision may result in the implant's loosening [55]. Other procedures that have been developed for damaged cartilage are microfracture [10], autologous-matrix induced chondrogenesis [11], autologous chondrocyte implantation, autologous cultured chondrocytes on porcine collagen membrane [12]. However, long-term clinical follow-ups have revealed durability issues with all the above-mentioned procedures [13]. Therapeutically, nonsteroidal drugs, corticosteroids, and hyaluronic acid just relieve the pain in the short term and are pushed out of the joint within a few days [13].

Therefore, TKR/THR is the only clinical solution for older patients. However, there is not much attention for developing procedures and treatments suitable for younger patients suffering from dysfunctional cartilage to eliminate or at least postpone the need for TKR/THR. Young patients between the age of 20-25 years old have reported the highest incidence of joint injury [33]. It turns into OA by 35-40 years old and implementing TKR/THR is high-risk at this age. If TKR, for instance, is performed at the age of 35-40 years, then based on 15-20 years' service life of prosthesis, patients may need revision surgery at the age of 55-60 years. Revision surgery could potentially lead to disability at this age due to the loosening of the prosthesis. In this case, a novel orthopedics implant with minimally invasive surgery that could mimic the mechanical and

biological behavior of the native cartilage has been highlighted among researchers as a better alternative to TKR surgery for younger patients [56].

2.4 MECHANICAL CHARACTERISTICS OF ARTICULAR CARTILAGE

AC can withstand imposed load under its lifetimes which is estimated at 100-200 million loading cycles [57]. AC is categorized as viscoelastic due to variations of its deformation under various strain-rate [58]. It is anisotropic since the tensile stiffness varies with the direction of loadings [59]. Furthermore, AC is inhomogeneous and performs diverged mechanical functions of tension and compression through the thickness from the superficial to the deep zone [60]. AC incorporation with the synovial fluid, which is incompressible and pressurizes noticeably, supports a significant portion of joint contact pressure [35]. These mentioned properties provide a unique cartilage structure to withstand cyclic loading from the body and transfer those loads smoothly to the bones.

AC tolerates contact pressures in the range of 3-5 MPa during the walking state in hip and knee joints [61]. Moreover, cartilage compressive and shear modulus are reported to be less than 1.5 MPa and 0.5 MPa, respectively. Its Poissons's ratio also ranges from 0.34 to 0.48 [2]. AC is also classified as a poroelastic material as its stiffness is highly dependent on strain rate [62]. Fig. 2.4 (a) shows that at low strain rates ($0.01>\dot{\varepsilon}(t)$) AC responses is consolidation-type deformation, which is stiffness-dependent. In contrast, at higher strain-rates ($0.01\leq\dot{\varepsilon}(t)$) hyperelastic deformation mechanism is dominant that results in high stiffness according to the classical elastic deformation process shown in fig. 2.4 (b) [63].

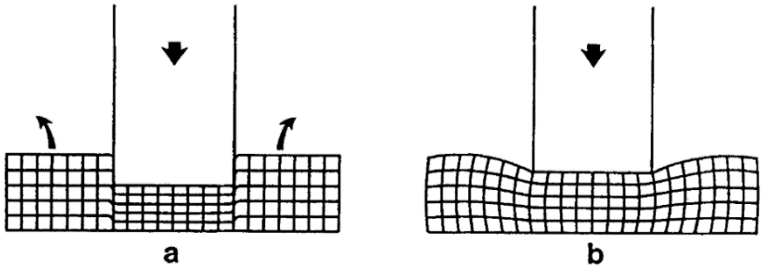

Figure 2. 4 Compressive response of AC representation of (a) consolidation type deformation observed in the low strain rate regime, and (b) hyperplastic deformation in the high strain-rate regime [63].

Eric et al. [64] studied the correlation of cartilage stiffness and strain rate and reported that strain rate increases from 2.7 x 10^{-3} sec^{-1} to 3.5 x 10^{-2} sec^{-1} by increasing stiffness. Their studies employing a wide range of strain rates showed two primary mechanical responses for AC, which is presented in Fig. 2.5 (a). At low strain rates, stiffness increases considerably by a minimum increase in strain rate. In contrast, at the upper strain rates regime, stiffness does not vary significantly when the strain-rate increases. As indicated in Fig. 2.5 (b), there is a critical point beyond which the stiffness does not change much by high-strain rate loading. It indicates that the compressive response of AC is strain-rate dependent at a low strain-rate regime.

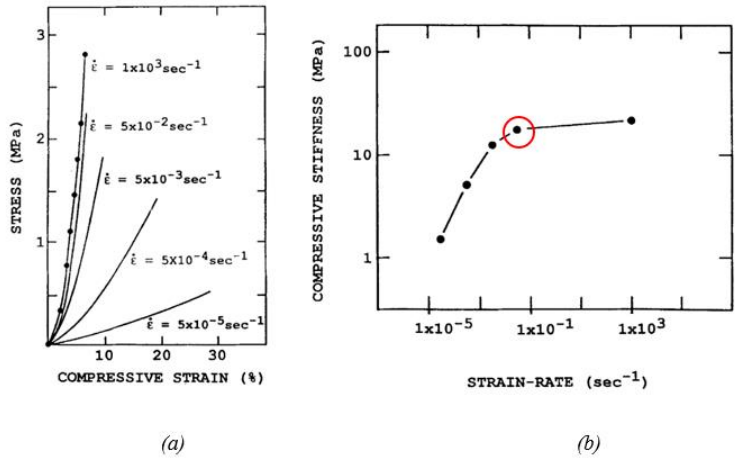

Figure 2. 5 (a) Compressive stress-strain curves at various strain rates (b) Compressive stiffness versus strain rate[63]

ECM significantly affects the mechanical properties of AC. AC exhibits time-dependent responses with viscoelasticity, poroelasticity, or the combination of both phenomena [65]. Research studies demonstrate that AC responds to the loads based on PGs and chondrocyte arrangement [41, 66]. However, cartilage's viscoelastic properties support the continuity of the inner tissue interactions by solid and fluid phase incorporation and fluid migration rates through the solid architecture [67]. Therefore, categorizing AC as viscoelastic or poroelastic material is highly dependent on several test factors, such as the size of the indenter, indentation depth, and strain rates. Joseph et al. [65] demonstrated that the AC neither follows the classical poroelastic nor the viscoelastic model; In fact, the best model characterizing AC is a nonlinear biphasic material.

As AC is a heterogeneous, anisotropic, and multiphasic biomaterial, the mechanical properties depend on its different zones. AC with three main zones and variation of collagen fibrils, PG and water contents in different layers show different responses based on the structure depth or thickness. AC with its relative strength through its thickness is in accordance with its non-homogeneity [68]. Therefore, to analyze the AC responses under loadings, the nonhomogeneous poroelastic model has been recommended [69]. This model presented that the collagen fibril reinforces the cartilage through its thickness resulting in stress-strain ranges. This range is not limited just to the axial-loading direction but also to the radial direction due to the pressurized pores by the interstitial fluid.

Hydration and dehydration are factors that affect the dissipation of pressure energy [70]. AC dissipation response is analyzed by uncoupling poroelastic and intrinsic viscoelastic mechanisms. In the dehydration state, energy dissipation reduction presents the essence of hydration in both poroelastic and viscoelastic functionality [70]. Several elements affect the mechanical properties of AC; however, researchers have circumnavigated through the complexities using customized techniques. For example, the sample-specific tissue composition has been used to predict the compressive mechanical behavior [71].

Depth-dependent mechanical properties of cartilage were also attained with optical imaging techniques like relaxometry by Magnetic Resonance Imaging (MRI), which has demonstrated that under similar loading, different deformation patterns at different anatomical sites [72]. Cartilage degeneration is associated with deformation and its mechanics patterns before morphological symptoms. This finding complies with the depth-dependent mechanical properties under contact loading [72].

The cyclic loading effect on cartilage compaction was highlighted when its relaxation time was altered [62]. Moreover, static and dynamic loadings are other factors that significantly affect stress distribution over the cartilage. By dynamic loading, more uniform deformation across cartilage depth occurs, and this is because of substantial synovial fluid pressure in dynamic loading imposed on the cartilage compared to static loading. Thus, it exemplifies cartilage characteristics in reducing local strains in daily high intense physiological activities [73].

A method, known as Principal Component Analysis (PCA), has been developed to characterize cartilage mechanical properties with more abilities than conventional methods. This method is based on the surrounding tissue of the loaded area (L) and the transient strain (TS) of the AC during loading and unloading. L would be a benchmark to differentiate healthy and PG-depleted cartilage under loadings (deformation) and unloading (recovery) modes [74]. This framework is proving how PGs play a significant role in mechanical functioning.

2.5 TRIBOLOGICAL PROPERTIES OF ARTICULAR CARTILAGE

2.5.1 Wear and CoF of Articular Cartilage Components

Human knee or hip joints are subjected to up to one million cycles of loading per year during daily activities [75]. The rupture of the anterior cruciate ligament (ACL), or meniscal tears, is attributed to joints' misalignment, consequently affecting the joint kinematics, which increases the OA risk [76]. ACL and meniscus deficiency also cause excess tribological contact stresses due to instability of the joint and immediate fibrillation on the tibial plateau [77]. Several studies

have presented that cartilage properties vary as the function of local contact stresses and mechanical environment; however, tribological properties have been reported to be location-independent [78, 79]. Moore et al. [80] have shown that cartilage properties are location-independent and claimed that tribological properties also vary with respect to the local mechanics of the healthy joint. They found four primary tribological responses of the healthy cartilage: first, different regions have different damage tolerances. Secondly, material properties vary remarkably due to OA diseases. Third, different properties are the results of the healthy tibial plateau and OA cartilage. Fourth, OA tissues demonstrate different tribological performances that increase the shear stresses due to mechanical failure or biomechanical degradation [80]. Since cartilage is avascular, degenerated cartilage initiated from the superficial zone and propagated to the deep zone causes destruction of the layers through the thickness resulting in gradual material loss. Cyclic loading induces stress through the entire cartilage structure yielding microscopic damage [81]. The superficial zone in AC experiences shear stresses and cracks within its collagen fibres. Therefore, AC damage occurs when the fibres crack rate exceeds the cell repair rate [82], and this phenomenon is called AC wear-off. AC presents a rubbery surface with a meagre wear rate and CoF [36] but can be escalated by the absence of lubrication, abnormal loading due to varus or valgus knee alignment, ageing, and excess physiological activities [83].

Wear is the amount of material loss from the surfaces due to contacting asperities and friction. In AC, the wear mechanism is categorized as adhesive, abrasive, and fatigue wear [84]. Cartilage wear is because of PGs loss and alterations in the collagen network [85]. Cartilage wear could be initiated due to biochemical degradation and biomechanical factors like knee misalignment, which induces higher pressure on either the medial or lateral side of the knee joint [86]. Most of the studies have fallen short of quantifying wear mechanism due to its complex nature; hence only frictional properties have been investigated. Several studies used metal abrader against AC to quantify wear depth, and their results demonstrated that synovial fluid incorporation with trypsin effectively protects the cartilage surface against wear [1, 87]. Other studies showed that the wear rate increases with increased contact pressure, area of contact, and sliding speed [88, 89]. Wear

rate can be quantified by biochemical characterization of collagen and GAGs content [90]. Another method to capture wear depth and wear scar is surface topography, using scanning electron microscopy (SEM), transmission electron microscopy (TEM), atomic force microscopy (AFM), contact and non-contact profilometric methods [91, 92].

Quantifying wear in AC is complex because of the deficient wear volume of soft tissues. An experiment was conducted to assess wear in AC and cartilage specimens loaded against stainless steel ball by steady sliding motion with 4.62 MPa contact pressure. Collagen loss was monitored as the wear rate indicator, and the results showed a low wear rate (0.5μg/h at 4.62 MPa) in AC [2].

McCutchen [93] worked on the interstitial fluid and hypothesized that this fluid is the most load-bearing element in AC functioning. The author highlighted that since AC has deformable architecture, the interstitial fluid withstood most of the compressive state load. After this theory, Mow et al. [94] studied the biphasic structure and categorized it as incompressible and immiscible tissue. Katta et al. [78] then assessed that fluid could migrate through the porous AC architecture with tiny pore sizes in the range of 2.0-6.5 nm. In addition, Lati et al. [95] presented the triphasic theory, which considers monovalent ions in the interstitial fluid as the third phase. It showed that three elements of fluid, solid, and ion concentration are vital in identifying the compressive stiffness of cartilage. Joint under compressive loading pressurize the interstitial fluid in the tissue. Such a pressure gradient in the tissue supports a significant contribution of the applied loads until the fluid is exuded away at the very beginning of the unloading period [96]. By the fluid pressurizing phase, the applied load is gradually transferred to the soft cartilage tissue, while the imposed load on the fluid is also gradually dissipated. At the equilibrium state, however, the load is tolerated by the soft cartilage tissue. Therefore, the solid phase of cartilage incorporated with interstitial fluid deprives CoF between cartilage mates. It can be maintained at a very low level as long as sufficient interstitial fluid is lubricating superficial layers of the cartilage [79].

Rehydration, contact stress, sliding contact materials and speeds are proportionally related to AC lubrication [97]. The sliding speed and stroke length are primary factors for controlling CoF and rehydration time. These factors control the wear in the cartilage surface as fluid carries the maximum load and results in a very low CoF in AC [98]. Contact stress was also reported to impact CoF significantly; increasing contact stress resulted in the reduction of CoF [99]. On the other hand, it has been shown that experimental parameters and rehydration would change the trend of decreasing CoF by increasing contact stress [79]. Consequently, Katta et al. [99] demonstrated that with increased contact stresses from 0.2 to 0.5 MPa, CoF decreased upon regular rehydration. Most of the cartilage frictional studies conducted have been based on the linear relationship between the applied load and CoF; however, further study is needed to investigate this relationship by a nonlinear trend.

Krishnan et al. [100] investigated friction in AC under cyclic compressive loading with various frequencies (0.05, 0.5, and 1 Hz). They reported that cyclic loading does not decrease CoF by increasing the interstitial fluid's pressurization compared to the static loading. Their study showed that relocation of contact areas effectively lowered CoF rather than the cyclic loading. On the other hand, another study showed that contact stress and stroke length (for rehydration process time) affect CoF detrimentally [101].

While fluid lubrication has been highlighted as a critical element of CoF variations in experimental studies [80, 102], boundary lubrication shows a remarkable improvement since cartilage is biphasic and retains fluid in its superficial layer [103]. By lubricant depletion, the CoF is mostly altered as a function of surface chemistry [78]. Boundary lubrication has been recognized for its usefulness in tissue engineering purposes, joint lubrication, cartilage substitution therapies, and several other applications [96].

Biological factors also have a significant impact on CoF in cartilage. GAGs/PGs formation and existence result in fluid pressurization and consequently variation in tribological properties [104]. These materials exhibit resistance against the interstitial fluid flow, leading to a low

permeability rate (~10-15 to 10-16 m^4/Ns) [105]. Ageing or joint disease leads to a reduction of GAG [106], which effectively increases the CoF rate [107]. Chondroitin sulfate is recommended in case of GAGs depletion; however, lubrication conditions must be considered [108]. Diffusing chondroitin sulfate into the cartilage reported results in a deficiency of ECM integration with chondroitin sulfate, and after imposing load, it is exuded out [78]. Collagen, another major component of cartilage, has also been reported to be effective in reducing CoF, and the lower level of collagen could exacerbate friction [109] and reduce water contents [110]. The SAL contains sulfated sugars, glycoproteins, and lipids, which can be removed by wiping, resulting in higher friction than the unwiped surface [105].

2.5.2 Boundary Lubrication

Transition time in joint is shifting of dynamic to static loading or vice versa. When dynamic loading is gradually transformed to static loading, dissipating energy is mitigated by the interstitial fluid, and it permeates into the cartilage. At this stage, cartilage components absorb the synovial fluids, which initiate the boundary lubrication process [111]. Therefore, it yields cartilage-on-cartilage contact that increases CoF.

Several studies have demonstrated the role of synovial fluid in minimizing CoF drastically under boundary lubrication regimes [112, 113]. Radin et al. [114] demonstrated that the proteinaceous layer has a load-bearing duty and not hyaluronic acid (HA) in the synovial fluid. In contrast, other researchers have shown that HA significantly supports the interstitial fluid in withstanding load [109, 115, 116]. Tests using HA one healthy and dysfunctional cartilage for both humans and bovine showed a remarkable decrease in CoF [109]. This effect is limited to lowering CoF in dynamic loading, even under static pressure, while boundary lubrication occurs. HA penetrates into the cartilage structure and surrounds the chondrocytes, which preserves the CoF levels [116].

Lubricin, a mucinous glycoprotein, is another component of synovial fluid has been reported that lack of lubricin in synovial fluid resulted in inadequate boundary lubrication and increases wear in cartilage [91]. This research showed that in the presence of lubricin, adhesion between contacting cartilage is minimized, and this process yields decreased friction upon boundary lubrication [91].

As another component of synovial fluid, phospholipids contributed significantly to boundary lubrication due to the hydrophobic nature of its fatty acid [117]. Hills and Crawford [118] reported that phospholipids are a component of lubricin in the boundary lubrication, whereas lubricin and HA only supported the phospholipids. Furthermore, Pickard et al. [119] demonstrated that elimination of phospholipid from the cartilage increases the CoF of cartilage minimally. Their study was just limited to the short time; however, no remarkable effect was reported at a prolonged time regarding the cartilage friction properties.

According to the literature, all mentioned components of synovial fluid effects boundary lubrication, and isolating any component can compromise the boundary lubrication process. Moreover, the biomechanical and biochemical synergies may also be insufficiently controlled, as it is in a synovial joint. Nevertheless, all these findings are the expedient benchmark to characterize wear and CoF in AC.

2.6 TISSUE ENGINEERING OF ARTIFICIAL CARTILAGE

Cartilage tissue engineering has been investigated extensively by researchers since this tissue is avascular, and confined migration of chondrocytes reduces its self-recovery considerably. Therefore, the essence of artificial cartilage motivates researchers to design and manufacture materials mimicking the mechanical and tribological responses of the native cartilage. Polymeric hydrogels have been highlighted as candidates for this application as they resemble the biomechanical, biochemical, and architectural properties of native cartilage [120]. Hydrogels have also appealed to researchers due to their biocompatibility [121], nontoxicity effects, and no stimuli on the immune system [16]. Hydrogels are categorized as natural and synthetic and can

be modulated with cell-free or cell-laden scaffolds. Some of the cell-free scaffolds have been presented with the use of bacterial nano-cellulose [122], polyethylene glycol (PEG) in combination with HA [123], collagen-hydroxyapatite hybrids [124], aragonite-hyaluronate membranes [125], acrylamide (AAm) hydrogels [7], alginate (Alg)/chitosan compounds, agarose/polyglycolic acids (PGA) [126], and porous polycaprolactone (PCL) [127]. The mentioned scaffolds were used clinically; however, after clinical follow-up in the longer term, they were rejected due to the lack of strength and durability. The following sections describe some of the common materials used in the manufacture of hydrogels.

2.6.1 Hydrogel Materials

2.6.1.1 Hydrogel Classifications

Hydrogels are classified based on raw materials, chemical composition, physical structure, type of crosslinking, physical appearances and electrical charge, presented in Table 2.1 [128].

Table 2. 1 Classification of Hydrogels

Classification of hydrogels based on	Ref.	Subdomains	Features
Source		Natural origin Synthetic origin	—
Polymeric composition	[13, 128]	Homopolymeric hydrogels	Network formation by single species of monomer
		Copolymeric hydrogels	Network formation by various monomer species with at least one hydrophilic monomer
		Multipolymer hydrogels	Synthesized by two independent crosslinked natural or synthetic polymer
Physical structure and chemical composition	[129]	Amorphous	-Non crystallized polymer chains contain an abundant amount of water

			- Mechanically weak - Very soft and homogenously heparinized
	[130]	Semi-crystalline	- Moderately water-swollen hydrogels. - Mechanically stable and performing melt-processability, and self-healing function
	[131]	Crystalline	- Structurally unique and hierarchical - Morphologies depend on their molecular architectures
Type of crosslinking	[132]	Chemically crosslinked (permanent joints)	Covalent bonding between polymer chains
		Physical crosslinked (transient junctions)	Physical interactions between chains result in chain entanglement, hydrogen bonding, hydrophobic interactions, and crystallite formation
Physical appearances post-polymerization		Matrix, film and Microsphere	—
Network electrical charge	[133]	Non-ionic (neutral)	Less toxic to the cells in vitro
	[134]	Ionic (including anionic or cationic)	high strain sensitivity and many superior mechanical properties
		Amphoteric electrolyte	—
	[135]	Zwitterionic (polybetaines)	Anti-polyelectrolyte" behavior, unusual pH sensitivity, and temperature sensitivity

2.6.1.2 Polymer Materials Used in Medical Applications

Table 2.2 presents comparative advantages and applications of the wide range of materials in synthesizing polymeric hydrogels and mostly for medical applications.

Table 2. 2 The most commonly used polymers in medical applications

Hydrogels	Ref.	Advantages	Applications
Acrylamide	[136]	- High level of toughness & stretch ratio - Similar elastic properties to that of native cartilage	The base of the most polymeric hydrogels
Acrylic Acid	[137]	- Great impact on tensile strength and elastic modulus - Usage amounts effects on more crosslinking and shorter polymer chains, yields higher toughness - Usage results in nonlinearity in mechanical response - High capacity in water retention for swelling applications	Used in synthesizing hydrogels
METAC*	[138]	- Deprive wear loss rate - Retain water in the hydrogel matrix and decrease CoF	Utilized in hydrogels that must be riched of water in prolonged time in biomedical and pharmaceutical applications
Hyaluronic acid	[139]	- Tissue healing, expansion of cell proliferation, and migration - Angiogenesis - Inflammatory response control	For treatment purpose of osteochondral diffusion, enhancing chondrogenesis within the damaged tissues
Cellulose	[140]	- Special fibrous nanostructure, with excellent mechanical and physical characteristics	Methylcellulose includes producing thermosensitive hydrogels applicable in drug delivery systems
Dextran	[141]	- Biodegradable - Biocompatible - Bioadhesive	Wound healing, Relief patient pain, Hard for installation and removal
Alginate	[142]	- Biocompatible - Availability and reproducibility - Low cost	Wound healing, Encapsulation of therapeutic agents, Tissue engineering applications
Chitosan	[143]	- Biocompatibility - Biodegradability - Non-toxicity - Biological characteristics	Hydrogel synthesized by Chitosan and beads applicable to embedding drugs for transport bioactive substances. Drug delivery applications

Gelatine	[144]	- Biopolymer's biotoxicity - Biodegradability - Potential to induce cell migration	The optimal candidate for applications for extracellular matrix (ECM), 3D structure, Cell transplantation
Polyvinyl alcohol (PVA)	[145]	- Biocompatibility - Biodegradability	An ideal option for tissue engineering applications, appropriate for mimicking tissue, vascular cell culture, nontoxicity, and mechanical strength

METAC: *2-(methacryloyloxy)ethyltrimethlammonium chloride*

2.6.2 Synthesis of Hydrogel

2.6.2.1 Crosslinking Approaches

Various crosslinking approaches have been reported to synthesize hydrogels, such as chemically modified processes, crystallization processes, free-radical polymerization, and ionic polymerization [146]. Table 2.3 presents four prevalent approaches that are used to synthesize hydrogels for medical applications.

Table 2. 3 Crosslinking methods to design hydrogels [147]

Methods	Ref.	Categorize		Advantages
1.Chemically crosslinked gels	[148, 149]	I.	Crosslinking by radical polymerization	Water-soluble polymers can be done with an initiator and catalyst. Such a system is very efficient, and at ambient temperature, gel forms quickly. Water solubility, short-chain, and solubility activity.
		II.	Crosslinking by chemical reaction of interdependent groups	A group of polymer chains can be connected with covalent linkages due to their interdependent reactivity.
		III.	Crosslinking by high energy irradiation	-

	[150]	IV.	Crosslinking using enzymes	In an equilibrium state (more than 90% water content), gelatine is formed.
2. Physically crosslinked gels	[147]	I.	Crosslinking ionically	Very effective on the self-healing properties of hydrogels.
	[145]	II.	Crosslinking by crystallization	By the process of freeze-thawing, a very elastic gel is formed.
	[151]	III.	Physically crosslinked hydrogels from by graft copolymers	The uniform structure is formed in water
3.Crosslinking by hydrogen bonds	[152]		-	Swelling is a function of pH
4. Crosslinking by protein interactions	[153]	I.	Use of genetically designed proteins	By manipulating the genetic Deoxyribonucleic acid (DNA) code, physical and chemical properties are controllable parameters (More related to Genetic Engineering).
		II.	Crosslinking by antigen-antibody interactions	Good for drug delivery to target specific antigens.

Among the methods mentioned above, free-radical polymerization is a prevalent method used to synthesize hydrogels for biomedical application [154].

2.6.2.2 Free Radical Polymerization

Free radical polymerization (FRP) is a capable technique to produce about 50% of monomers to polymers [155]. The major advantage of FRP is its insensitivity to monomer and impurities compared to ionic polymerization [156]. It can be applied in normal room conditions, which minimizes the cost of production. A broad range of monomers can be utilized in FRP to turn to polymers which is the great advantage of this technique [157].

Free radical polymerization involves the conversion of monomers into polymers through the initiation, propagation, and termination steps. The ‘’*initiation’’* process involves the production of radicals that start the reaction with the monomer. An existing free-radical interacts with the monomer resulting in a new radical, which in turn opens another molecule monomer. This process repeats to result in a polymer, and this step is called ‘’*propagation*’’. The polymerization reaction stops when the last radical of one polymer chain meets another chain with the free radical, and when they combine, the polymerization process is completed, hence the “*termination*” step [158].

2.6.3 Bilayer Hydrogels

Bilayer hydrogels comprise a porous architecture layer integrated with a bulk layer covalently. The porous architecture is the result of the interruption in the polymerization process. The porous layer benefits hydrogel in water retention, impact on diffusion rate, minimizing CoF and wear rate [124, 138]. Gong et al. [159] developed a bilayer hydrogel with varying crosslinking degrees in the top layer. A lower degree of crosslinking resulted in high porosity, and the hydrogel had a higher fluid retention capacity, which consequently minimized the CoF. The bilayer architecture formation in hydrogels is due to branch dangling chemical phenomena [159]. A branched dangling polymer chain is achieved by polymerizing the monomers, while in contact with a hydrophobic surface. Hydrogen-rich moieties are located within close vicinity of the hydrophobic surfaces yielding a low density highly porous structure. This is attributed to the high concentration of hydrogen affecting the propagation step of polymerization. The bulk area, which is far from the hydrophobic surface, could accomplish the polymerization process due to hydrogen deficiency in this zone. Consequently, a very dense structure is formed, and the bulk area's strength enhances compared to its porous counterpart [160]. Therefore, a hydrogel with a porosity gradient could be attained.

2.6.4 Hydrogel Network Systems

A number of hydrogel systems have been reported in the literature, namely, interpenetrating networks (IPN), semi-interpenetrating networks (semi-IPN), double networks and dual networks hydrogels [53, 161]. IPN networks consist of two or more networks that are chemically crosslinked [162]. In semi-IPNs, consist of blends of one or more polymers without them being chemically connected. Semi interpenetrating networks are achieved using only initiator and monomer; however, full-IPNs are formed using monomers, initiator, and cross-linker [163]. Double networks (DN) hydrogel is a structure of two networks entangled jointly that each network carries a specific mechanical property, as one network carries ductility and the other one supports rigidity, which yields a higher toughness [164]. Arakaki et al. [61] manufactured double network hydrogel using poly-(2-Acrylamido-2-methylpropane sulfonic acid)/poly-(N, N'-dimethyl acrylamide) (PAMPS/PDMAAm) DN hydrogel for rabbit knee cartilage. They conducted the animal study, and for the first 12 weeks, the surface structure of the gels was not affected and reported a CoF of ~0.029. They showed the type of polymer, monomer, and crosslinker concentration were instrumental for attaining enhanced compressive strength. Furthermore, Gong et al. [165] have also reported that the mentioned parameters affected the compressive strength PAMPS hydrogels. Single network (SN) hydrogels, on the other hand, fracture easily compared to DN hydrogels. Fig. 2.6 illustrates compression test results for SN and DN hydrogels.

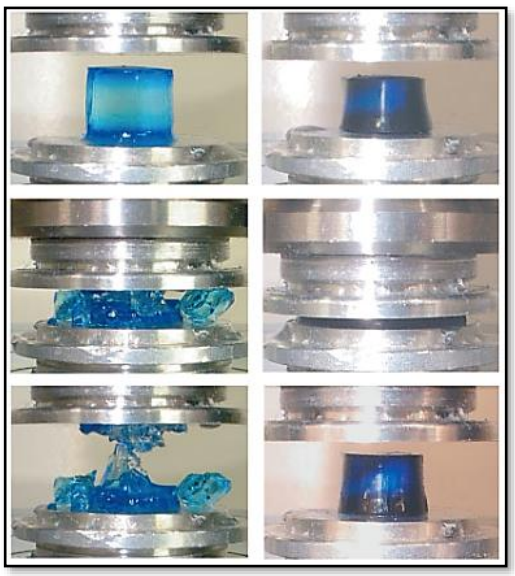

(a) (b)

Figure 2. 6 Compressive tests demonstrate that how DN gels sustain high compressive strain while single network breaks easily a) PAMPS-1-4 SN gel, b) PAMPS-1-4/PAAm-2-0.1 DN gel. Fracture stress: PAMPS SN gel, 0.4 MPa, PAMPS/PAAm DN gel, 17.2 MPa [128]

Furthermore, the tests showed that a SN hydrogel's fracture-toughness is low and would fail at minimal compressive loading. However, DN hydrogel endures superior compressive load and the ability to return to its original shape. Thus, the crosslinking density of the first and second networks of DN hydrogels are essential considerations for hydrogel synthesis [166]. A DN hydrogel consisting of a highly crosslinked first network and loosely crosslinked second network demonstrated analogous elastic modulus. Fig. 2.7 shows the schematics of IPNs, double and dual hydrogels network systems.

a)

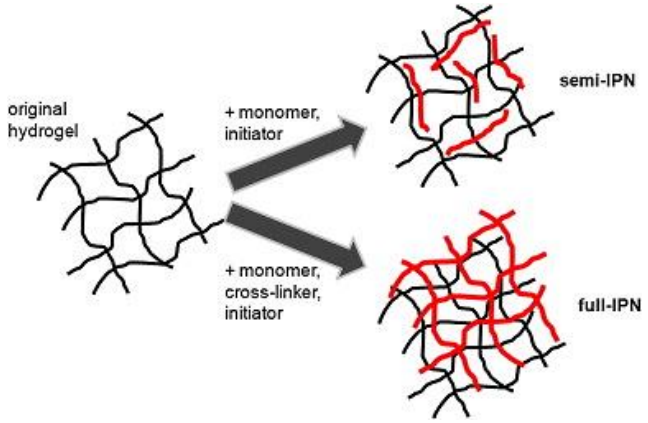

b)

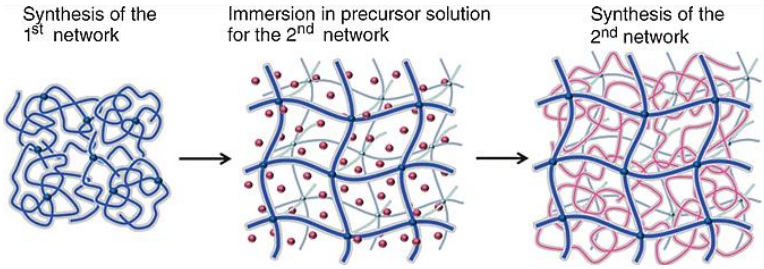

c)

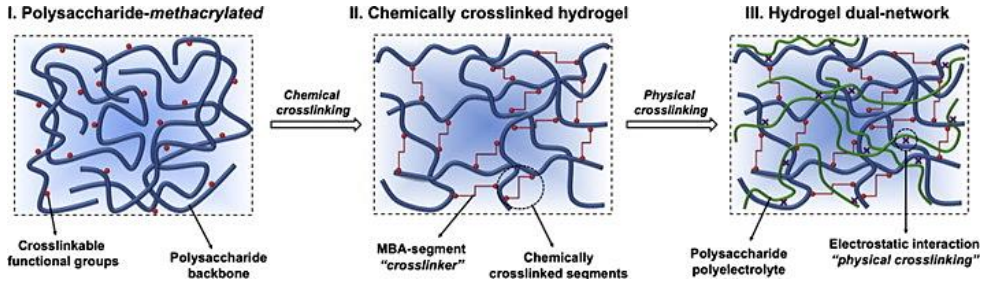

Figure 2. 7 Hydrogel network systems in the form of a) IPNs [163], b) Double networks[167] and c) dual networks [168].

Among hydrogels, IPNs hydrogels have presented improved tribological and mechanical properties compared to single network hydrogels [169, 170]. AC, as mentioned previously, is nonlinear, anisotropic, viscoelastic, and inhomogeneous material. Three-dimensional (3D) woven structure infused by IPN hydrogels reported mimicking the properties of AC [171, 172]. Furthermore, the IPN structure would establish an environment for cell seeding followed by cell

differentiation which enhances the biological properties of the implant and affects osseointegration. However, a polymeric hydrogel with sufficient mechanical load-bearing response and optimum tribological properties similar to that of AC is still a challenging subject [53, 146, 173].

2.6.5 Mechanical and Tribological Testing of Articular Cartilage and Hydrogels

AC as a soft tissue articulates the full range of motions, and experiences complex loading scenario, which is compression, tension, shear and friction [174, 175]. The combination of architecture of ECM and synovial fluid associated with poroelasticity and fluid pressurization dissipate stress imposed on the joint [176]. Figure 2.8 demonstrates that the type of tests has been conducted on AC from 2009 to 2018.

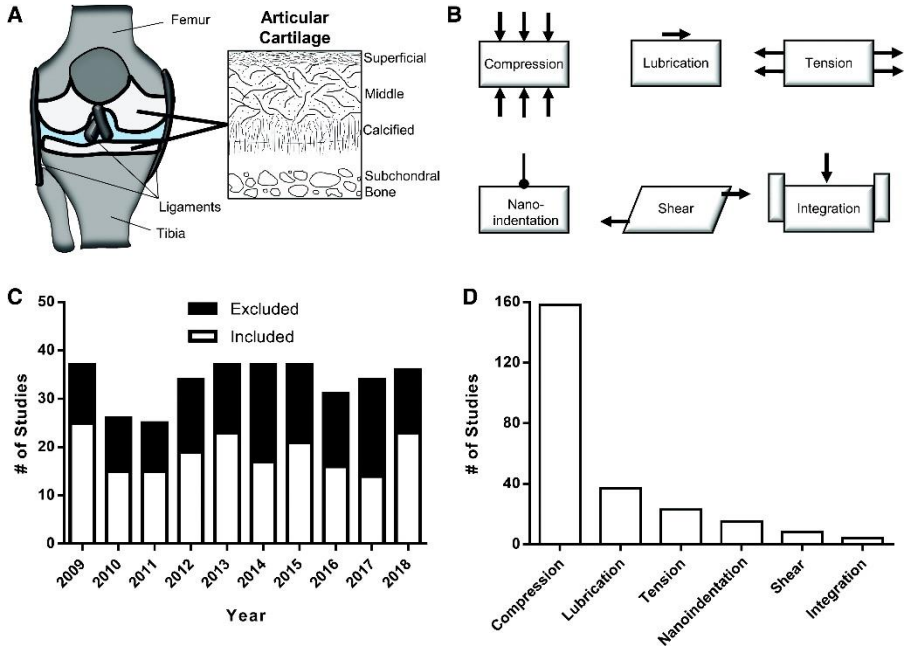

Figure 2. 8 (A) Anatomy of the knee joint, showing the femur, tibia, and ligaments, with AC (in white). Schematic of AC architecture showing the anisotropic alignment of collagen bundles. (B) Schematics of standard modes of articular cartilage mechanical testing (compression, lubrication, tension, nanoindentation, shear, integration). (C) A systematic review of "articular cartilage mechanical testing" from 2009 to 2018, showing excluded and included studies. (D) Breakdown of testing type (n = 197 studies), showing the overwhelming majority of studies (80.2%; 158/197) reporting data from compression testing [177].

2.6.5.1 Compression or Ramp Tests

Most studies focused on assessing recovered tissue based on biochemical, gene expression, or histological aspects[178, 179]. Comprehensive protocols for mechanical evaluations showed a lack of standardization for their unit reference. Therefore, remarkable tolerances in the reported data are inevitable. Test parameters are primary factors that are affecting results. The compression testing is categorized as unconfined, confined, and in situ. For the confined compression test, a porous plate or indenter is used to let fluid flow out of the tissue as illustrated in Fig. 2.9.

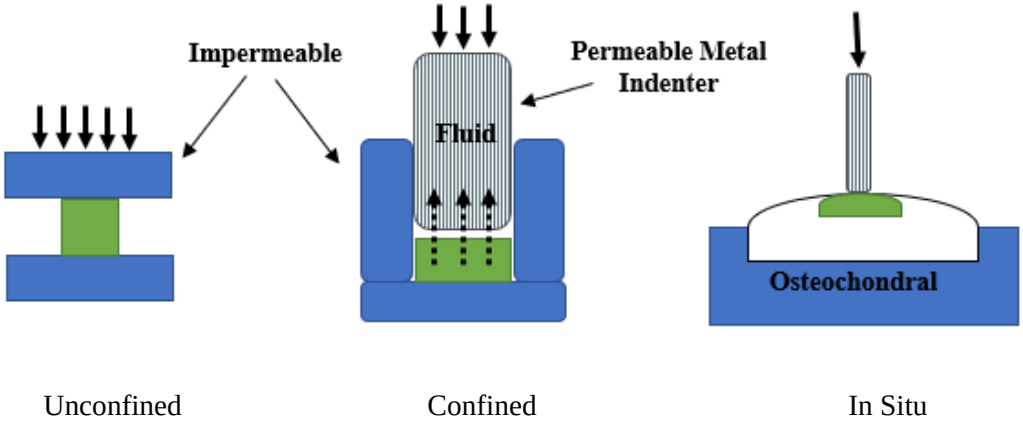

Figure 2. 9 Compressive testing configurations

Four test configurations are commonly used to characterize cartilage mechanical responses, which are ramp, stress relaxation, creep, and indentation tests. The ramp test load varies (load) while the deformation (strain) rate is held constant, and the tissue stress response is recorded. In the stress relaxation test, strain is imposed to a certain level and is held under a specific time to monitor stress distribution over the structure. In the indentation test, a load with a constant rate compresses the sample to a certain thickness to measure elastic modulus and hardness of the tissue. The most utilized test configuration in studies from 2009 to 2018 according to Jay et al. [91] are listed in Table 2.4.

Table 2. 4 Mechanical test configurations applied for cartilage tissue during 2009-2018.

Test	Unconfined	Confined	In Situ
Ramp	59	3	17
Stress Relaxation	41	10	21
Creep	2	5	13
Dynamic	26	2	8

The low permeable tissue in AC incorporated with interstitial fluid and pressurization mechanism absorbs impact loadings. Thus, the ramp test has been configured to simulate the load-bearing properties of the tissue. After recording the stress-strain response by the ramp test, the first-order differential equation of the curve, which is the slope of the stress-strain curve, results in the tangent modulus of the tissue. Tangent modulus quantifies softening and hardening of the material and plastic deformation beyond yield stress [151]. Softened materials endure a higher load before ultimate failure compared to hardened materials and are suitable for replacing tissues that undergo large deformations [22]. Two factors that considerably affect the tangent modulus are strain rate and strain point. Healthy knee cartilage typically experiences average strains under 10% [59] and a maximum of 17% [180]. While the tangent modulus is estimated by laying on the curve less than 10% strain at different strain points, as shown in Fig 2.10; therefore, tangent modulus data would not be clinically helpful. But it shows at each strain point how hard or soft tissue responses are. This is relative to the micro-architecture of the tissue matrix, porosity, and fluid flow rate within the matrix [128].

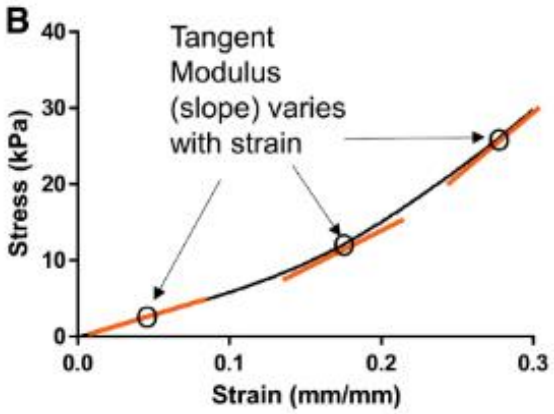

Figure 2. 10 Tangent modulus of stress-strain curve for articular cartilage [177]

2.6.5.2 Stress Relaxation Tests

Stress relaxation is the second-ranked standard test, according to the literature survey presented in Table 2.4. Viscoelastic properties of tissue benchmark energy absorption and dissipation during physiological activities [181]. Therefore, the viscoelastic properties of cartilage enable the tissue to withstand immense continual strain [182]. Numerous methods have been applied to characterize the viscoelasticity of the native or artificial cartilage. A typical test is the stress relaxation and rheometer test. Tuncaboylu et al. [183] applied a rheometer on their synthesized hydrogels to analyze relaxation modulus and reported that hydrophobic associations could perform as additional crosslinks and improve the toughness. AC fracture toughness is proportionally associated with stress relaxation [57].

2.6.5.3 Tribological Testing of Articular Cartilage and Hydrogels

In the tribology testing of both native and engineered cartilage, there are two methods of testing the lubrication properties; the first method is sliding mate with a specified stroke length, which yields matrix deformation. The CoF would be very low as the fluid resistance is against imposed load in the active deformation region. It is reported that the load support can be analyzed by Peclet number, where low friction occurs by the condition of Pe>>1 and connective fluid velocity surpasses diffusive fluid velocity [35, 96]. The second method of lubrication analysis is aimed more at boundary lubrication which is a stationary contact area. In this method, a sample

is compressed to a solid mate, and CoF is recorded as the fluid pressure drops to the ambient pressure [102]. Therefore, interstitial fluid pressure lessens, and only contact pressure between two solid mates determines the CoF associated with the biochemical and articular surface. Thus, this method is suitable to analyze boundary lubrication and its biomolecular interactions. It is worth mentioning that a correct interpretation of using the two methods is necessary and depends on the surface and pressuring mechanism. If a tissue provides excellent permeability, which increases the localization of lubricants, it would have a relatively low CoF in stationary and high CoF in migrating contact areas. In contrast, a tissue with a remarkable pressurizing fluid mechanism but poor in boundary lubricants would have a relatively low CoF in migrating contact area and high CoF in stationary contact area [177].

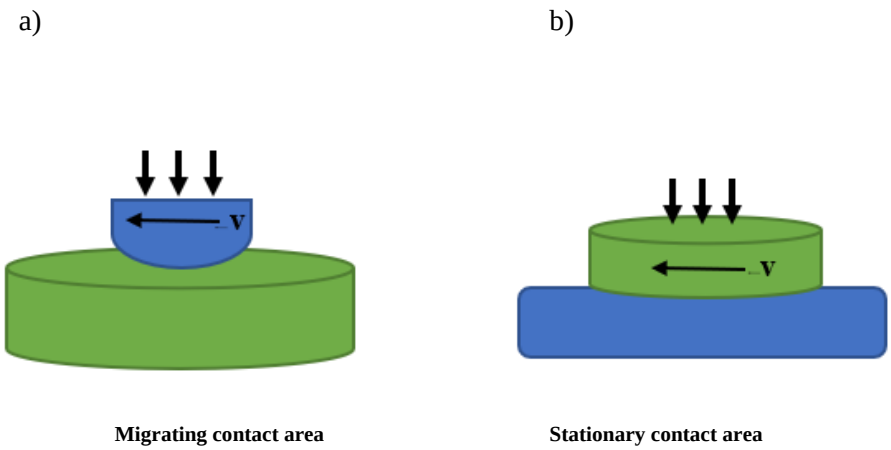

Figure 2. 11 Lubrication (a) migrating contact area and (b) stationary contact area

It has been highlighted that compression tests are essential with modelling of viscoelasticity responses according to required tests of the United States Food and Drug Administration (FDA) and International Cartilage Repair Society (ICRS) [14, 184]. Moreover, The American Society for Testing and Materials (ASTM) standard is focused on confined creep testing as a requirement for mechanical evaluation of designed tissues [185]. Alternatively, creep or stress relaxation is needed to quantify material properties recommended by ASTM. A systematic review of literature from 2009 to 2018 [177] showed only 11.4% of studies had performed stress relaxation or creep tests, which demonstrates that most studies did not meet the requirements of the FDA and ICRS

guidance documents. FDA and ICRS also recommend other tests to sufficiently approve the mechanical assessment of a native or artificial cartilage as outlined in the following table.

Table 2. 5 Mechanical testing types, modes and configurations suggested by FDA [184], ICRS [14] and ASTM [185].

		FDA	ICRS	ASTM
Test Type	Compression	✓	✓	✓
	Lubrication and friction		✓	
	Shear	✓		
	Tension	✓	✓	
	Integration/fixation	✓		
	Wear	✓	✓	
	Fatigue		✓	
Mode	Quasi-static	✓	✓	✓
	Dynamic	✓	✓	
Configuration	Unconfined	✓	✓	
	Confined	✓	✓	✓
	Indentation	✓	✓	

2.7 MECHANICAL PROPERTIES OF HYDROGELS

Crosslinking process within polymer chains improves the compressive strength, stretch-ability, and toughness of the hydrogels to withstand shear or compressive stresses. There are two conventional crosslinking approaches. Covalent crosslinking enhances materials' strength and dissipates mechanical energy against deformation, whereas ionically crosslinked augments self-healing properties and controls degradation of the polymeric network [53, 138, 186]. Furthermore, it was reported that ionically crosslinked hydrogels using Fe^{3+} or Al^{3+} also exhibited enhanced mechanical strength [187]. Crosslinking density affects the polymer chain length, and consequently, different properties can be achieved [188]. The dangling chains phenomenon exploits the hydrophobicity and hydrophilicity interaction to form a low-crosslinked density that

improves lubricious fluid retention [189]. The high-crosslinked density, however, results in a bulk layer that enhances structure load-bearing [187].

An improvement in the mechanical properties mitigates the lubrication properties of hydrogels. Subsequently, research on having a load-bearing structure with a sufficient lubricational threshold has not yielded the desired success; therefore, this subject warrants further research attention. It has been proven that monomers molar ratio, initiator, and crosslinking degree determine the mechanical properties of hydrogels [190]. Zhang et al. [138] reported that the mechanical properties of bilayer hydrogels improved notably by meticulously increasing monomer (AAc) content. They showed by increasing the molar ratio of their monomers from 25% to 35%, and tensile strength was enhanced two-fold. Increasing the amount of AAc resulted in ultimate tensile strength and elastic modulus increase. However, when AAc was more than 50%, hydrogels become very brittle and stiff, resulting in inferior tensile properties [151], and were not suitable for practical applications. They also reported that less AAc in the total amount of monomers leads to less crosslinking, and a longer length of polymer chains results in material ductileness. Xu et al. [188, 191] found that the titanium nanocomposite hydrogels having 10% AAc had significant tensile strength and enhanced water stability (low swelling ratio) compared to the higher molar percentage of AAc. Optimum AAc amount improves the mechanical strength and affects the nonlinearity of the hydrogels, which is a premium consideration in tissue engineering applications [137]. Arjmandi et al. [53] reported that their hydrogel's mechanical properties improved by increasing crosslinking concentration up to 21% and 32% for elastic modulus and hardness, respectively. Trivalent cations (Al^{3+}or Fe^{3+}) also presented a momentous factor in increasing the strength and stiffness when hydrogels were synthesized using alginate monomer [192].

Among polymers, alginate and polyacrylamide (Alg/PAAm) have been reported to provide a high level of toughness and stretch ratio [136, 193]. The elastic properties, furthermore, were reported to be similar to that of AC [169]. Alg/PAAm also proved a 3-fold decrease in CoF

compared to either Alg or PAAm as single network hydrogels [186]. Alg, however, has some disadvantages such as low tensile properties and difficulty in sterilization and controlling the hygiene process during synthesis. Its impurities may also affect material properties [194, 195]. To sum up, optimum amounts of AAc, AAm, Alg, and relevant crosslinking ratios would significantly improve both the mechanical and tribological properties of hydrogels. Table 2.6 summarizes the mechanical properties of some common polymers. The elastic modulus of ICRS is also presented in three different grades.

Table 2. 6 Mechanical properties of commonly used polymers to synthesize hydrogels for artificial cartilage implants.

Hydrogels Compositions Researchers/year	**Ref.**	**Primary crosslinkers (MBAA)**	**Secondary crosslinking**	**Elastic Modulus**	**Compressive Stress**
PAAm-Alg Arjmandi et al./2019	[22]	(0.06 w/w %) 4 wt% SNPs	$CalCl_2$ (10wt%)	180 kPa	0.18 MPa
	[53]	(0.06 w/w %)		120 kPa	—
PAAm-Alg Zhai et al./2015	[196]	(0.06% wt%) SNPs (6wt%)	$CalCl_2$ (0.5 Mole/L)	110.9 kPa	2.0 MPa
		(0.06% wt%) TNPs (6wt%)		133.2 kPa	3.0 MPa
PAAm-Alg Yue et al./2019	[197]	(0.25% wt%)	$CalCl_2$(0.5 Mole/L)	—	0.29 MPa
κ carrageenan/PAA Tarashi et al./2019			Cooling and UV light techniques	160 kPa	21.7 MPa

PAAm-Alg+OA-POSS Bahrami et al./2019	[164]	(0.23wt%)	OA-POSS	240kPa	2.2 MPa
PAAm-AAC-METAC	[187]	(0.05wt%)	Fe^{3+}	—	45 MPa
Articular Cartilage	[179] [33]	Grade 1: 0.50 ± 0.14 MPa Grade 2: 0.37 ± 0.13 MPa Grade 3: 0.28 ± 0.12 MPa			0.1-2.0 MPa

[a]*Human Elastic Modulus calculated under unconfined compression mode [45].*

**DMAA: N,N-dimethyl acrylamide*
**AAc: Acrylic Acid*
**AAm: Acrylamide*
**METAC:2-(methacryloyloxy)ethyl trimethylammonium chloride*
**PVA: Poly Vinyl Alcohol*
**AlG: Sodium Alginate*
**OA-POSS: Octa-aminopropyl polyhedral oligomeric silsesquioxane hydrochloride salt*
**SNPs: Silica Nanoparticles*
**TNPs: Titanium oxide Nanoparticles*

2.7.1 Viscoelastic and Poroelastic Relaxation

Viscoelastic and poroelastic are associated with the rate of fluid migration within the networks, and their interaction with polymer chains results in dissipating energy [198]. Therefore, the assessment of hydrogel materials and their viscoelastic or poroelastic relaxation response is essential in designing tissues where they are subjected to high-impact loads. Hydrogels are formed by fibre networks similar to fibrin and collagen in AC and can be categorized as viscoelastic due to the exhibition of stress relaxation [24]. A nano-porous hydrogel structure, like acrylamide hydrogels, performs minor viscoelasticity and is nearly elastic [68]. It was reported that stress relaxes promptly when the hydrogel is crosslinked ionically compared with covalently crosslinked [199]. Zhao et al. [199] showed that the binding and unbinding of alginate hydrogels that are crosslinked ionically show stress relaxation responses. By exerting a force that results in unbinding of ionically crosslinked fibres, divalent cations detach from the anions of alginate chains and re-bond with another anion. In contrast, the covalently crosslinked network does not

detach and re-attach fibres. Thus, instead of detaching, it yields a longer time to relax the stress [200]. The covalently crosslinked hydrogels exhibited time-dependent mechanical properties.

It is highlighted that an abundant amount of water in hydrogels also affects viscoelastic responses. Fluid motion within the network would significantly impact dissipating energy from external loadings [199]. Hong et al. [201] formulated a coupled mass transport theory and large deformation within the hydrogel network. The motion of fluid inside the network and the resistance of the porous structure against the fluid migration yield to macroscopic mechanical relaxation, which is different from relaxation resulting from structural deformation in the network. This phenomenon is called poroelasticity and is characterized by diffusion coefficient D of the fluid in the network [202] and can be obtained by the following equation:

$$D \sim Er^2/\eta \tag{2.1}$$

where E is the elastic modulus, r is the pore radius of the polymer network, and η is the fluid viscosity in the hydrogel. According to the equation, the rate of relaxation depends on poroelasticity. As mentioned above, regarding the fluid migration, the smaller pore size results in slower fluid migration and thus slower stress relaxation. Therefore, diffusion rate D, and geometric scale L of the sample are inversely proportional to the time of stress relaxation. A smaller L yields faster stress relaxation due to the fluid migration at a shorter distance. However, the rate of deformations of a hydrogel is independent of the geometric scale [199]. In addition, viscoelastic responses are always attributed to fluid flow and network deformation. Therefore, when $L >> \sqrt{D\tau_v}$ which was obtained for hydrogels when the sample scale is large enough to prevent the fluid from migrating to the end, viscoelastic relaxation occurs before poroelastic relaxation [203]. If we consider two states of time required for hydrogel to reach viscoelastic and poroelastic relaxation, therefore, $t \sim \tau_v$ is the time of viscoelastic relaxation from deformation and $t \sim \tau_p$ is the time of poroelastic relaxation resulting from fluid flow. Then, the following states presented in Table 2.7 would apparently occur in hydrogels that might be considered as the key parameter of relaxation time that effects on results.

Table 2. 7 Time states of viscoelastic and poroelastic relaxation in polymeric hydrogels [204].

Time states	Viscoelastic relaxation	Poroelastic relaxation	Material behavior	modulus	Fluid migration
$t<<\tau_v$ $t<<\tau_p$	×	×	Purely elastic solid	Unrelaxed	Ignorable
$t<<\tau_v$ $t>>\tau_p$	×	✓	Behave as an elastic solid	Unrelaxed	Conspicuous
$t>>\tau_v$ $t<<\tau_p$	✓	×	Behave as an elastic solid	Relaxed	Ignorable
$t>>\tau_v$ $t>>\tau_p$	✓	✓	Behave as an elastic solid	Relaxed	Conspicuous

Therefore, it is essential in the design of artificial cartilage to assess the viscoelastic and poroelastic time of relaxation based on material properties.

2.8 TRIBOLOGICAL PROPERTIES OF HYDROGELS

Wear is the loss of material, a continuous damage process due to the sliding of contact mates throughout cycles. Wear, V is defined as the total volume of material loss. Wear rate (*w*) reported by Archard et al. [205] is defined as volume loss per unit sliding distance. Archard's equation predicts that the wear rate is proportional to the normal contact pressure and inversely proportional to the hardness of the material surface:

$$\mathrm{w} = \frac{\mathrm{V}}{\mathrm{s}} = \mathrm{K}\frac{\mathrm{P}}{\mathrm{H}} \tag{2.2}$$

where *W* is the total volume loss in [mm^3], *P* is the normal load in [*N*], *H* is the hardness of the material, *s* is the sliding distance, and K is the so-called wear coefficient a constant that is usually

determined by experiment for two specific contact partners under certain environmental conditions.

A conventional system for analyzing tribological parameters is the pin-on-disk tribometer, where a small pin slides on a larger circular disk. The sliding motion is between the specimen and the rotating disk. Several types of motions and sliding between solids have been introduced (i.e. sliding wear, rolling wear, impact wear and oscillation wear) [206]. The dominant wear mechanisms are abrasion, adhesion, surface fatigue, and tribochemical reactions. Abrasive wear is the subtraction of a soft material by a hard adjacent surface [207]. The most substantial part of the abrasive wear is caused by tangential sliding motions and removal of the microscopic asperities. Adhesive wear is associated with an increase in the CoF, μ between the interfaces [207]. Up to μ=1.0, the presence of friction can be explained by adhesion itself, which means that frictional resistance is caused by asperities coming into contact and adhering to one another. Corrosive wear is a mechanism of materials and environment interface; development of worn surface may yield to different scenarios as relative motions of the bodies. Finally, wear due to fracture is a description of the removal of chunks of material due to microcracks occurring within material either due to surface cracks or subsurface cracks [79]. One of the conventional approaches to control wear and friction is lubrication. The lubricating region is described as load transition between surfaces through a pressurized lubricant film and is defined through a film parameter by the following equation:

$$\Lambda = \frac{h}{\sqrt{R_{q1}^2 + R_{q2}^2}} \tag{2. 3}$$

where Λ is lubrication regimes, h is the film thickness, R_{q1} and R_{q2} are the surface roughness of each surface in contact. If Λ is less than one, it is considered to be a circumstance of boundary lubrication, where all of the load transfer occurs across asperities with the presence of a molecularly thick layer of a boundary species. If $1<\Lambda<3$, then full film lubrication occurs when

the load between asperities is transferred across a pressurized lubricant, and asperities are rarely in contact. Full film lubrication is categorized in thin-film ($3 \leq \Lambda \leq 10$) and thick film ($\Lambda \geq 10$); however, such a distinction is not applicable for orthopedics implants [208].

Film parameter has a significant impact on friction and wear by which a small increase by Hersey number associated with the film thickness results in a significant decrease in wear rates. Therefore, consideration of fluid film in the design of orthopedics implants maximizes design efficiency. The following figure shows the effect of lubrication type on the coefficient of friction.

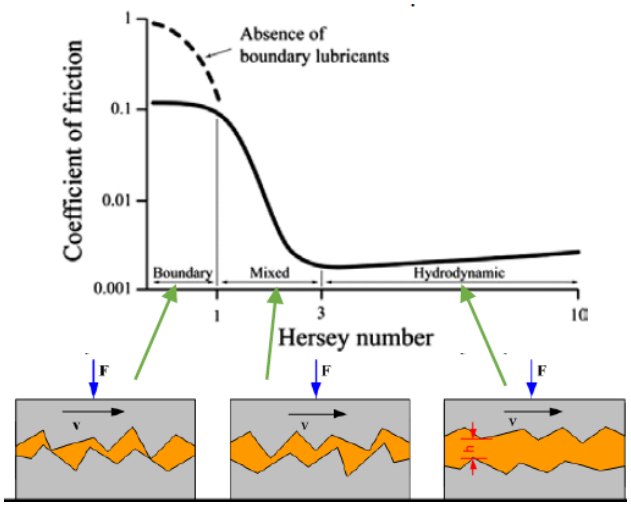

Figure 2. 12 The effect of lubrication type on friction coefficient [208].

Cartilage wear and degeneration are trackable by magnetic resonance imaging (MRI) that can show the initiation and propagation of cartilage wear [209, 210]. Moreover, the worn surface can be observed using SEM, as shown by Fig. 2.13.

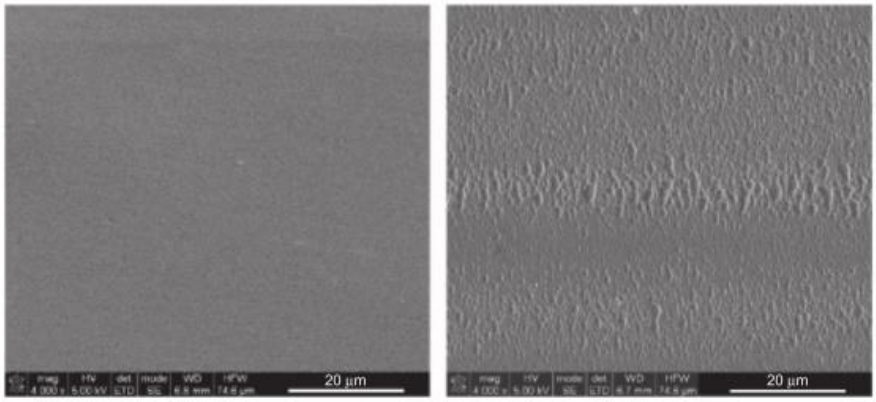

(a) (b)

Figure 2. 13 *Worn surfaces resulting from sliding against articular cartilage under (a) p=3.5 MPa and (b) p= 5.0 MPa[36].*

By increasing the load factor during the wear test, the surface becomes pitted, and wear particles are accumulated. AC tends to wear off by ageing and physiological activities; thus, measuring tribological properties is of the essence in artificial engineering of the cartilage. A study on the frictional response of hydrogels demonstrated that it does not follow Amonton's law $F = \mu W$ that is related to solids friction [160]. Sliding velocity and contact pressure play significant roles in the sense of frictional force.

Bilayer hydrogels that consist of a bulk layer for bearing load and a thin porous layer to retain fluid and minimize the CoF have been developed recently [138, 187]. In these bilayer hydrogels, the bulk layer exhibited significant compressive strength up to 0.35 MPa. The reciprocating sliding test reported a 0.038 of associated with its lubricious layer. However, the lubricious layer was worn after a few thousand cycles due to its low network density. Surface network density is inversely proportional to water retention, which in turn influences the CoF. CoF value in hydrogels depends on types of crosslinking [138], crosslinking density [8], and type of lubricant [79]. Zhang et al. [132] achieved ionic crosslinking by 1-day immersion of their bilayer porous hydrogels in 3% sodium alginate solution (SA), which decreased the CoF up to 18%. It shows that ionic interactions enable the polymer matrix to trap the lubricant resulting in a remarkable

CoF reduction. They found that two days of immersions of their bilayer hydrogels in SA showed the best results for decreasing CoF to 0.025. Crosslinking density is proportionally related to the mesh size and showed a remarkable correlation at the transition of low to high frictions [211].

In an earlier study, the lateral and normal friction forces were not directly correlated to the stiffness but varied with the hydrogel architecture and composition [212]. The contact pressure and pore pressurization within interconnected channels are the key factors that control hydration levels in tribological assessments [202]. The contact pressure experienced by AC was reported in the range of 0.1-2.0 MPa in the hip and knee joints [97, 178]. By increasing contact stress on AC, the CoF decreases [99]. However, research showed that experimental parameters and rehydration would change the trend of decreasing CoF by increasing contact stress [213].

Beyond CoF values, the determination of lubrication mechanisms in hydrogel has rarely been addressed. The effects of load and speed on lubrication regimes have been studied with the aid of the classical engineering Stribeck curve [214]. They found that hydrogels are not covered the engineering Stribeck curve regimes, and the main regimes were developed: mesh-confined, elastoviscous transition, and fluid film.

In the engineering system, a prompt transition occurs over narrow ranges of the Hersey number, which is also the dimensionless fluid thickness. It is worth mentioning that stiff engineering materials have elastic moduli in the scale of GPa; therefore, the hydrodynamic fluid film would form by increasing speed or decreasing load. However, hydrogels with conformational surfaces with respect to contacting mate and a much lower range of elastic modulus (kPa) do not fall into this lubrication regime. Therefore hydrogels are viscoelastic materials, and their wear behavior is similar to that of rubbers; thus, fatigue and adhesion wear mechanisms are dominant [215].

Furthermore, the effects of applied load and sliding speed on shifting wear mechanisms have been investigated recently, and it was shown that unlike applied load, sliding speed has a minor

influence on the wear mechanism [216]. Addressing these tribological properties is essential to ensure hydrogels under various contact pressures and sliding speeds can perform similar to AC. [214].

A knee joint represents a situation of soft elastohydrodynamic lubrication (EHL). Artificial implants are examples of hard EHL. Hard EHL can be very successful in tribological situations, but only when the lubricating fluid has superior high-pressure rheology. This is not the case for synovial fluid [217]; thus, the soft EHL results in thicker lubricant films than hard EHL in vivo. To this end, a porous architecture of polymer would mimic natural cartilage in terms of EHL lubrication and yields significant performance to conventional fully dense polymers.

Table 2. 8 Effects of monomers and polymers materials on hydrogels' CoF.

Author	Ref.	Year	Materials	CoF	Findings
Gong et al.	[160]	2001	PAMPS	0.001	Polymers with dangling chains reduce CoF substantially
Covert et al.	[97]	2003	PVA-c	*Stc.:0.285 Dyn.: 0.143	Friction significantly depends on material stiffness and toughness
Yasuda et al.	[136]	2005	PAMPS	0.040	Excellent wear properties compared to UHMWPE
Lin et al.	[218]	2009	PAAm-Alg-SNPs	0.00026	The incorporation of nano-silica significantly increased the compressive strength and fracture toughness but lowered the cross-linking density and CoF
Arkaki et al.	[219]	2010	PAMPS/PDMAAm	0.029	Low CoF on normal cartilage, no significant detrimental effects on counterface cartilage
Liao et al.	[186]	2013	PAAm-Alg-caprolactone	0.150	Tough material and potential for cell-based artificial cartilage
Li et al.	[220]	2016	PVA on cartilage	0.114	The CoF significantly depends on load and speed.
Zhang et al.	[138]	2017	PAAm-AAc-METAC	<0.07	Salt leaching method was used to modulate porosity on the surface of the hydrogel, and it reduced CoF.
Arjmandi et al.	[53]	2018	PAAm-Alg	0.01	Less material was removed under higher sliding speed in their tribology tests.

Li eat al.	[221]	2020	PAAm & different crosslinking concentratio ns	0.008-0.04	In the low normal force regime, friction is mainly adhesion-controlled and increases with polymer volume fraction. In the high normal force regime, friction is predominantly load-controlled and shows a slow increase with normal force.

**Stc:Static*
**Dyn: Dynamics*
**PAMPS: Poly 2-acrylamido-2-methyl-1-propanesulfonic acid*
**PVA-c: Poly vinyl-alcohol cryogel*
**PAMPS: Poly(2-acrylamide-2-metyl-propane sulfonic acid) and polyacrylamide*
**PAMPS/PDMAAm: Poly-(2-Acrylamido-2-methylpropane sulfonic acid)/poly-(N,N'-dimetyl acrylamide)*

It is evident from the literature that the crosslinking density and volume fraction of monomers showed a significant impact on the reduction of CoF. Furthermore, some studies showed that test parameters like type of lubricant solution, the sliding mates material determinately affect the final results. Using polydimethylsiloxane PDMS and steel or alumina ball would yield similar trends in but different values in friction results on the same hydrogel composition.

2.9 STRENGTHENING HYDROGELS WITH NANOPARTICLES

2.9.1 Nanoparticles in Hydrogel Synthesizing Process

There are five approaches, shown in Fig. 2.14 [212], to utilizing nanoparticles in hydrogels networks system as follows:

1) Synthesizing hydrogels by suspending nanoparticles within the hydrogel

2) Placing nanoparticles after gel formation

3) Reactive nanoparticle formation within a preformed hydrogel

4) Applying nanoparticles as a crosslinker to the hydrogel

5) Utilizing nanoparticles, polymers, as well as gelators to form the hydrogel

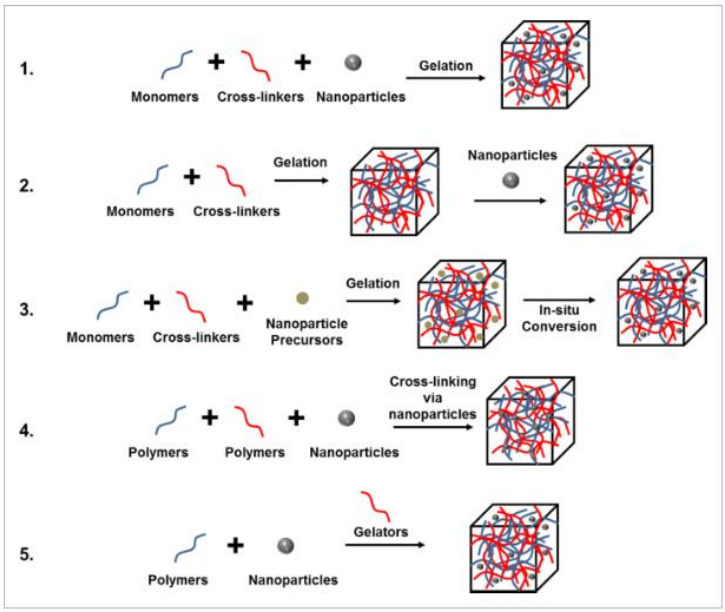

Figure 2. 14 *Five methods used for synthesizing nanoparticle-reinforced hydrogels [212].*

2.9.2 Nanoparticles Dispersion in Polymeric Hydrogels

TiO_2 nanoparticles (TiO_2 NPs), due to their low toxicity, excellent biocompatibility, low-cost, and high-level stability have been explored for the synthesis of polymeric hydrogels for medical applications [222]. However, due to the hydrophobic nature of these nanoparticles, having a homogenous solution that affects mechanical and tribological properties would be challenging. These challenges are because of TiO_2 NPs surface and electrostatic attraction among particle molecules [223]. TiO_2 NPs tend to agglomerate due to solution ionic strength (IS), pH level, surface charge, or coating [224]. Using different techniques may affect the tendency of nanoparticles to aggregation. Some researchers have reported these techniques, which are ultrasonic irradiation, stabilize TiO_2 NPs in an aqueous medium, electrostatic stabilization, controlling pH level of the solution by neutralizing acidity level, and coating the surface of nanoparticles by surfactants [225]. Moreover, overcoming the van der Waals attraction of nanoparticles by utilizing steric or electrostatic stabilization is the critical factor to suppress nanoparticle aggregation or agglomeration effectively.

Ultrasonic irradiation was an effective method to disperse NPs, which depends on the solvent type, concentration, and suspension volume. Two ultrasonic irradiation methods, bath and probe sonications, are commonly used, although probe sonication showed a better result [224]. Even using probe sonication is not the permanent solution to suppress aggregation. Stabilizers were reported to have prolonged effects on dispersed particles. As mentioned earlier, steric and electrostatic stabilization takes place when charges accumulate by the particle surfaces. More than 30 mV or less than -30 mV surface charge on the TiO_2 NPs yields no aggregation. Moreover, having higher than 1 % TiO_2 NPs concentration in the AAm-based hydrogels composition resulted in sedimented particles even if a long homogenization process was used [18].

Some monomers of hydrogel compositions have a high acidity level, for instance, AAc, which can affect NPs dispersion. The hydrodynamic size of nanoparticles can be tuned by modifying the pH level of the solution. TiO_2 and SiO_2 particles have a positive surface charge when the pH level is low, and on the opposite, negative surface charge when the pH level is high [226]. Fig. 2.15 demonstrates aggregation and agglomeration, which are essential parameters in the dispersion process.

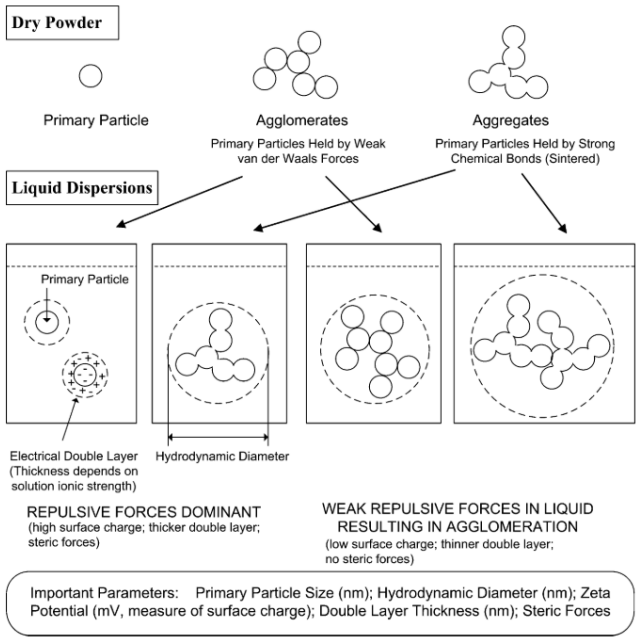

Figure 2. 15 Different modes of particles in both dry and dispersed in liquid [226]

2.9.3 TiO_2 & Silica Nanoparticles Mechanical and Tribological Properties

The recent studies focused on composite hydrogels reinforced by nanoparticles [160, 227]. Nanoparticles have the potential to strengthen hydrogels against wear or frictional motions. TiO_2 NPs reported as a promising candidate for their effective cross-linkages with monomers, which results in significant mechanical properties, promising water-stability (swelling ratio), and unique water-activated shape memory behavior [228]. Fig. 2.16 shows the bonding of TiO_2 with polymer chains in nanocomposite hydrogels (NCHs).

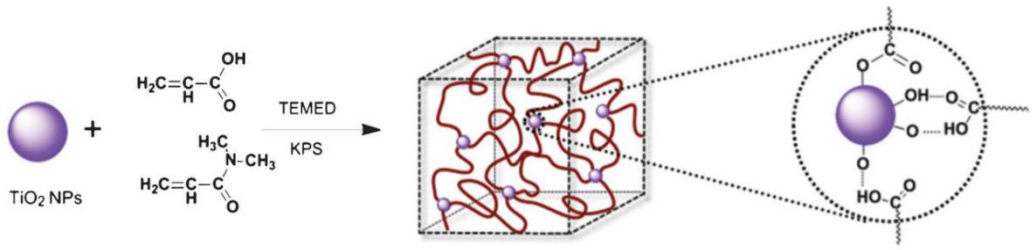

Figure 2. 16 *Formation of titanium oxide nanoparticles gels and its bonding to the polymer chains, full-line and dash line is the covalent bonds and hydrogen bonds, respectively [228].*

Conventional hydrogels made by the chemical crosslinking approach were reported to have weak mechanical properties compared to hydrogels crosslinked covalently and ionically [191]. However, NCHs reported higher strength, improved sliding wear resistance, anisotropy, and potential self-healing property compared with double-network hydrogels (DNHs), topology hydrogels (TPHs) and micromolecular microsphere hydrogels (MMHs). The swelling ratio is a crucial factor for hydrogels in biomedical applications, which supports water-stability within the hydrogel and can be achieved by utilizing titania NPs [191]. The superior mechanical strength of hydrogels is associated with the equilibrium swelling state. Seddiki et al. [152] reported that TiO_2 NPs and a high dosage of crosslinking agents (15%) are vital factors affecting swelling ratio. Besides, it has been reported that carboxyl groups formed complexes with TiO_2 NPs via different methods to crosslink polymer chains [8].

The concentration of TiO_2 NPs is a critical point in the reinforcement process since this substrate act as a crosslinker. The higher concentration of NPs, which is inversely proportional to the structure mesh size, would produce a higher degree of crosslinking [18]. Consequently, with smaller mesh-size, hydrogels would imbibe less fluid in the networks, which affects stress distribution over the structure. Due to this fact, the poroelasticity and viscoelasticity relaxation time would also be affected.

Silica nanoparticles (SNPs) have also been utilized to synthesize artificial cartilage and have demonstrated appreciable mechanical and biological properties [229, 230]. Incorporating SNPs within polymer networks improves tissue adhesion, stiffness, and shear modulus [231]. Furthermore, SNPs, interlaced with polymer chains, enhance hydrogel elasticity [25]. Zareie et al. [21] showed that by increasing SNPs amounts in the polyacrylamide networks, the number of tie points in each entanglement increased, and the compressive strength of hydrogel reached 26.2 kPa.

Besides improving mechanical strength, SNPs have promoted the degree of crosslinking in very weak chemically crosslinked PAAm hydrogels, which have interestingly presented the ability of SNPs to function as a crosslinker [25]. Arjmandi and Ramezani [22] reported that SNPs interact with PAAm chains resulting in network crosslinks through hydrogen bonds.

Unlike other NPs, SNPs showed a significant impact on initial shear modulus and viscoelastic properties since they could immobilize the polymer chains and form NPs-polymer interphases [20]. SNPs reported increasing the number of tie points in each entanglement, which results in the improvement of the compressive strength [21]. SNPs also enhance slower chain kinetics and relaxation due to tough NPs-polymer bonds [22]. Polymer bonds relax promptly when NPs are located far from chains [23]. Viscoelasticity of the SNP loaded nanocomposite hydrogels (NCHs) was studied extensively and found to be similar to that of AC [25]. AC exhibits a time-dependent response associated with viscoelasticity, poroelasticity, or the combination of both phenomena [65, 232].

Tribologically, SNPs showed the dominance of adhesion mechanisms rather than other wear mechanisms, although fatigue wear took place with surface pitting at higher applied loads [233]. Utilizing 1%-4% SNPs into the PAAm-Alg network resulted in low Cof values in the range 0.0035–0.0055, which is comparable to the CoF of AC (0.0001) [22]. It is attributed to the strong interfacial NPs-polymer bonding in the hydrogel matrix. The contact pressure and pore pressurization within interconnected channels are the key factors that control hydration levels in tribological assessments [202]. SNPs also affect mesh patterns, and therefore, are strongly correlated with the lubrication regimes [233]

2.10 SUMMARY

In this chapter, a comprehensive review of the literature for the AC was presented. First, the architecture of the AC, its compositions and the role of each component on mechanical and tribological properties were discussed extensively. It was explained that damaged cartilage cannot recover itself due to its avascular nature. Then, osteoarthritis roots and treatment methods were presented with conventional TKR/THR solutions as the ultimate treatment being highly invasive and with significant disadvantages, especially for younger patients, and the need for revision surgery due to the limited service life of TKR/THR implants were discussed. To address the gap in the treatment of younger patients with OA, developments of artificial cartilage by different synthesizing processes, materials and their pros and cons were described. The required standard and necessary tests for artificial cartilage to assess its mechanical and tribological properties are based on the International Cartilage Repair Society (ICRS), Food and Drug Administration (FDA), and American Society for Testing and Materials (ASTM) were briefly reviewed. Viscoelastic properties were found as the critical point in the design of engineered soft tissues and the techniques to tune viscoelasticity to perform optimum responses under different loading scenarios were reviewed. Parameters and conditions that result in poroelastic and viscoelastic relaxation were introduced.

Advanced bilayer hydrogels were discussed as promising candidates for artificial cartilage. Both the load-bearing and lubricious layer were investigated recently; however, the weak point of the proposed lubricious layer was found to be its limited strength and service life under cyclic sliding tests. NPs, on the other hand, are utilized in hydrogel systems to reinforce the mechanical and tribological properties that were mentioned in the recent findings.

According to the literature survey, some of the research gaps are highlighted as follows:

- Tribological assessment of bilayer NCHs reinforced by TiO_2 NPs and SNPs remained mostly intact.
- The effects of NPs on strengthening mechanical and tribological properties of the lubricious layer have not been discussed yet.
- Assessment of the viscoelastic or poroelastic relaxation in NCHs according to network topography was not addressed sufficiently, which is critical in the design stage of bilayer hydrogels.

In this research, we aimed to address the mentioned gaps, and the questions associated with the research include:

- What are the optimum parameters in NCHs that maintain both mechanical and tribological properties at the same time and respond analogously to native cartilage?
- To what extent NPs affect the reinforcements of the lubricious and bulk layers and what is their contribution in reducing friction and wear?
- What are the dominant wear mechanisms and lubrication regimes, and how would they be mapped when NPs are used in hydrogels?

CHAPTER 3

MATERIALS AND METHODS

3.1 DEVELOPMENT OF BILAYER HYDROGEL IMPLANT MATERIAL

3.1.1 Conceptualization of the Structure

The proposed implant concept is based on the native cartilage structure with gradual stiffening through the thickness and full interpenetrating (full-IPN) bilayer hydrogel, which is strengthened by TiO_2 and Silica NPs separately. The implant was conceptualized as a plug roughly 3-4 mm in thickness. The lubricious or porous layer is formed by using the concept of the branched dangling polymer chain. Hydrophobicity of the mold or substrate initiates heterogenous formation during the polymerization process. Such heterogeneity is a phenomenon that causes gradient network density. This phenomenon affects the crosslinking process near the hydrophobic surface with excessive hydrogens that interrupts the polymerization process; therefore, the polymer chains are not completed in their propagation steps, resulting in a porous layer side of the implant plug. Bulk area, however, by a certain distance from the hydrophobic surface polymerization process is complete, and polymer chains propagate through the networks. Consequently, a very dense structure is formed by which the compressive strength of the bulk area is more than the porous layer [160]. The bilayer hydrogels, which include porous and bulk zones, result in two advantages: the first is the ideal structure for interstitial fluid retention that minimizes friction and wearing off the implant surface due to its hydrated networks and exhibiting similar to boundary lubrication of the superficial zone in cartilage. Second, the bulk layer, which is very dense, mimicking the deep

zone of the cartilage, therefore withstands against applied load. The components of the bilayer hydrogel are illustrated in Fig. 3.1.

To reinforce both the lubricious and bulk layers and improve the mechanical and tribological properties of the implant against wear or shear forces, TiO_2 and SiO_2 NPs were utilized. TiO_2 NPs increase the stretchability for shear forces and deformability. Incorporating SNPs within polymer networks improves tissue adhesion, stiffness, and shear modulus [231]. Hydrogel implant was synthesized by the free radical polymerization method to achieve a chemically (covalent) high-density crosslinked network along with the ionic or physical crosslinked networks to advance it with self-healing and energy-dissipation features.

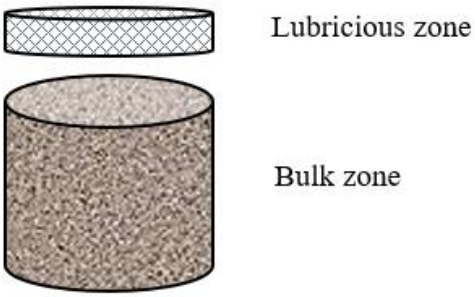

Figure 3. 1 Schematic of the bilayer hydrogel including bulk and lubricous layers.

The proposed implant supports both required mechanical and tribological properties close to the native cartilage properties, and minimally invasive surgery compared to total joint replacement is a big advantage, especially for younger more active patients with OA.

3.1.2 Materials

Monomers used in this study include Acrylamide (AAm), acrylic acid (AAc), N, N′-methylenebis acrylamide (MBAA), 2-(Methacryloyloxy)ethyl]trimethylammonium chloride solution (METAC), alginic acid sodium salt from brown algae (Alg), TiO_2 NPs, SiO_2 NPs (SNPs), ammonium persulfate (APS), N,N,N′,N′ tetramethyl ethylenediamine (TEMED), and calcium chloride ($CaCl_2$) were all purchased from Sigma-Aldrich (Sigma-Aldrich, St. Louis, MO). Silica-

NP powder (99 % purity, 20 nm NP size, hydrophilic) and TiO_2-NP powder (100 % purity, 21 nm NP size, hydrophobic), was purchased from Sigma-Alderich (Sigma-Alderich, Auckland, New Zealand)

3.1.3 Nanocomposite Bilayer Hydrogel Synthesizing Process

Many parameters must be controlled in order to manufacture high-quality hydrogels. In this section, some of the critical bottlenecks will be disclosed**.** Free radical modulated polymerization method at ambient temperature was used to synthesis PAAm-PAAc-Alg-METAC IPNs. First, AAm (26.6 w/v%) as the base material was decanted in 10 ml deionized water (DI water). After attaining a homogenous solution, AAc (12.6 w/v%) was added, followed by METAC (0.18% w/v%). Alg was stirred by 50^{o}C temperature on a hotplate stirrer separately and then added to the AAm-AAc-METAC solution. Then crosslinker MBAA (0.19 w/w %) was added gently, and the stirring process was continued until all MBAA particles were dissolved in the solution homogenously. Ultrasonic homogenizer sonicator, cell disruptor mixer 450 W, 10-300ml was used with 3mm tip to disperse the NPs in DI water in 25 minutes by the set power of 225 W (50% of the total power) and then added to the prepared solution. 5 mm gap was considered between the tip and the bottom surface of the baker to maximize the power of sonication on the dispersion process and prevent splashing the solution out. Fig. 3.2 shows the sonication process.

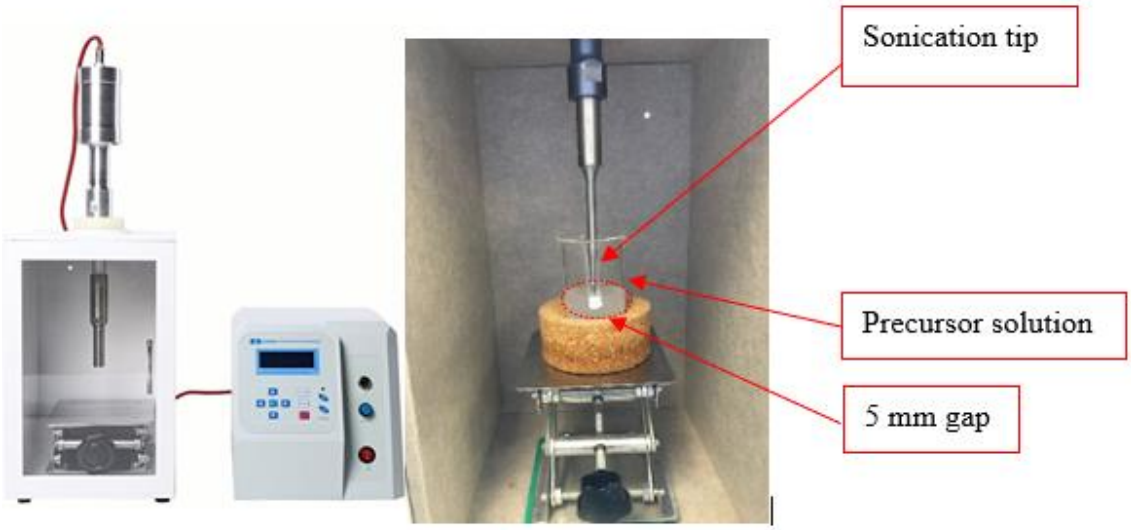

Figure 3. 2 Ultrasonic homogenizer sonicator and dispersion process by using probe sonication machine

By achieving a homogenous solution after adding dispersed particles to AAm-AAc-Alg-METAC solution, APS as an initiator was added and stirred for 10 minutes. Then, the solution was degassed by nitrogen dioxide to remove oxygen as a free radical sweeper, which interrupts acrylamide polymerization [53]. Free radical is a crucial factor in polymerizing hydrogels. Therefore, a factor that affects as a sweeper of free radical is oxygen and must be removed during the synthesizing of the hydrogel by degassing process [53]. A typical degassing process is using nitrogen gas [187]. Some of the experimental studies utilized argon gas for degassing process [151]. Degassing should be processed preferably before adding the catalyst to remove oxygens [234]; however, Tsioptsias et al. [235] mentioned that degassing can be conducted by sonication, whenever required. The presence of bubbles is a potential risk in crack initiation and propagation under mechanical loadings and tests that must be removed from the solution. It is worth mentioning that, depending on the precursor solution's viscosity, introducing high-pressure nitrogen gas into the solution results in trapping bubbles. Therefore, nitrogen gas pressure and time of degassing are the two critical factors in free radical polymerization. Fig. 3.3 shows solutions/ hydrogels with and without bubbles.

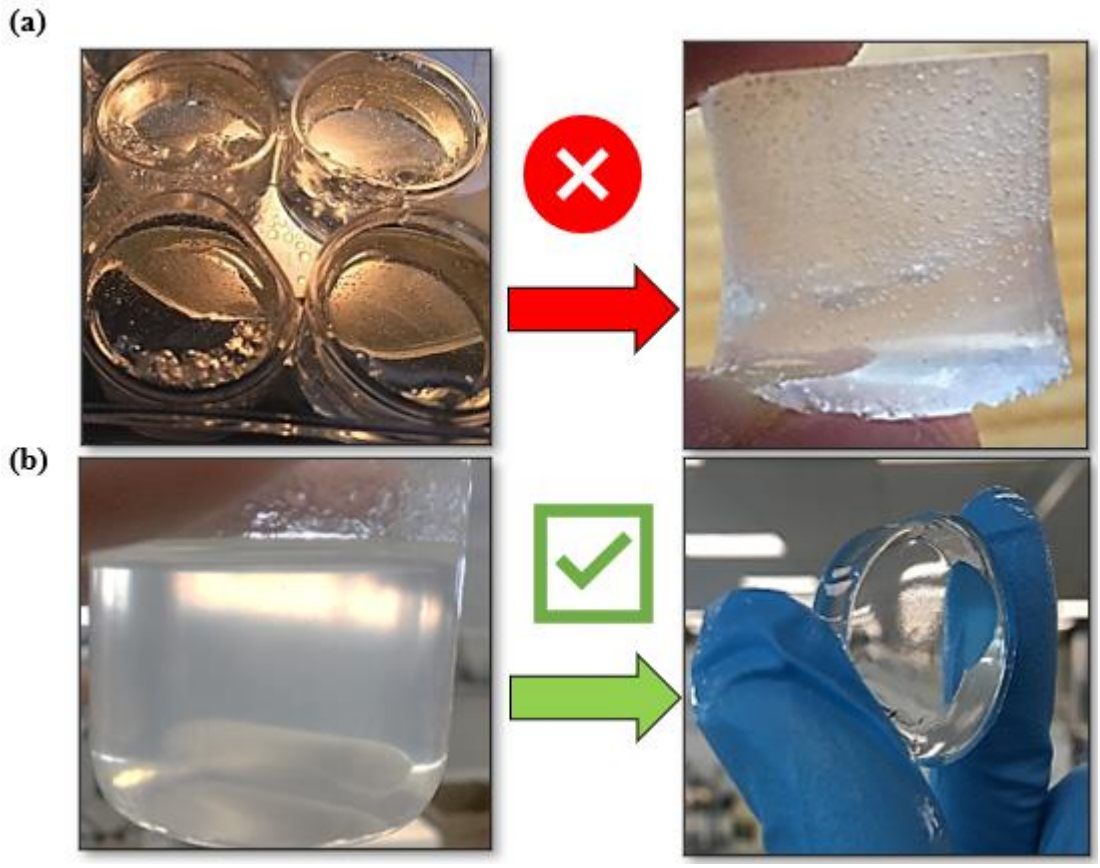

Figure 3. 3 Solutions and hydrogels with (a) bubbles (b) bubble-free

Polystyrene petri dishes purchased from Interlab Ltd were used to cure the solution at the incubator room for 24 h and 35^{o}C constant temperature. Cured hydrogels were then immersed in 16.0 w/v% $CaCl_2$ solution for 24 h to form the ionic crosslinks as the second network.

A range of different loadings (0.05wt%, 0.2wt%, 0.4wt%, 0.6wt%) was used to prepare the samples to study the effect of NPs on the mechanical and tribological properties of hydrogels. All four concentrations in nanocomposite hydrogels (NCHs) were tested, and results were compared with non-reinforced hydrogel (NRHs), which is hydrogel without NPs. It is worth mentioning that many attempts were made to add more than 0.6wt% SNPs, but the cured hydrogels were very brittle; therefore, SNPs concentration could not exceed 0.6wt% for this NCH. Also, over 0.6 wt% TiO_2 NPs resulted in sedimentation in the solution before the curing process. Using more than 1 wt% TiO_2 NPs resulted in excessive heat generation during the curing process and caused melting

of the mold. Further to the generated heat, propagation and termination steps in the polymerization process were affected and led to foamy hydrogels, as shown in Fig. 3.4.

Figure 3. 4 Generated heat in the polymerization process due to utilizing more than 1 wt% TiO_2 NPs

After several attempts with different monomers amounts in the solution, crosslinkers, and NPs, the optimum formula was found, as mentioned in this section. It is worth mentioning that our NPs were utilized in the polymerization process without any modifications or surfactants that were discussed in the literature, which is cost-effective in the manufacturing process of reinforced bilayer hydrogels. In addition, AAc with a very acidic level (2.0 pH level) was another bottleneck of the manufacturing process in the sense that after adding dispersed TiO_2 NPs all particles aggregated or agglomerated. Many attempts were made to neutralize acid up to different levels (6.0-6.30 pH), and we found even after neutralizing with NaOH reported by Masiak et al. [236], hydrogels were cured in less than 2 minutes, which should not occur in the free radical polymerization process according to the literature. Kango et al. [237] were able to penetrate the accumulated nanoparticles and activate them to form the chains and separate the nanoparticles or disperse them homogenously. Since monomers have low molecular weight compared to TiO_2 NPs, (AAc MW:72.06 g/mol, AAm MW:71.08 g/mol, TiO_2 NPs MW:79.87g/mol), NPs would sediment after mixing with the monomers. Sodium Alginate has a high molecular weight of 216.121 g/mol, which helps disperse NPs inside the solution and prevent sedimentation. Finally, to this end, the

neutralizing process was eliminated, and many more try and error attempts were performed on adjusting the viscosity of the hydrogel by alginate amounts and attain homogenously dispersed particles. Finally, the standard process of synthesizing bilayer nanocomposite hydrogel, and its networks strengthened with NPs with a lubricious layer on top and bulk layer at the bottom was established as is shown in Fig. 3.5.

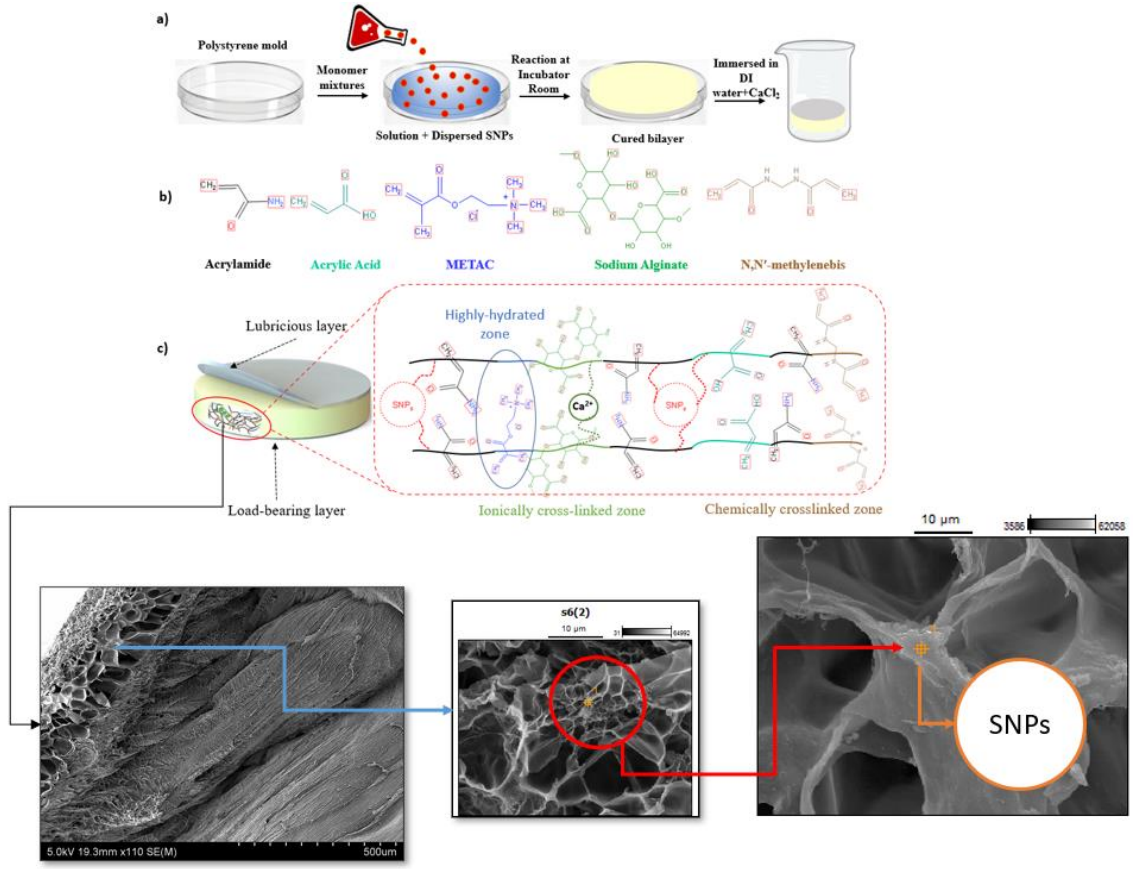

Figure 3. 5 Bilayer hydrogel (a) synthesizing process, (b) Utilized materials, (c) final networks and implant.

Once the solutions were cured at the incubator room with a constant and controlled temperature (35^{o}C) for 24 h, hydrogels were removed from the mold gently. Hydrogels, then immersed in a 16.0 wt% $CaCl_2$ solution in 100 ml DI water for 24 h to form the physical or ionic crosslink network. Then, samples in $CaCl_2$ solution were washed off several times with DI water and decanted in a clean beaker filled with fresh DI water for a few days to wash away all non-reacted monomers and carbons from the surface. Every day, water was changed with fresh DI water with

a controlled resistivity meter (>12-16 MΩ-megohm). Next, samples were placed in the incubator room to dry them thoroughly and prevent thriving algae on the surface before mechanical or tribological tests. Samples were immersed in DI water 72 h prior to each test to get fully hydrate and be ready for mechanical or tribological tests.

3.2 EXPERIMENTAL PROCEDURE

3.2.1 Indentation Tests

The localized properties of each specimen, such as elastic modulus and hardness, were determined by indentation tests. ASTM E2546 Standard [238] was used to calculate the elastic modulus and hardness of hydrogels. TA XT Plus texture analyzer (Stable Micro Systems, Godalming, UK) with an attached 50N load-cell was used with a spherical indenter and 1.2 mm indentation depth. A cross-head rate of 1.2 mm/min was set up to record the force with respect to indentation depth. All required parameters to calculate the elastic modulus and hardness from the unloading part of the force-displacement data are illustrated in Fig. 3.6.

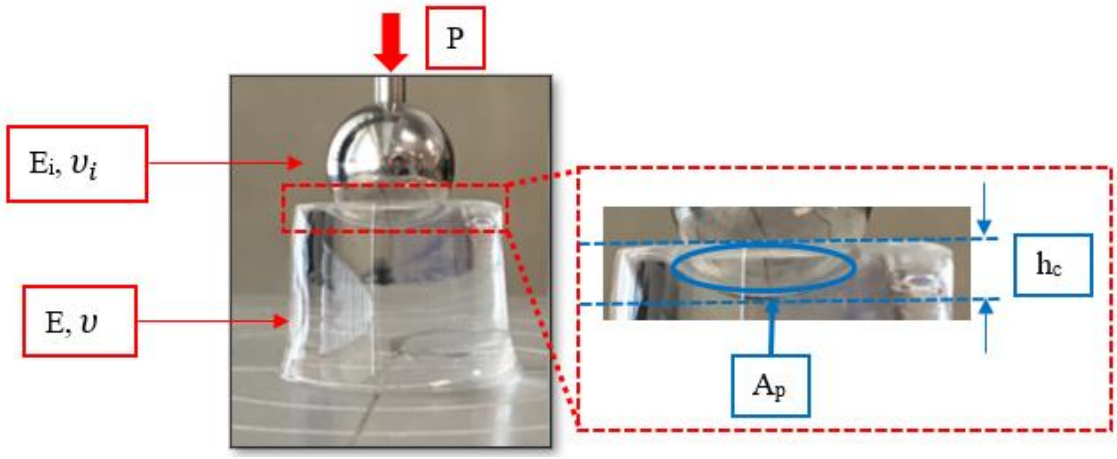

Figure 3. 6 Indentation tests parameters to evaluate elastic modulus and hardness.

The unloading part of the load-displacement data was used to calculate the elastic modulus and hardness by the following equations:

$$E_r = (\frac{S}{2})\sqrt{\frac{\pi}{A_p}} \tag{3.1}$$

where S is the contact stiffness, obtained by 50% slope of unloading curve and A_P, the projected contact area can be obtained from Eq. (3.2) specified for the spherical indenter. Here, R is the radius of the indenter, and h_c is the contact depth that can be determined by Eq. (3.3):

$$A_P = 2\pi R h_c \tag{3.2}$$

$$h_c = h_{max} - \frac{3P_{max}}{4S} \tag{3.3}$$

where h_{max} is the indentation depth, and P_{max} is the peak force at h_{max}. Furthermore, the elastic modulus, E, and hardness, H, can be attained by equations (3.4) and (3.5), respectively:

$$\frac{1}{E_r} = \left(\frac{1-\upsilon^2}{E}\right) + \left(\frac{1-{\upsilon_i}^2}{E_i}\right) \tag{3.4}$$

$$H = \frac{P_{max}}{A_p} \tag{3.5}$$

where υ_i and E_i are Poisson's ratio and elastic modulus of the indenter, respectively, while υ and E are the Poisson's ratio and elastic modulus of the hydrogel specimen. υ =0.5 was assumed in the calculations since hydrogels retain abundant water and can be considered as an incompressible fluid [239, 240].

3.2.2 Unconfined Compression Test

Compression tests were carried out using The same mentioned instrument with a 50N load-cell and cylindrical indenter that compresses samples at different strain rates (0.01 s^{-1}, 0.1 s^{-1}, and 1 s^{-1}), to mimic the range of the strain rates experienced by the articular cartilage [63]. Pre-load of

0.1 N was applied before the initiation of each test in order to have consistent results. Sample responses were recorded as a load-displacement graph, and then engineering stress-strain data were obtained by using Eq. (3.6).

$$\sigma = A + Be^{(C\varepsilon)} + D^{(E\varepsilon)} \tag{3.6}$$

where σ is compressive stress, ε is the strain, and coefficients A-E are curve fitting constants. A differential equation code was developed using Matlab software (Mathworks, USA) to calculate the first-order differential equation of two-terms exponential growth, five parameters of compressive stress, then to attain data for tangent modulus, which is the slope of compressive data at five different strain points.

3.2.3 Viscoelastic Characterization

As the hydrogels are categorized as polymeric materials, they would perform a time-dependent mechanical response, assessed by a stress relaxation test. Samples were compressed to 50% strain by the mentioned testing instrument in the indentation section, then the load was held constant for 1h, and the previously mentioned instrument recorded the reaction force vs. time. The recorded force will then be converted into engineering stress at time t. Stress-time data were curve fitted using Eq. (3.7), adapting previously reported works on the viscoelasticity of hydrogels [241, 242].

$$\sigma(t) = \sigma_f + ae^{(-bt)} + ce^{(-dt)} \tag{3. 7}$$

where σ_f is the maximum stress value (within t=3600s), and coefficients a-d are material constants obtained by curve fitting.

3.2.4 Friction and Wear Characterization

Tribological tests were conducted using the Rtec tribometer (Rtec-instruments, San Jose, CA, USA). The test setup for each specimen is demonstrated in Fig. 3.7. Tribological measurements

were performed with a ball-on-plate configuration in a linear reciprocating motion. The samples were sliding against a 4mm diameter sliding that is a common counterface to assess orthopedics materials [79, 187, 243]. A 10 N load cell was attached to the tribometer and a range of different frequencies were used in the sliding wear tests to meet the walking, jogging and running speeds as is experienced by the articular cartilage. Fig. 3.7 shows tribology test setup and components in detail.

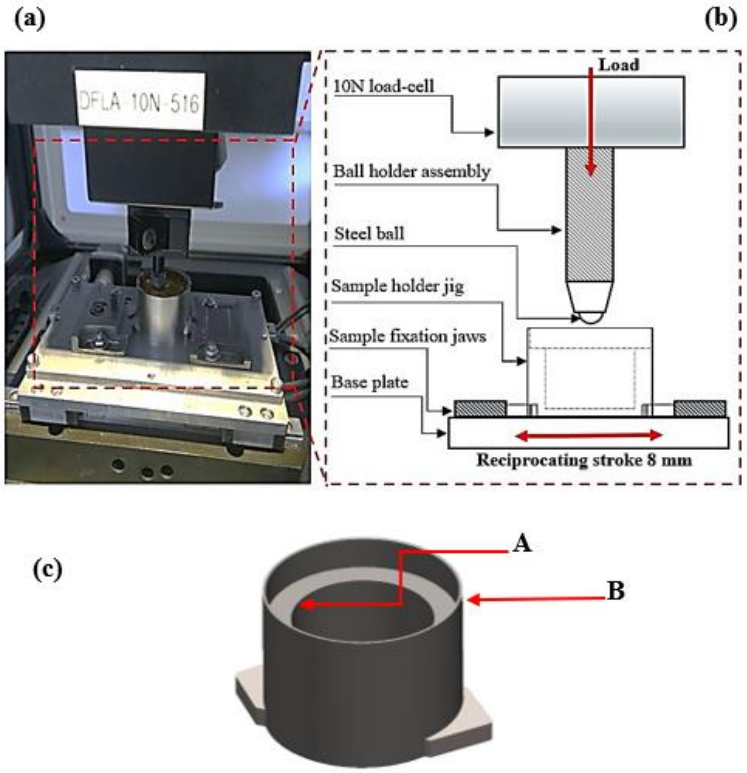

Figure 3. 7 (a) Experimental setup of wear and coefficient of friction testing instrument (b) schematic illustration of hydrogel specimen sliding against a steel (c) design of the hydrogel holder, point A is the edge that sample swells up to that and depth A-B was embedded for lubricating fluid.

All tests were conducted at room temperature on the samples in their equilibrium state. The equilibrium state was achieved by placing dried hydrogels in the hydrogel holder was shown in Fig. 3.7 (c) for three days before each test. Samples swelled in the holder up to the edge of point A. The lubricant was filled up to the edge of point B. Tests were conducted with and without lubricants and controlled by regular intervals to have consistent results. All tests were conducted

with the same steel ball, and a reciprocating-based plate with 8 mm stroke was set with various sliding speeds and loads to mimic the native cartilage physiological activities conditions according to the following table. Fresh bovine serum (contains on average 65 g/ml albumin protein) for lubricated tests was obtained from Auckland Biosciences Ltd. (Auckland, New Zealand).

Table 3. 1 Summary of the parameters of the tribological test to assess wear and coefficient of friction.

Experimental setup	Test variables		Test conditions
Set 1	0.5 N	Constant speed [80 mm/s]	Lubricated **&** Dry
	0.7 N		
	0.9 N		
Set 2	50 mm/s [f=3.125 Hz]	Constant load [0.7 N]	
	80 mm/s [f=5 Hz]		
	110 mm/s [f=6.875 Hz]		

To evaluate the tribological performance of the proposed hydrogel, an experimental study was designed according to Table 3.1. Set 1 were set up to cover ranges of loads (0.5N, 0.7N, 0.9N) with an average speed (80mm/s) by both dry and lubricated conditions and Set 2 to cover ranges of speeds (50mm/s, 80mm/s, 110mm/s) with an average load (0.7N) by both dry and lubricated conditions. In total, 60 tribology tests (3 replications for each) were conducted to compare the results. The ranges of loads were determined according to the ranges of contact pressure experienced by articular cartilage (0.1-2.0 MPa) [97, 178, 220]. The corresponding contact pressures for each applied load were determined by using pressure-sensitive films (Fujifilm Prescale LLLW & LLW ranges) inserted between steel ball and hydrogels specimens prior to a quasi-static loading. The pressure-sensitive film is a Mylar-based sensor film that reveals the distribution and magnitude of pressure between any two matings by crushing microbubbles and reading scales associated with the relevant pressure. It was observed the load range of 0.5-0.9 N correlated to the contact pressure of 0.210-4.50 MPa for NRHs and 0.335-4.85 MPa for NCHs, which is much higher than the ranges of cartilage contact pressure. Sliding speed, on the other hand, is selected in the range of cartilage sliding rate under walking, jogging, and running activities

[97]. Based on the 8 mm stroke length incorporated with the relevant frequencies that were set to mimic physiological activities, 151.515, 208.33 and 333.33 minutes were associated with 1000 meters of total sliding distance for all experiments. The surface roughness of each sample was analyzed by a 20X confocal objective of the optical profilometer module of the Rtec tribometer.

3.2.5 Assessment of Wear Profile

Upon completing the tribological tests, wear profiles were plotted and measured using Taylor Hobson 50 stylus profiler (Taylor Hobson, AMETEK, PA, USA). A diamond tip stylus was used to record the depth and width of the wear scars as is illustrated in Fig. 3.8. Three points were selected on the wear track for depth and width measurements to attain the average cross-sectional area by curve fitting the wear profiles. The plotted curve was then imported to Java-based image processing software (Image J software, National Institute of Health, USA) to measure the wear profile surface area. Wear volume was then calculated by multiplying the average surface areas by the sliding stroke (8mm).

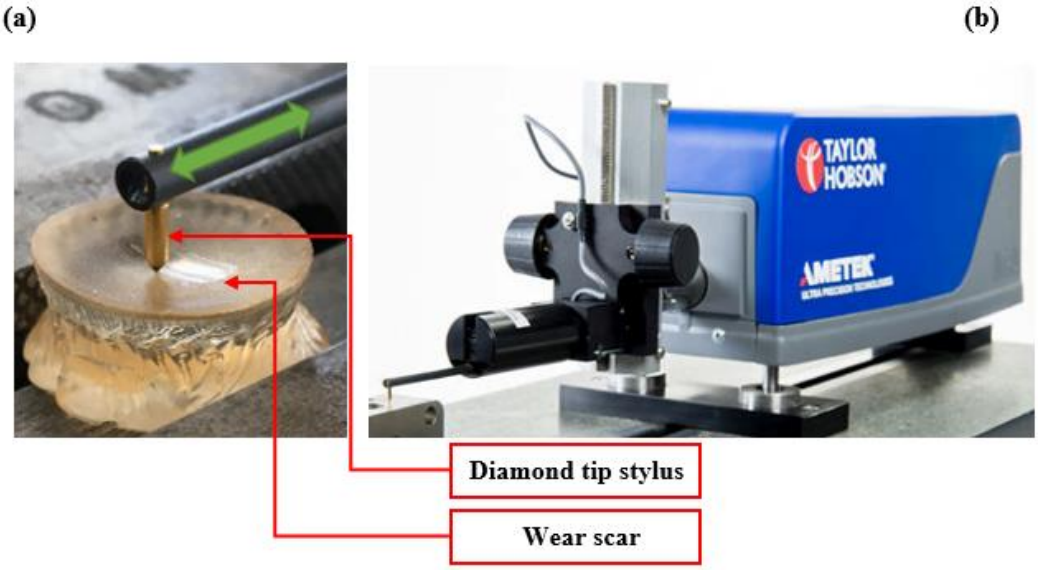

Figure 3. 8 (a) Diamond tip stylus and hydrogel with wear scare (b) Taylor Hobson stylus profilometer.

3.2.6 SEM and EDS Characterization

To obtain SEM images, samples were kept in an incubator room at a constant temperature of 35 ^{o}C for 240 h to get dried completely. Then, samples were shrunk in size using sandpaper attached to a rotary disk. It is worth mentioning that only non-treated sides of the samples were cut, and the treated surface remained intact to avoid any damage to wear scar. A vacuuming tube was held near the cutting region to ensure dust was sucked away thoroughly. Then samples were placed in a thin-layer plastic tube covered with a cap and immersed in liquid nitrogen for 10 minutes to freeze the structure slowly. Next, samples were lyophilized at 10 µBar for 72 h. Afterwards, samples were sputtered with Platinium powder using a sputter coating machine (Hitachi E-1045, Japan) at 25 mA for 100 seconds as shown in Fig. 3.9 (a). Finally, samples were mounted on a metallic jig shown in Fig. 3.9 (b) and loaded to the SEM machine (Hitachi SU-70, Japan) at an accelerating voltage of 5.0 kV to capture bilayer cross-sections as shown in Fig. 3.9 (c). The Energy-dispersive X-ray Spectroscopy (EDS) module of SEM was used to characterize chemical elements making up the networks. NPs amounts and distribution were also monitored under this module. For the EDS process, an accelerating voltage of 15.0 kV was set and magnified up to 4K to characterize the chemical elements in the networks.

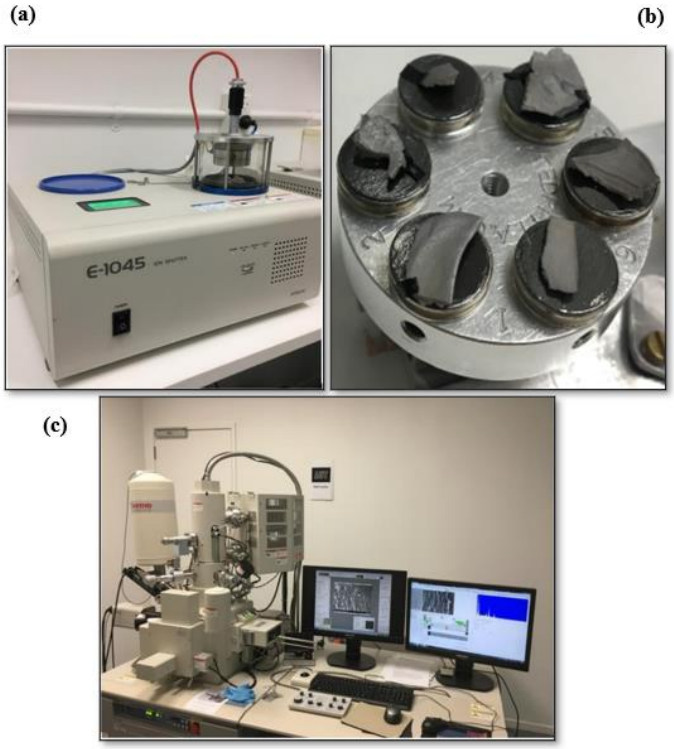

Figure 3. 9 (a) Hitachi SU_70 SEM, (b) Hitachi, E-1045 ion-sputter coater, (c) metallic jig to mount samples

3.3 STATISTICAL ANALYSIS

The samples were analyzed in triplicates and results were presented as mean ± standard deviations. Statistical analysis were performed using two-way ANOVA with post-hoc Tukey test to determine the statistical significance of NRH and NCH sample comparisons with 95% confidence level. One-way ANOVA, with post-hoc Tukey test, was further applied to the experimental data of individual samples..

CHAPTER 4

MECHANICAL AND MICROSCOPICAL CHARACTERIZATION OF BILAYER HYDROGELS STRENGTHENED BY TiO_2 NANOPARTICLES

4.1 INDENTATION AND MATERIAL PROPERTIES

The force versus indentation depth for all TiO_2 concentrations is plotted in Fig. 4.1 (a). By adding TiO_2 NPs, elastic modulus and hardness were increased significantly for all NCHs, except for 0.05 wt% NPs concentration that showed minor improvement compared to NRHs. The elastic modulus and hardness of 0.2 wt% NCHs increased by 286 % and 300 %, respectively, compared to NRHs that is shown in Fig. 4.1 (b). However, by increasing NPs composition, the improvement of elastic modulus of 0.4 wt% and 0.6 wt% NCHs were levelled down by 14.2 % and 12.5 %, respectively, compared to 0.2 wt% NPs.

(a)

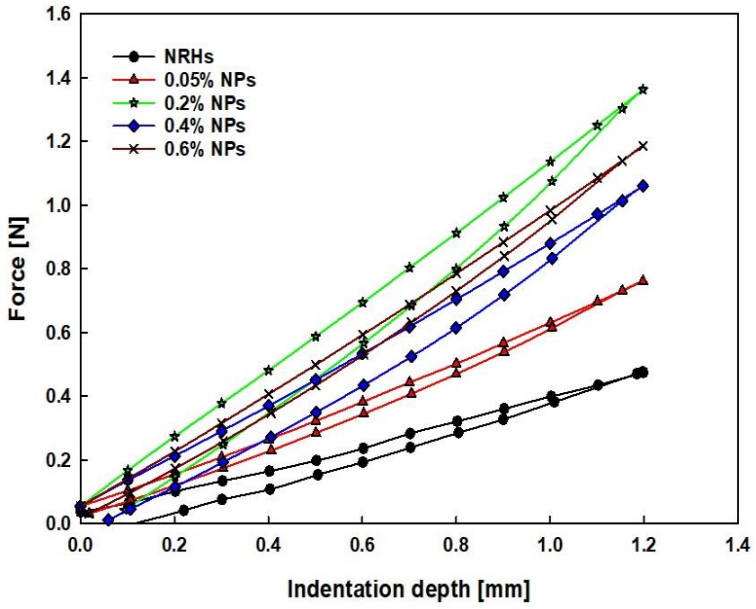

(b)

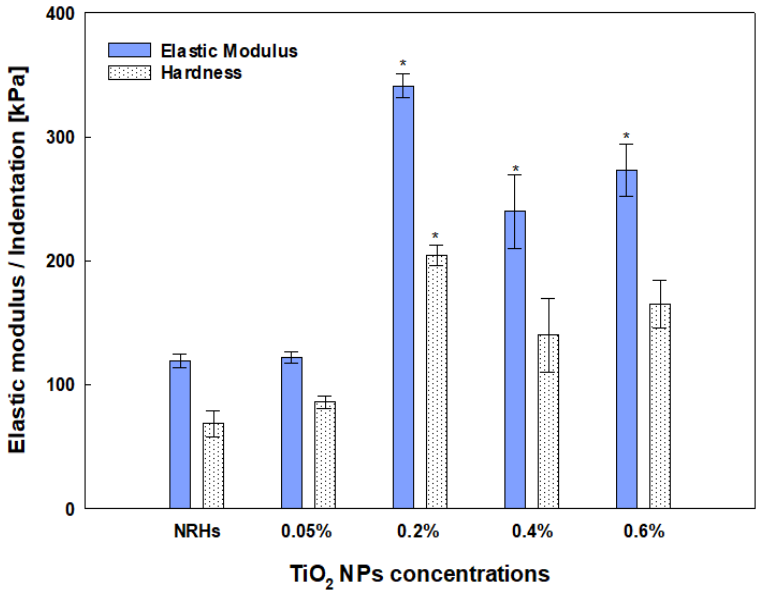

*Figure 4. 1 The indentation responses of hydrogel samples strengthened with TiO_2 NPs and NRHs (Mean (n=3) ± SD), $p<0.05$ for all NCHs (a), and (b) the elastic modulus and hardness of hydrogels, * represents p-value and statistically difference ($p<0.05$).*

Introducing nanoparticles to the hydrogel networks minimizes the porosity as NPs integrate into the network chains and consequently enhance the elastic modulus and hardness. However, more concentrations of NPs in the network tighten up the chains, and this phenomenon yields an

increase in stiffness and brittleness of the material [18]. This could be the result of interlocking more chains by NPs and a lower degree of freedom within chains. It is worth mentioning that many attempts were made to add NPs with more than 0.6wt%, but particles sedimented in the solution even with more sonication power and time. This phenomenon has also been reported by Toledo et al., who have highlighted that using higher concentrations of TiO_2 NPs (>1wt%) resulted in sedimentation in their solution [18]. Crosslinking density has a significant contribution to elastic modulus and hardness. Arjmandi et al.'s study showed that doubling crosslinking agent concentration improved the elastic modulus and hardness of Alg/PAAm hydrogel by up to 21% and 32%, respectively [53]. TiO_2 NPs react with polymer chains as a crosslinker [191] and therefore, increase the material properties. However, an additional amount of crosslinker would decrease the fracture toughness of the chains.

Distribution of the load between two networks, which are entangled together, is the benefit of double network hydrogels in the design of tough hydrogels. Elastic modulus, hardness, compressive strength, and viscoelastic responses improved by using TiO_2 NPs [48, 191]. The incorporation of TiO_2 NPs supports the crosslinking process as a crosslinker and binds with polymer chains [227]. Fig. 4.1 (a) shows that 0.2wt% NPs loading enhanced the toughness of the material. It can also be observed from Fig. 4.1 (b) that the elastic modulus and hardness of the 0.2wt% NPs loaded hydrogel were the utmost compared to other NCHs and NRHs. From the experiments and literature, accretion of crosslinking density yields higher rigidity and strength. Also, by increasing NPs concentration up to 0.2wt% NPs, polymer chains binding develops in its optimum state by using the mentioned monomers and polymerization formula in the method section. However, introducing more NPs concentrations shortens the polymer chains and decreases the degree of freedom of chains which would result in less elasticity [152]. The secondary network has also been reported as the key parameter of material brittleness or ductileness [167]. As the second network concentration in this study remained constant for all samples, just TiO_2 NPs concentration was modified in the first network; therefore, the required conditions for a tough network would be satisfied. The first requirement of tough hydrogels

reported to have short first network strands and long second network strands $N_2>>N_1$ and the second condition reported to have low first network concentration and high second network concentration $c_2>>c_1$, which is satisfied for all samples, as the second network concentration was 16.0wt%. Therefore, from Fig. 4.1(b), from 0.05wt% to 0.2wt% NCHs is the transition to ductile material, and from 0.2wt% to 0.6wt% is the transition of the ductile to brittle gradually. As Klein et al. [46] reported, the low density of polymer chains causes low elastic modulus and corresponds to the large polymer molar mass, and based on this fact, samples with 0.2wt% NPs demonstrated the uppermost density of polymer chains. These study results are tally with modified and unmodified TiO_2 NPs used in Toledo et al. [18] study, where, by loading more than a certain amount of NPs, their hydrogels modulus decreased similar to our findings.

4.2 COMPRESSIVE RESPONSE WITH RESPECT TO STRAIN RATE

Hydrogels crosslinked by ferric iron and $CaCl_2$ separately to form the second network. Although ferric iron covered the whole sample and the lubricious layer was covered by a thick-coated layer, after the compression test, the samples crosslinked by ferric iron were severely deformed and the inner structure crushed. In contrast, the samples crosslinked by $CaCl_2$ maintained their properties and returned to its original shape after 95 % strain. Figures for the compressive tests of both ferric iron and $CaCl_2$ can be found in the supplementary information document.

Fig. 4.2 shows the stress-strain responses of NCHs and NRHs. The compression tests were conducted under $0.01s^{-1}$ strain rate and all samples were compressed to 85 % of their initial thickness. All samples except NRHs did not fail by 85 % compressive strain, which is showing improvement of polymer bonds by adding NPs. NRHs samples failed at nearly 75 % strain. The highest compressive strength was obtained by reinforcing hydrogel with 0.2 wt% and 0.6 wt% concentrations of NPs. By the low rate of strain, hydrogels are imposed to stress distribution in a long time (~40 min) and therefore, consolidation type of deformation, which is stiffness dependent, would take place similar to the native cartilage [63].

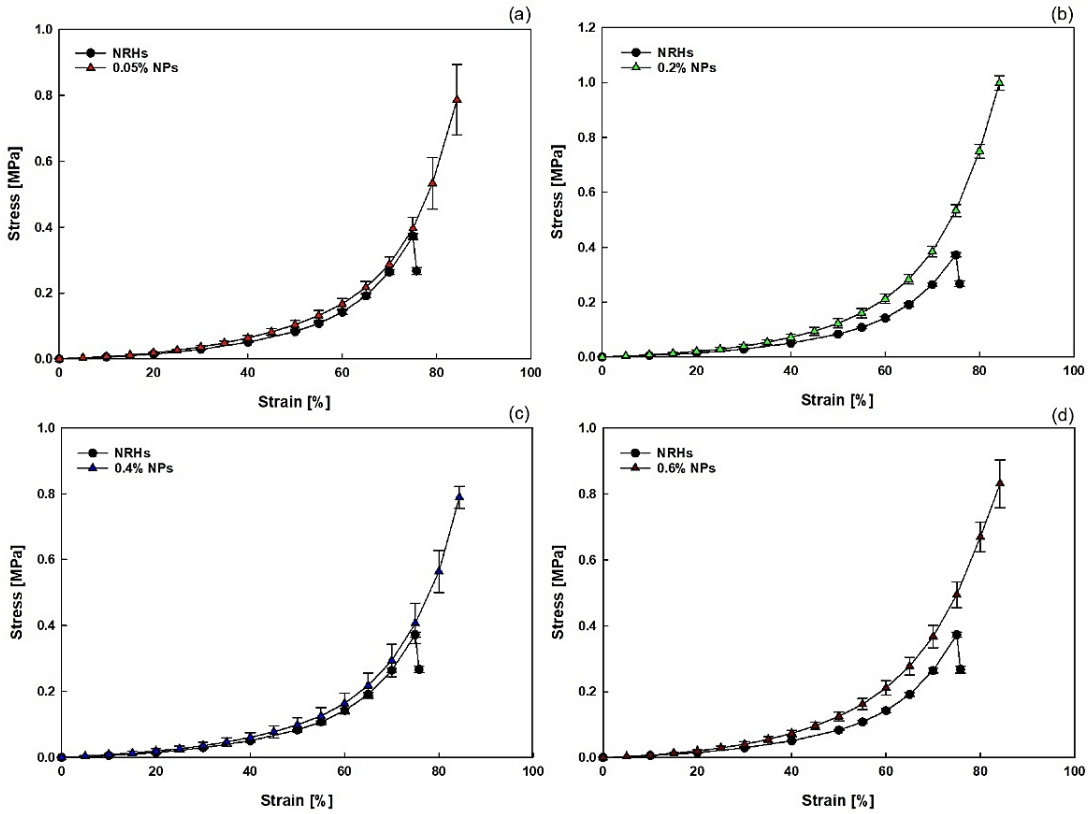

Figure 4. 2 Compressive stress-strain responses under 0.01 s−1 strain rate (Mean (n = 3) ± SD) for NRHs with: (a) 0.05 wt% NPs, (b) 0.2 wt% NPs, (c) 0.4 wt% NPs and (d) 0.6 wt% NPs.

Fig. 4.3 shows compressive stress with respect to strain up to 85 % by the strain rate of $0.1s^{-1}$. Hydrogels are incompressible structures with their compressive stress responses highly dependent on strain rates. Both NCHs and NRHs at higher strain rates reached 85 % compressive strain. 0.2 wt% NCHs demonstrated the highest compressive strength reaching 1.2 MPa at 85 % strain, superior to NRHs with 0.5 MPa. By this strain rate, no damage, crack, or rupture occurred for all. Samples with 0.4 wt% NPs are the second-highest regarding the stiffness with nearly 1.1 MPa. By increasing the amount of NPs to 0.6 wt%, the strength of the networks depreciated.

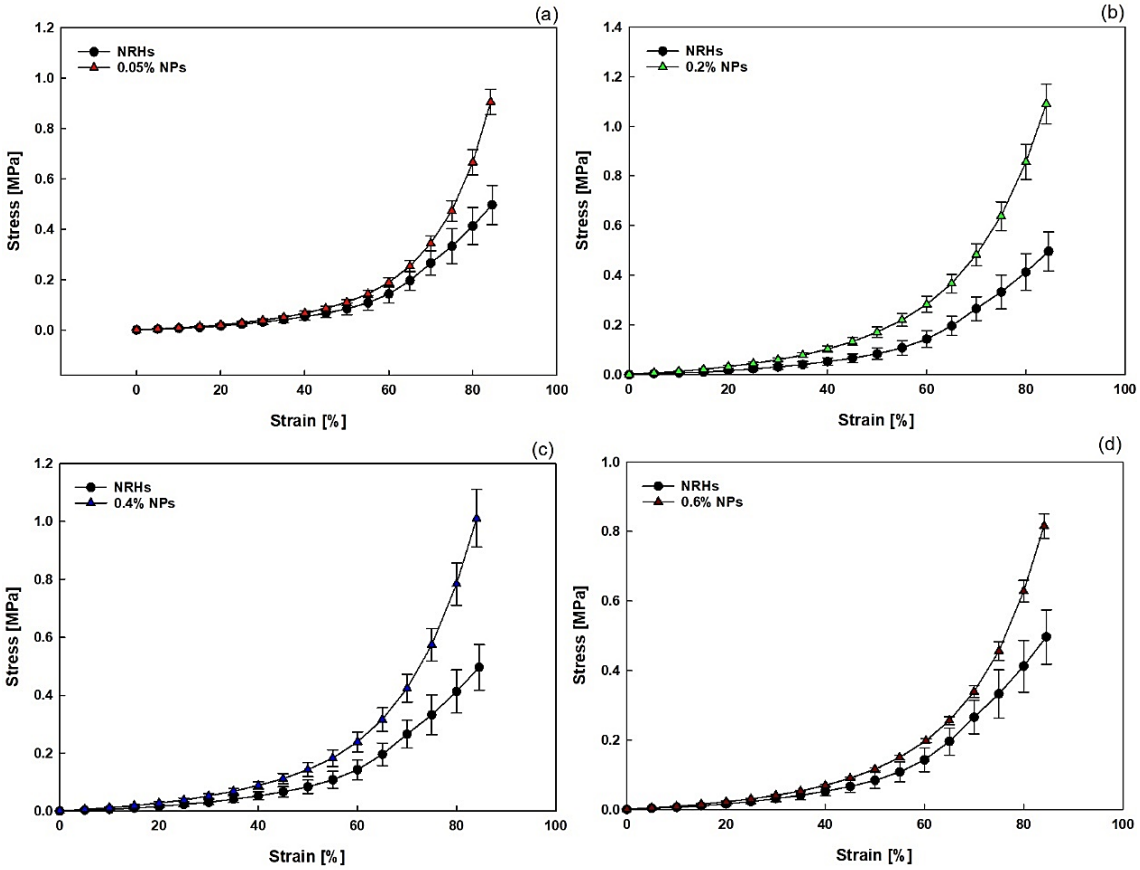

Figure 4. 3 Compressive stress-strain responses by 0.1s^{-1} strain rate (Mean (n=3) ± SD) for NRHs with: (a) 0.05wt% NPs, (b) 0.2wt% NPs, (c) 0.4wt% NPs and (d) 0.6wt% NPs.

At the strain rate of 1.0s^{-1} shown in Fig. 4.4, stress distributions over the networks within a concise time (< 1 min) do not permit the water contents diffusing out of the hydrogels. The hyper elastic deformation, which is independent of the strain-rate, results in the stress absorption of the networks with dissipating energy by the fluid. At a high strain rate regime, the compressive strength of hydrogels showed nearly 30 % improvement in samples with 0.05 wt%, 0.2 wt% and 0.6 wt% concentrations of NPs compared to NRHs. This is due to the transition of consolidation-type deformation to hyper elastic deformation at higher strain rates, which is similar to the articular cartilage deformation mechanism [63].

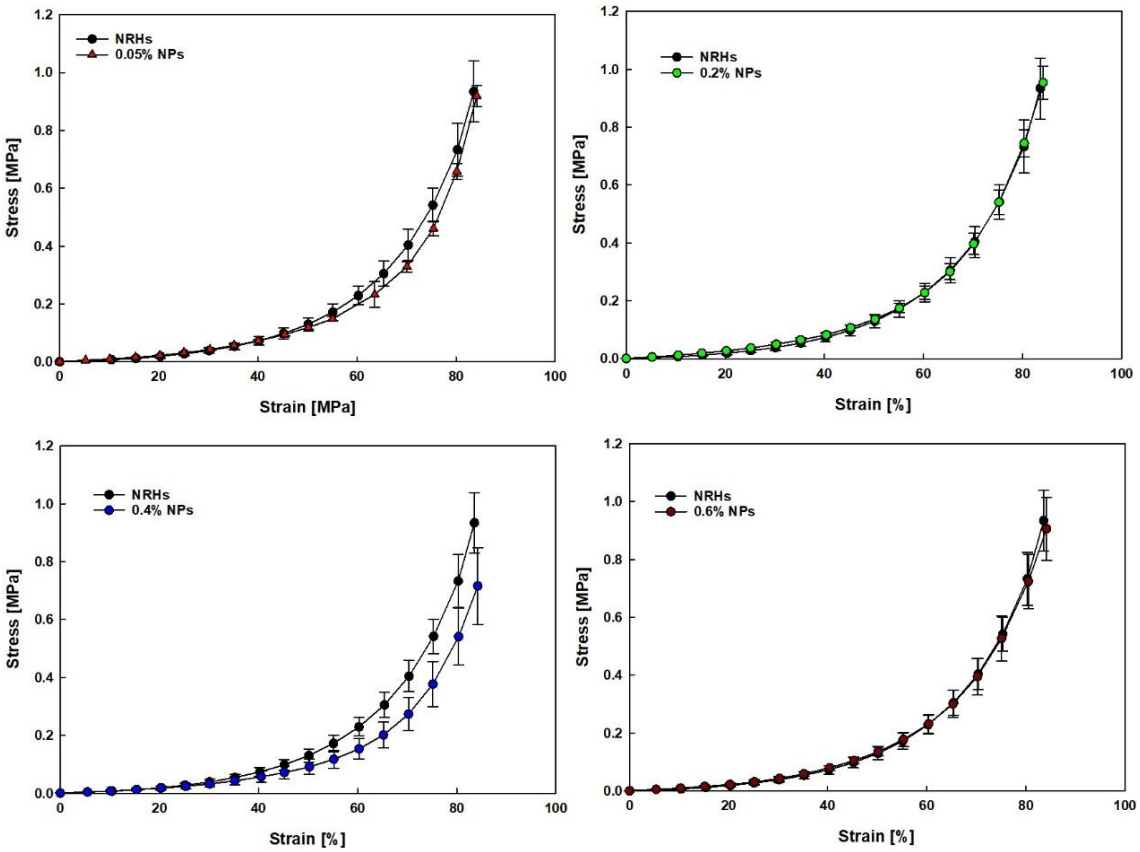

Figure 4. 4 Compressive stress-strain responses at 1.0s^{-1} strain rate (Mean (n=3) ± SD) for NRHs with: (a) 0.05wt% NPs, (b) 0.2wt% NPs, (c) 0.4wt% NPs and (d) 0.6wt% NPs

The higher concentration of NPs, which is inversely proportional with the structure mesh size, would result in promoting the degree of crosslinking [18]. Consequently, by the smaller mesh size, hydrogel would uptake less water volume trapped in the networks, which affects stress distribution over the structure. From Fig. 4.2, a rupture occurred in NRHs below 80% strain due to the less retained water and the rapid rate of pumping water out in comparison with other samples by the slowest strain rate. Fig. 4.2 showed NRHs with the lowest compressive strength, and softer material is not a suitable load-bearing candidate. Fig. 4.4 showed a similar pattern compared to the strain rate of 0.01s^{-1}; however, with higher compressive strength and extensive stress tolerated by all samples, similar to the native cartilage with increasing strain rate, stiffness increases [63]. No rupture or breakage of structure binding occurred as the stress was imposed

over the networks in a shorter time. It is worth highlighting that the maximum compressive stress demonstrated by 0.2wt% NCHs reached 1.2 MPa, which is in the range of articular cartilage compressive stress (0.26-1.37 MPa) [244].

4.3 COMPRESSIVE AND TANGENT MODULUS

The compressive test is a reference for hydrogel's strain-dependency response. Poroelasticity response according to the amount of water uptake in hydrogels and retaining a high amount of water (>75%) yields exceptional mechanical properties. Articular cartilage immersed in synovial fluid incorporating with the cartilage structure and the rate of defusing fluid in and out make it poroelastic and strain-dependent [63, 232]. The manufactured bilayer hydrogel was functioning similarly to the native cartilage when a porous top layer was placed in the structure. It is validated from Fig. 4.5 (b), where samples responses are distinguished at different strain rates.

(a)

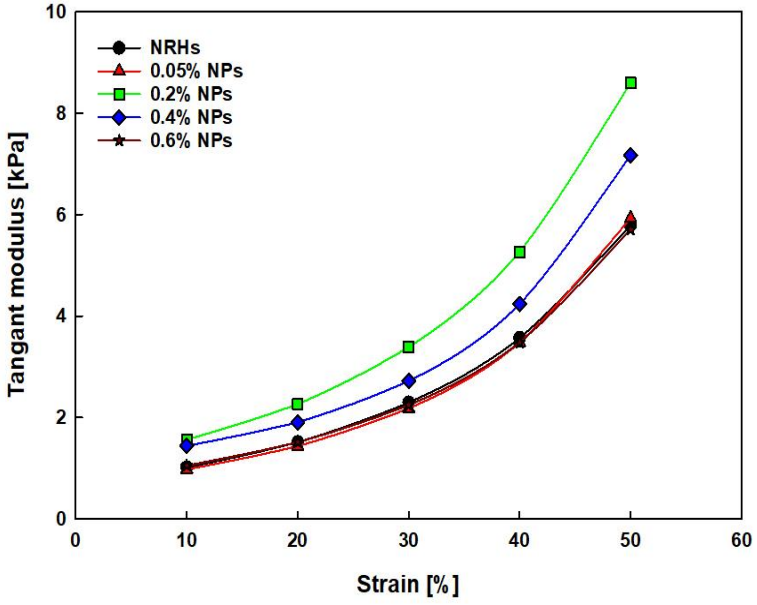

(b)

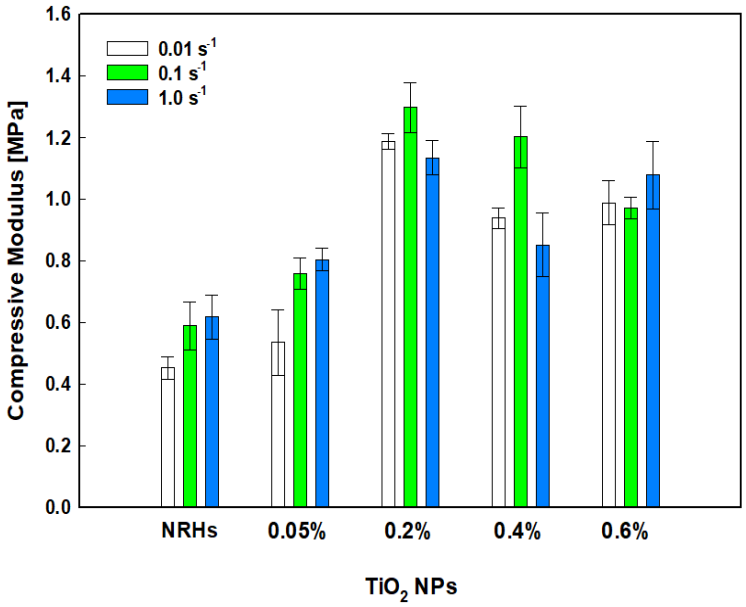

Figure 4. 5 (a) The compressive tangent moduli of all samples (mean (n=3) ± SD) as a function of strain under 0.01s^{-1} strain rate, fitted by nonlinear regression, (b) Compressive modulus of hydrogel samples (mean (n=3)) at different strain rates with 85% strain.

The compressive tangent moduli were computed by differentiating stress-strain data at specified points to monitor the behavior of a material, whether it is linear or nonlinear, as shown in Fig. 4.5(a). The compressive tangent moduli responses show nonlinearity of the material and its strain-dependency, which is desirable in the design of biomedical tissue applications. Fig. 4.5(b) demonstrates compressive moduli for all strain rates (0.01, 0.1 and 1s^{-1}) with the same trend observed for elastic modulus and hardness. According to the results, samples with 0.2wt% concentration on NPs showed 1.2-1.4MPa compressive modulus in all tested strain rates. Samples with 0.05wt%, 0.4wt% and 0.6wt% concentrations of NPs are presenting analogous results in all strain rates. Fig. 4.5(b) shows 0.2wt% NCHs as the utmost compressive modulus. It demonstrates that this sample has the most strain-dependent response, which is desired in the design of biomimetic structures. Table 2.6 in the literature chapter presents the results of the recent studies on mechanical properties of AAm, AAc and Alg with $CaCl_2$ ionic crosslinked single layer hydrogels with and without NPs, similar to the hydrogels proposed in the current study. The proposed NCHs with 0.2wt% NPs exhibited 350 kPa elastic modulus, which is significantly

higher than those presented in Table 2.6. While the compressive strength of 0.2wt% NCHs is lower than some of the hydrogels reported in the literature; however, 1.2 MPa compressive strength is within the range of the compressive strengths reported for articular cartilage (0.1-2.0 MPa).

4.4 STRESS RELAXATION

Stress relaxation tests were performed by keeping the strain constant (compressed to half of the initial thickness) for one hour, and reaction stress versus time was recorded. The stress with respect to time is illustrated for all hydrogel samples in Fig. 4.6(A). Immediately after loading, a sharp decrease in stress could be observed, followed by a further gradual decrease, demonstrating stress relaxation due to unbinding chains or the movement of loose-end chains.

(A)

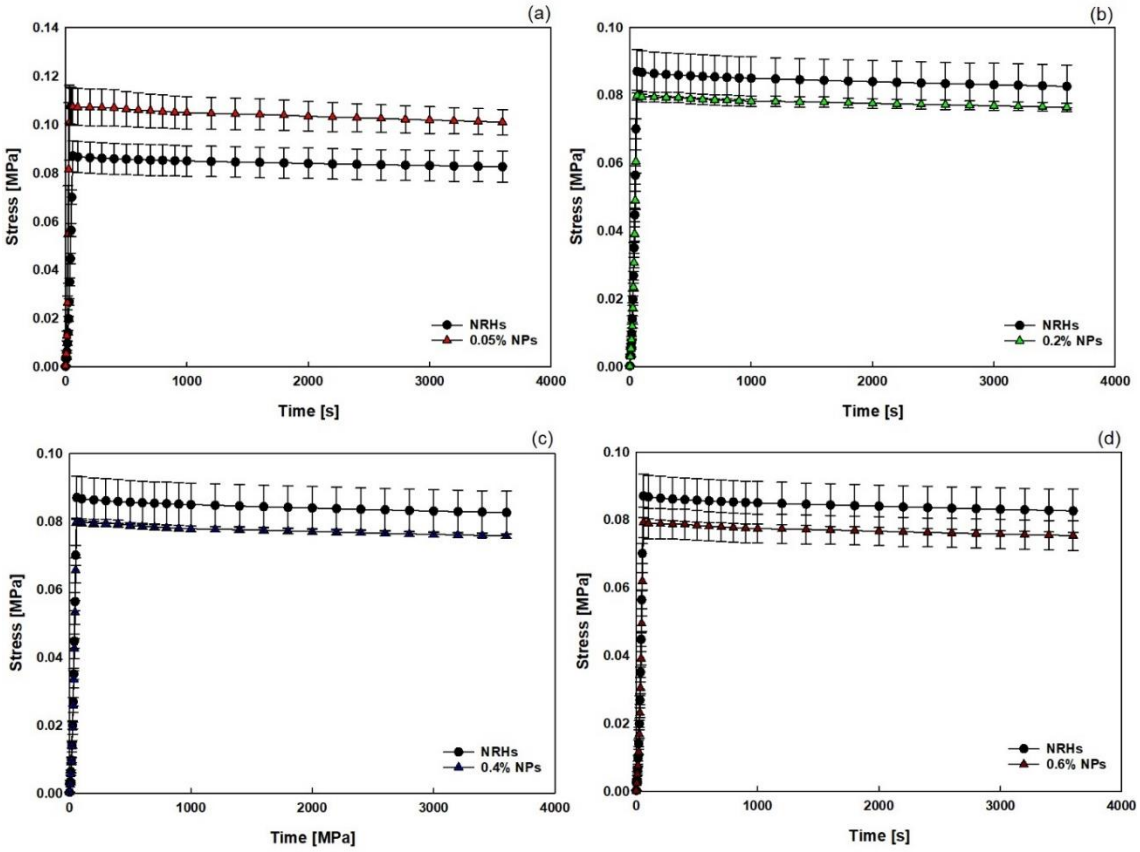

(B)

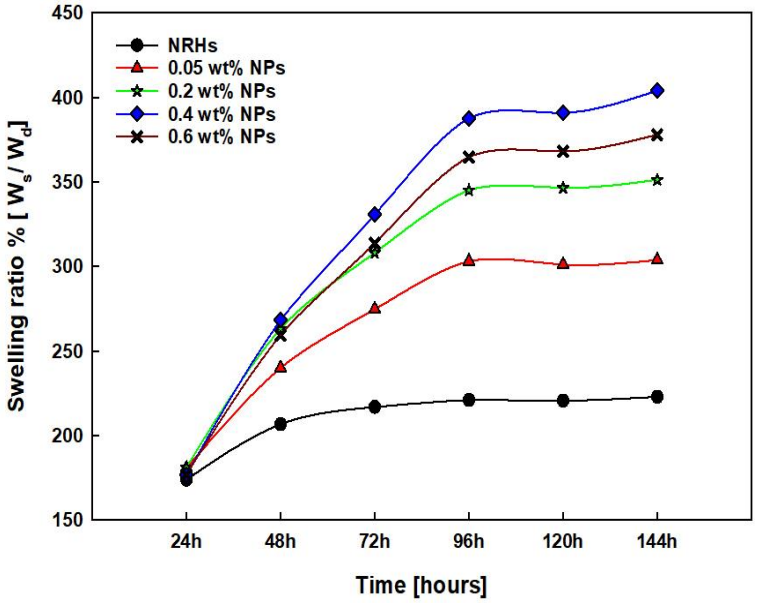

Figure 4. 6 A) Stress relaxation behaviour of NRHs compared with: (a) 0.05 wt% NPs, (b 0.2 wt% NPs, (c) 0.4 wt% NPs, (d) 0.6 wt% NPs at 50 % strain (Mean (n = 3) ± SD) and (B) The swelling ratio of NRHs and NCHs with respect to time.

Hydrogels with 0.6wt% NPs showed the lowest stress relaxation within the networks. Stress reduction within the timeframe is representative of the rate of induced plastic deformation. The optimum amount of NPs is a key point in the relaxation of stress [245]. Among all samples, 0.05wt% were inferior by the excessive peak stress compared to other samples.

A two-term exponential decay method was used to fit the stress relaxation data as previously described by (3.7). The fitting curve parameters are listed in Table 4.1 The viscoelastic model provided a good correlation with experimental data and verified as a capable model to predict stress distribution over the network at any given time.

Table 4. 1 Relaxation parameters for the NCHs and NRHs obtained from curve fitting.

Coefficient	NRHs	0.05wt% NPs	0.2wt% NPs	0.4wt% NPs	0.6wt% NPs
$\sigma_f/\ \sigma_0$	0.085	0.106	0.078	0.078	0.077
A	-0.051	-0.070	-0.047	-0.047	-0.047
B	0.024	0.056	0.023	0.025	0.023
C	-0.046	-0.055	-0.043	-0.042	-0.042
D	0.024	0.056	0.023	0.025	0.023

Results in Fig. 4.6(A) show that NRHs with 0.09 MPa peak stress initiated and decayed to 0.08MPa within 3600s. Regarding the bond breakage, results showed that by imposing load within 1h at 50% strain, bond rupture growth-rate was very slow as it is no indication of sudden drops in trends. A good correlation with the previously mentioned results, the sample with 0.2wt% NPs, is performing a meager transition of the load from the fluid phase to the solid phase of the hydrogels. It is also tangent with the previous study that found the higher crosslinking degree yields, the weaker viscous flow and consequently, larger plastic deformation [145]. It is worth mentioning that plastic deformation supports the crack blunting at higher strains, but is unlikely to contribute at low strains [246]. Stress relaxation study on the effects of NPs on the molecular displacement of polymer chains by imposing 0.2wt%, 0.4wt% and 0.6wt% NPs concentrations showed lower stress and reached a constant modulus in a shorter time.

Fig. 4.6(B) presents the swelling ratio of NCHs and NRHs after the hydrogel reached the swelling equilibrium. 0.6wt% and 0.4wt% NPs concentrations show the higher absorption of water, which is reasonable considering that the greater mesh size compared to other candidates and consequently higher capacity to retain water. According to a report, when nanoparticles are not effective in swelling ratio, it is attributed to a denser polymer matrix that masks the nanoparticle effect [247]. Therefore, samples with 0.05wt% and 0.2wt% NPs concentrations contained a denser matrix according to their low swelling ratio.

4.5 SEM CHARACTERISTICS

SEM images for all hydrogel samples were taken to characterize the bilayer feature and mesh size of each sample with different TiO_2 NPs concentrations. SEM images of NRHs are demonstrating a formed bilayer with a uniform cylindrical-shaped porous network with an average porous layer thickness of 140µm in Fig. 4.7 (b). The average diameter of pores is 10-12 µm in Fig. 4.7 (c). Uniform pores are formed on top of the bulk layer, and as it is illustrated in Fig. 4.7 (c), the porosity gradually shrinks in size from superficial through the bilayer thickness. Lin et al. [187] synthesized a bilayer hydrogel with an average pore size of 10 µm, which is similar to the average pore sizes of our non-reinforced bilayer hydrogels.

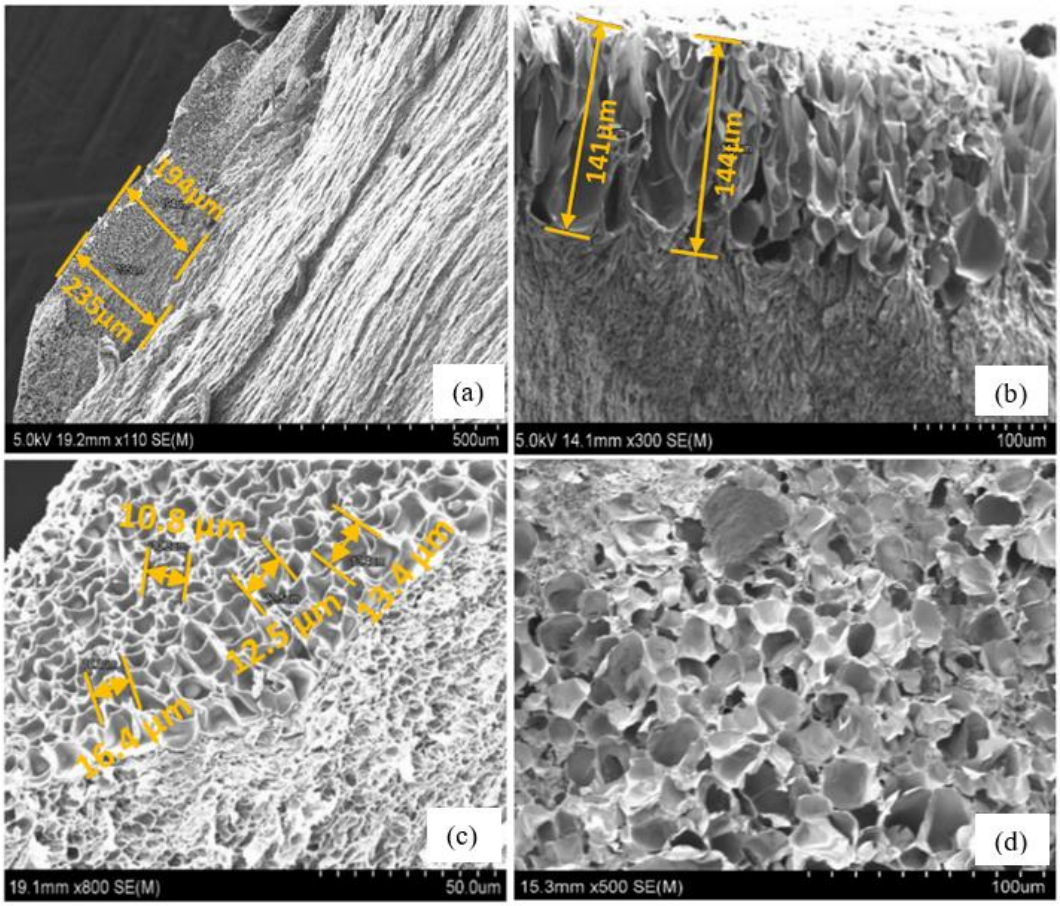

Figure 4. 7 The structure of the bilayer NRHs with different local magnifications (a) ×110; (b) ×300; (c) ×800 and (d) ×500.

The hydrogel strengthened by 0.05 wt% NPs showed smaller localized pores compared to other regions, as is shown in 4.8(c) with the red circles. It is because of the polymer chains connection network developed by TiO_2 NPs and extensive bonding to polymer chains within the networks. The porous layer thickness reached 1.40 mm maximum, which is a remarkable increase compared to the thickness in NRHs. It is demonstrated that introducing NPs to the networks locally affects the porosity with smaller pores than the NRHs.

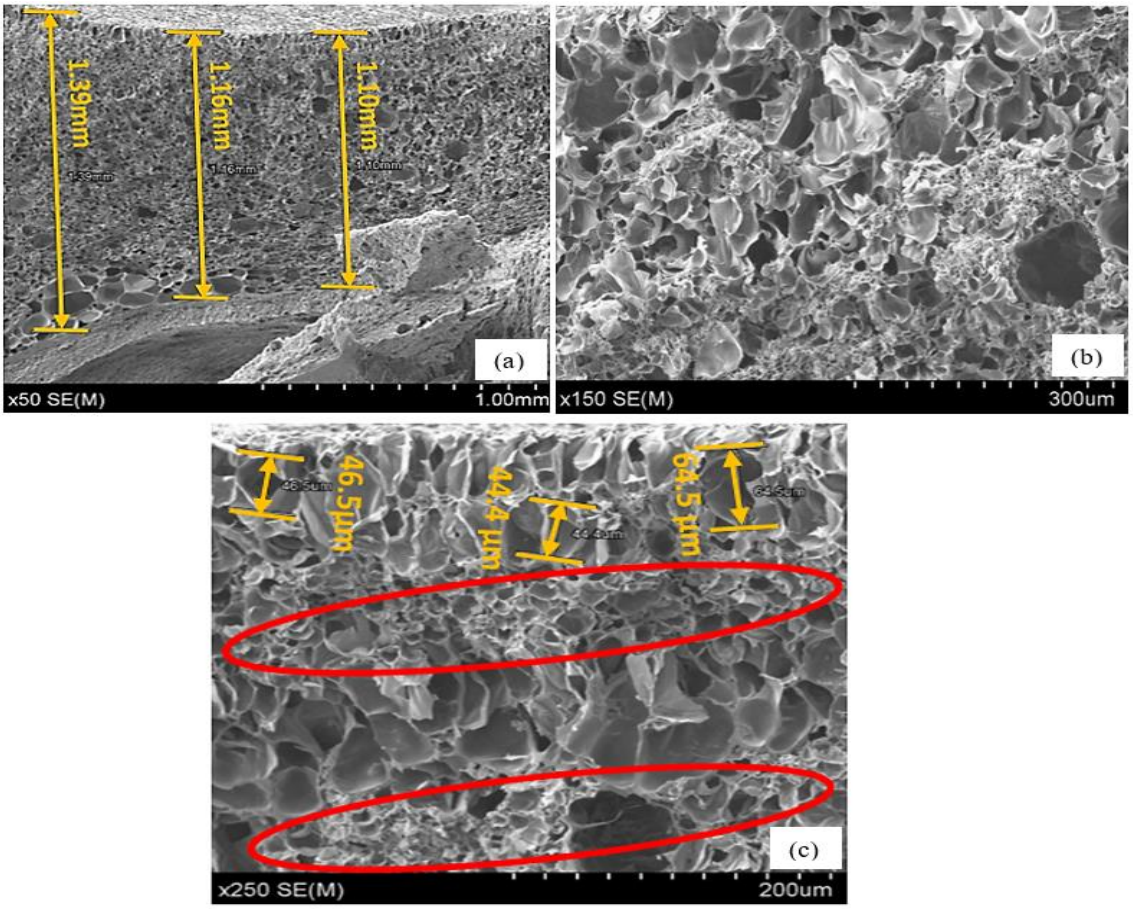

Figure 4. 8 The structure of the bilayer hydrogel strengthened with 0.05wt% NPs with different local magnifications (a) ×50; (b) ×150 and (c) ×250.

The porosity of the hydrogel samples strengthened by 0.2 wt% NPs was formed with the gradual shrink in pore size through the thickness of the porous layer with a total thickness of nearly 720 μm. As illustrated in Fig. 4.9(c), polymer chains formed to a string-like architecture on the surface of the porous layer. Similar to the hydrogel with 0.05 wt% NPs, the greater density

of NPs caused more bonding in some regions and a denser localized network in the porous layer, as is shown in Fig. 4.9 (b).

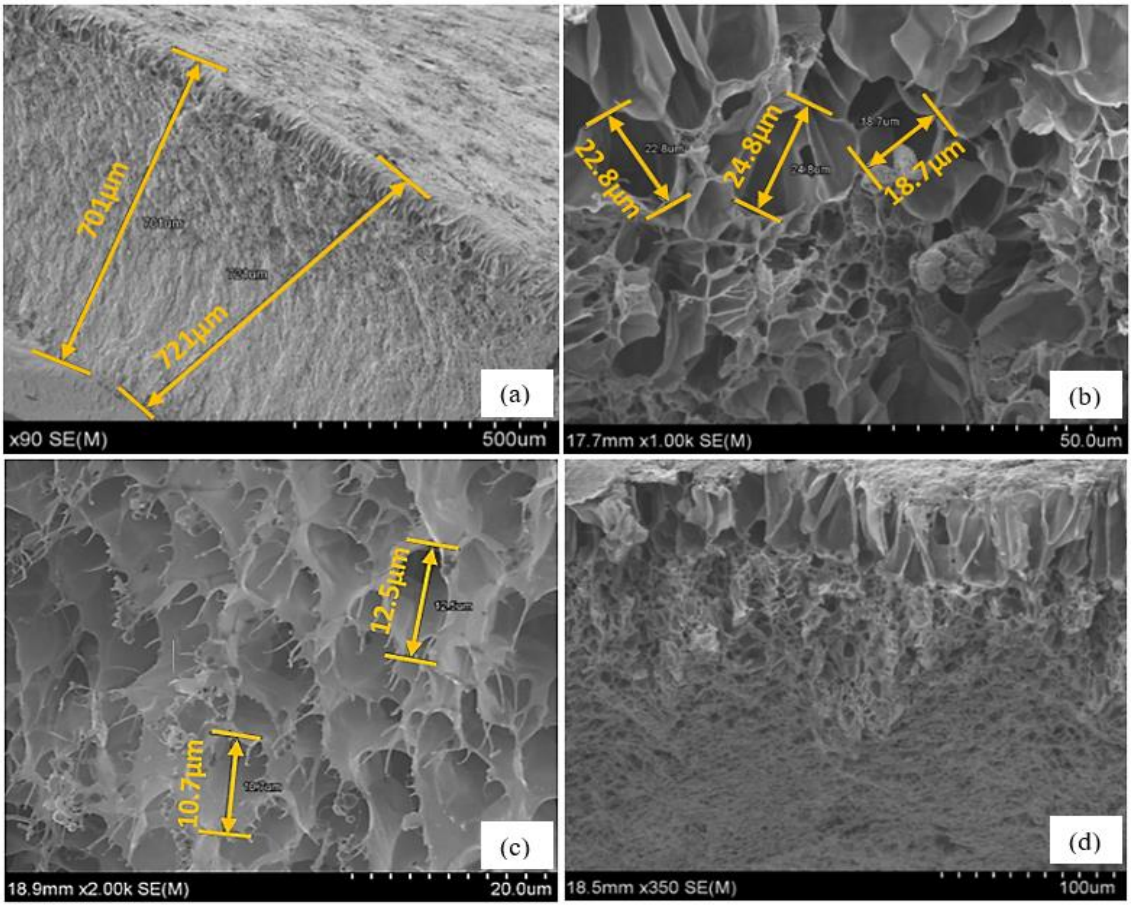

Figure 4. 9 The structure of the bilayer hydrogel strengthened 0.2wt% NPs with different local magnifications (a) ×90; (b) ×1k; (c) ×2k and (d) ×350.

For the hydrogel samples with 0.4 wt% NPs, pore sizes range between 1 μm and 30 μm with the localized polymer chains bonding. Longitudinal porous structures at the vicinity of the superficial zone are gradually shifted to spongy-like networks at other regions. SEM images for samples with 0.4 wt% NPs are shown in Fig. 4.10.

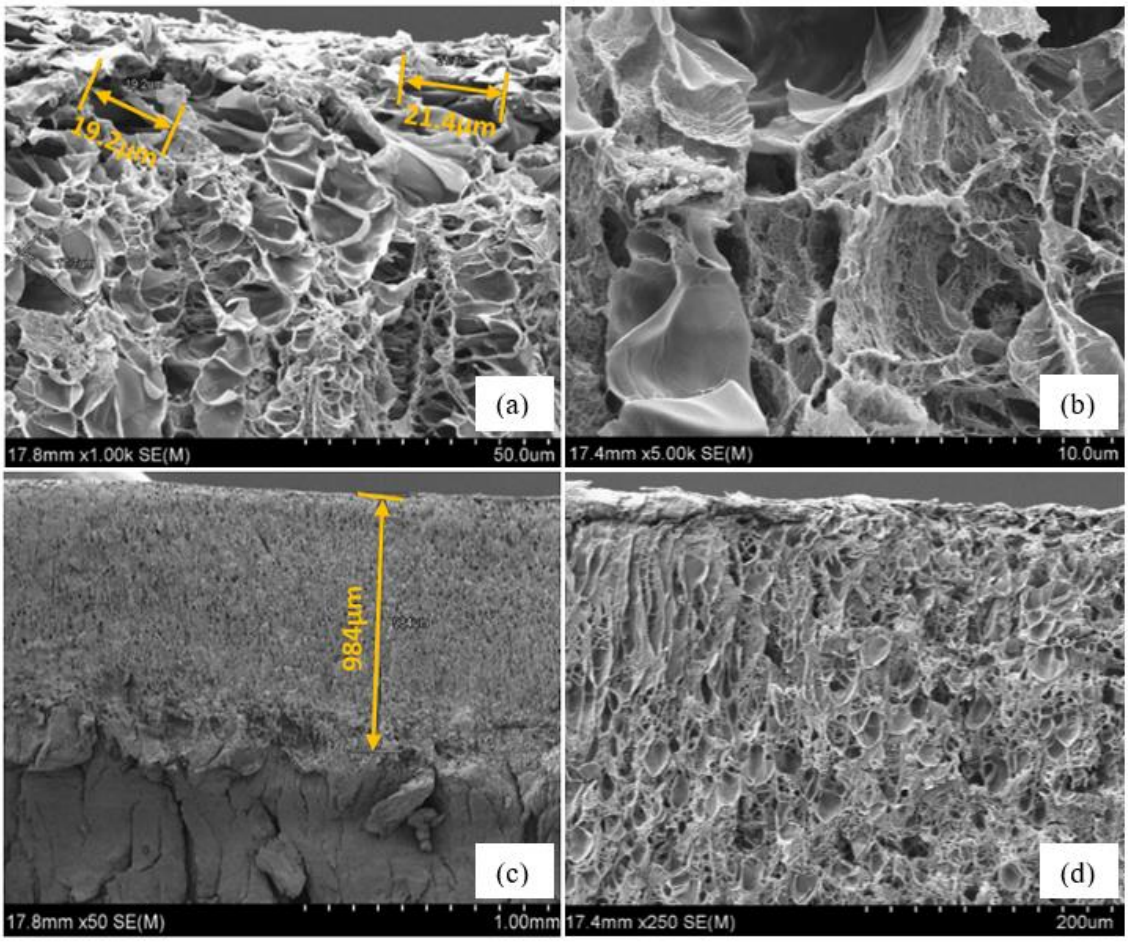

Figure 4. 10 *The structure of the bilayer hydrogel strengthened by 0.4wt% NPs with different local magnifications (a) ×1.0k; (b) ×5.0k; (c) ×50 and (d) ×250.*

The hydrogels strengthened by 0.6 wt% NPs demonstrated denser localized linkage to polymer chains compared to the other samples, and the high porosity resulted in pore sizes averaged in the range of 50 μm–90 μm showed in Fig. 4.11(b). The homogeneity of developed connections over the porous layer is the advantage of using a substantial amount of NPs relative to the other hydrogel samples. Porous layer thickness as is demonstrated in Fig. 4.11(a) reached 1.55 mm. Uniform networks, slimmed string-like fibres connected to the vicinity chains and thin plate-like architectures are the features of the hydrogels strengthened by 0.6 wt% TiO_2 NPs.

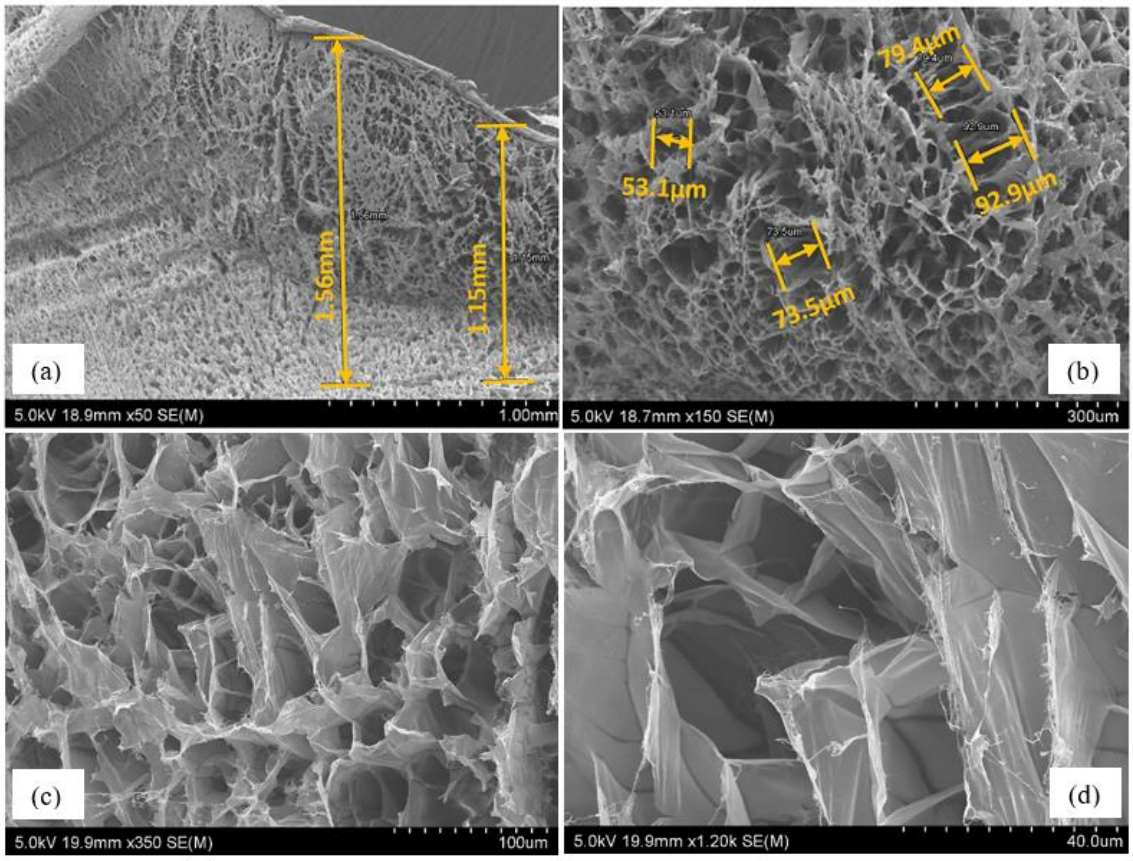

Figure 4. 11The structure of the bilayer hydrogel strengthened by 0.6wt% NPs with different local magnifications (a) ×50; (b) ×150; (c) ×350 and (d) ×1.20k.

SEM results showed how NPs binding with chains according to their weight percentage contribute to the networks. It is a clear picture of NRHs with uniform porosity over the top layer and small pore sizes 10−12 µm. Adding 0.05 wt% NPs to the networks, improved localized crosslinking and shrinkage of pores. Although the outstanding porous layer thickness ratio reached 1/14 in 0.05 wt% NPs concentrations, samples with 0.6 wt% NPs concentrations showed the highest capacity to retain water in their lubricious or porous layer. Sample with 0.2 wt% NPs demonstrated gradual shrinking of pore sizes from the top layer to the bulk layer, and this could be beneficial for developing cartilage implants with stiffness gradient through the thickness. The key points affecting the polymerization process are monomers, crosslinkers, and initiators, and introducing more NPs resulted in interconnecting polymer chains in the propagation stage of the polymerization process. The formation of the bilayer hydrogels, on the other hand, would be affected by the polymerization process near excess hydrogen source (polystyrene surface) [138].

Therefore, by curing time in the polymerization process, the amount of NPs and time are the keys that affect the thickness of the porous layer at the stage of interrupting polymerization.

4.6 DISCUSSION

Our results show that an optimum TiO_2 NPs concentration, improved elastic modulus and hardness of the bilayer hydrogels threefold. This could be the result of interlocking more chains by NPs and a lower degree of freedom within chains. It is worth mentioning that many attempts were made to add NPs with more than 0.6wt%, but particles sedimented in the solution even with more sonication power and time. This phenomenon has also been reported by Toledo et al., who have highlighted that using higher concentrations of TiO2 NPs (>1wt%) resulted in sedimentation in their solution [220]. By increasing NPs amounts to the system, the tie points of chains would increase and result in a stiffer network. Stiffer networks promote brittleness and reduce the stretchability of chains, which ended up in lower energy dissipation of the hydrogel.

Cartilage is a poroelastic material as it absorbs a significant quantity of water [248], hence its performance is highly dependent on the strain rate of the material and its stiffness in the compressive state [45]. Therefore, strain-dependency is a critical consideration in the design of polymeric hydrogels. 0.2wt% TiO_2 loading in the polyacrylamide/alginate/ acrylic acid hydrogel exhibited the best material stiffness and stress-strain responses. The higher crosslinking densities (0.4wt% and 0.6wt%) resulted in stiffer networks and that is why the compressive modulus of these two loaded NCHs were reduced due to a quicker rupture of the chains. This could be due to the shorter length of chains and reduced stretchability.

Viscoelastic responses improved for 0.2wt%, 0.4wt% and 0.6wt% NPs loadings compared to the non-reinforced hydrogel. The improved energy absorption by topping up NPs was due to boding dangling chains or long-length chains that might be incapable of relaxation of imposed stresses. The time-dependent viscoelastic response of the cartilage dissipates pressure energy on the joint by the interstitial fluid flowing through the porous matrix [3]. Polymeric hydrogels are also viscoelastic, and the effect of reinforcement on hydrogels against imposed load has been

reported recently [234]. The relaxation process is decisive in tissue engineering in the sense of load transfer, nutrient transport and cell behaviour [199].

A unique string-like pore on the surface of 0.2wt% NPs sample was observed, and the swelling ratio of this sample was at a moderate level (300%) compared to other concentrations. Water content retention also affects the modulus of elasticity and compressive strength [162] and is beneficial for biomedical applications. However, a high swelling ratio drastically degrades mechanical properties [249]. The reason is due to the difference of hyper-elastic deformation or consolidation type deformation as mentioned comprehensively in the literature chapter. The swelling ratio is a function of the degree of crosslinking [250]. The swelling mechanism is categorized into four types of non-porous, microporous, macroporous and super porous. Non-porous hydrogels have polymer chains that are tightly packed, similar to our 0.4wt% and 0.6wt% NCHs that is limiting the diffusion of a solvent through the free hydrogel matrix [247, 251]. Furthermore, the pore size of the super porous hydrogel has spherical shaped pores that are connected to form a capillary-like structure. This structure allows quick diffusion of water into the pores leading the hydrogels to swell [252]. The degree of swelling depends on many factors such as solvent nature, network density, and interaction of polymer-solvent parameters [253]. The swelling rate of hydrogel with AAc and N-isopropyl AAm is sensitive to pH as such their swelling, and de-swelling behavior is quite similar [254]. Smaller pore size is the result of a higher concentration of AAc; however, by increasing the amount of AAm, the swelling ratio also increases [162].

4.7 LIMITATIONS

The limitation for this part of the research was dispersing titania NPs in the DI water. Since this NPs is hydrophobic, some treatments were advised in the literature such as neutralizing or using a surfactant. However, the application of each proposed method impacted the polymerization process and deteriorated the lubricious layer. In this research extensive attempts were conducted to neutralize the acidity level of AAc monomer. However, we found that

neutralizing process could boost up polymerization in a very short time that certainly affects the quality of the crosslinking process. Also, due to the prompt polymerization, very irregular samples were formed and that could result in tissue rupture under the mechanical tests. Another limitation of this research was the measurements of the nitrogen degassing pressure inside the viscous solution. Since this is a very critical process, it is necessary to ensure degassing oxygens must be performed and would not introduce nitrogen more than required into the solution, which results in initiating more bubbles and trap in the viscous solution. It is essential to have a benchmark for degassing pressure by an apparatus, with which it records the imposed pressure from the nozzle tip according to the viscosity of the solution.

4.8 CONCLUSIONS

TiO_2 NPs have a significant impact on improving the mechanical properties of hydrogels, although the optimum amount of monomers along with NPs is playing a key role in this regard. Many attempts were conducted to achieve an optimum amount of monomers by which TiO_2 NPs dispersed in the solution without any surface modifications. Our study also showed the extent to which the optimum amount of TiO2 NPs improves mechanical properties while the excess amount of NPs minimizes material compressive strength and elastic properties. Samples with 0.2 wt% TiO_2 NPs in our formula showed the best results in all conducted mechanical tests. Moreover, the combination of large-size pores along with small-size pores at its inter-layer makes it a unique feature to retain more water. Maintaining both mechanical and tribological properties for hydrogel has been highlighted as a challenging topic in recent studies, as improving one could result in minimizing the other one. The proposed bilayer hydrogel showed significant material properties reinforced with the TiO_2 NPs compared to the recent studies, while its lubricious layer benefits tribological properties. Further investigations of the suitability of the manufactured bilayer hydrogels reinforced by TiO_2 NPs for the Tribological performance and wear resistance of the samples will be studied in the next chapters.

CHAPTER 5

ASSESSMENT OF MICROSTRUCTURAL AND MECHANICAL BEHAVIOUR OF BILAYER SILICA-REINFORCED NANOCOMPOSITE HYDROGELS

5.1 INDENTATION AND MATERIAL PROPERTIES

The force versus indentation depth for NCHs with different SNPs concentrations is plotted in Fig. 5.1(a). By increasing the amounts of SNPs in the network, hydrogels' load-bearing capability was improved. The hydrogel strengthened with 0.6wt% SNPs reached 1.0 N peak force. Fig. 5.1(b) shows that by adding SNPs, elastic modulus and hardness increased significantly in all NCHs. The elastic modulus and hardness at 0.6wt% NCHs increased by 155% and 165%, respectively, compared to NRHs. SNPs in the network react as a crosslinker, resulting in chain interlock in the system [21]. This phenomenon boosts the strength of the material due to an accretion crosslinking density and consequently enhances the modulus of elasticity and hardness [18]. Several studies reported that the optimum amount of monomers along with the crosslinker significantly enhance material properties [186, 196]. SNPs function as a crosslinker in the system, and the excess amounts of SNPs shorten the polymer chains, which results in material stiffness [255]. In the IPNs, the secondary network is the key for the end product to become either brittle or ductile [167]. In this study, parameters like secondary network density, monomers and crosslinker volume remain intact, while for each sample, SNPs concentrations were varied. Klein et al. [246] reported that low elastic modulus in their hydrogels corresponded to the low density of polymer chains and large polymer molar mass. Compared to our results, this finding verifies

that samples loaded with 0.6wt% SNPs exhibited the maximum elastic modulus because of their upmost polymer chain density. Moreover, the previous study by Zhai et al. [196] showed that utilizing the maximum concentration of SNPs (6.0wt%) in AAm-Alg hydrogel system resulted in 110.9 kPa elastic modulus. In comparison to our results, we could achieve a two-fold increase in elastic modulus (*E*~215 kPa) by using only 1/10 wt% SNPs used in their system. This is the result of optimum amounts of monomers and crosslinkers that was achieved by many attempts conducted at the hydrogel properties optimisation stage.

(a)

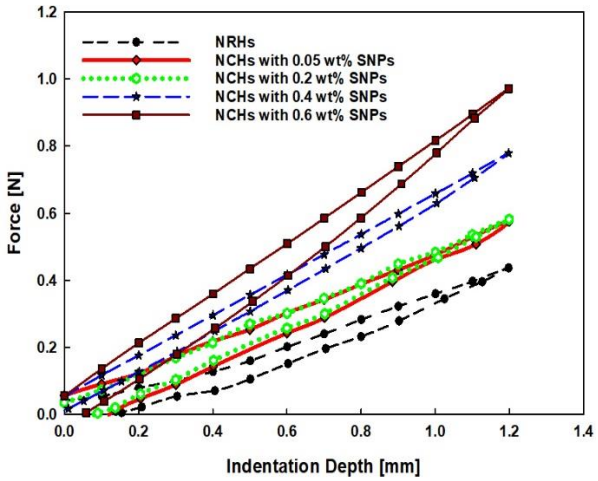

(b)

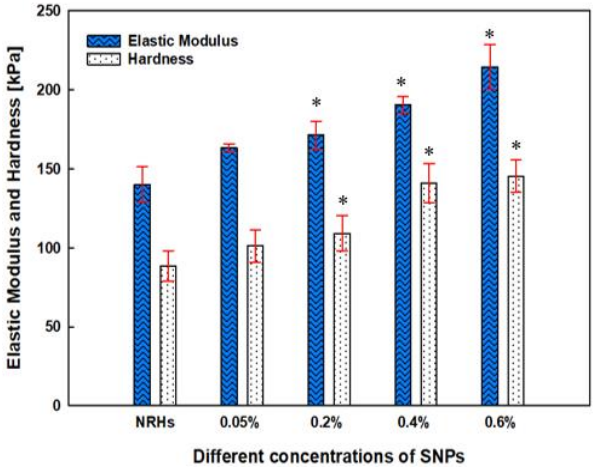

Figure 5. 1 (a) Indentation responses of hydrogel samples strengthened with SiO_2 NPs and NRHs, and (b) the elastic modulus and hardness of hydrogels (Mean (n=3) ± SD), [represents p<0.05, which indicates the significant difference of treated samples (NCHs) compared to NRHs].*

5.2 COMPRESSIVE RESPONSE WITH RESPECT TO STRAIN RATE

Fig. 5.2 demonstrates the compressive stress responses of NRHs. The compression tests were performed at three strain rates mentioned in the method section. NRH samples failed at nearly 76% strain under $0.01s^{-1}$ strain rate. Since the compressive strain rate is in the lowest regime and the fluid phase has enough time to migrate through the porous structure and diffuse out of the sample, therefore most of the stress would be carried by the solid phase. Thus, weak chains in the network could not tolerate the load and fail at their ultimate stress point that results in gel rupture or breakage. NRHs under $0.1s^{-1}$ experienced higher peak compressive stresses compared to $0.01s^{-1}$ strain rate. AC in lower strain rates responds in the form of consolidation type of deformation, which is stiffness dependent [63]. Due to this fact, by increasing the strain rate, stiffness would increase in AC. A similar response by a higher strain rate was exhibited in our polymeric hydrogels. The peak compressive stress in NRHs was attained at 0.75 MPa without failure at 85% strain.

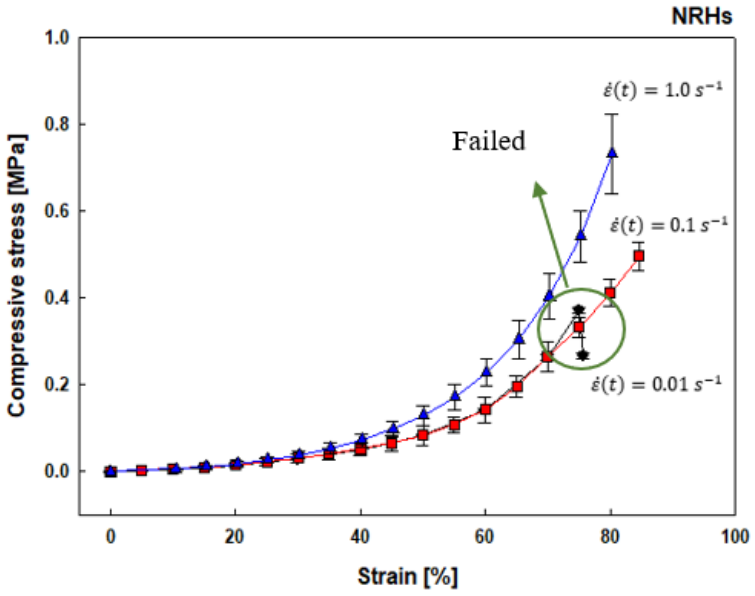

Figure 5. 2 Compressive stress-strain responses of NRHs at different strain rates ($0.01s^{-1}$,$0.1s^{-1}$,$1.0s^{-1}$) (Mean (n=3) ± SD).

Fig. 5.3 shows compressive stress-strain responses of all NCHs under different strain rates ($0.01s^{-1}$,$0.1s^{-1}$ and 1.0 s^{-1}). All NCHs compressed to 85% of the initial thickness, and only 0.05wt% NCHs failed at strain rate $0.01s^{-1}$. This is because of the minor amount of SNPs to the system, not enough to boost up the strength. By increasing the considerable amount of SNPs in the networks (SNPs > 0.05wt%), the compressive strength was increased due to the chain interlocks. The peak compressive stress in NRHs was attained at 0.75 MPa, yet adding 0.6wt% SNPs significantly increased the strength by up to nearly two-fold, to 1.4 MPa. This theoretically indicates that SNP has a significant impact on chain entanglement, which results in higher toughness. No crack or rupture was observed in samples when compressive loading was imposed at the strain rate of $0.1s^{-1}$. Since at higher compressive strain rate, less water would diffuse out of the sample compared to $\dot{\varepsilon}(t) = 0.01s^{-1}$, the retained water contributes to dissipating the load and energy imposed on the system. Microscopically, the same weak bonds that reached their ultimate strength under $\dot{\varepsilon}(t) = 0.01s^{-1}$ would withstand stresses under $\dot{\varepsilon}(t) = 0.1s^{-1}$, since the presence of the fluid phase, would minimize the continuously imposed stresses [73].

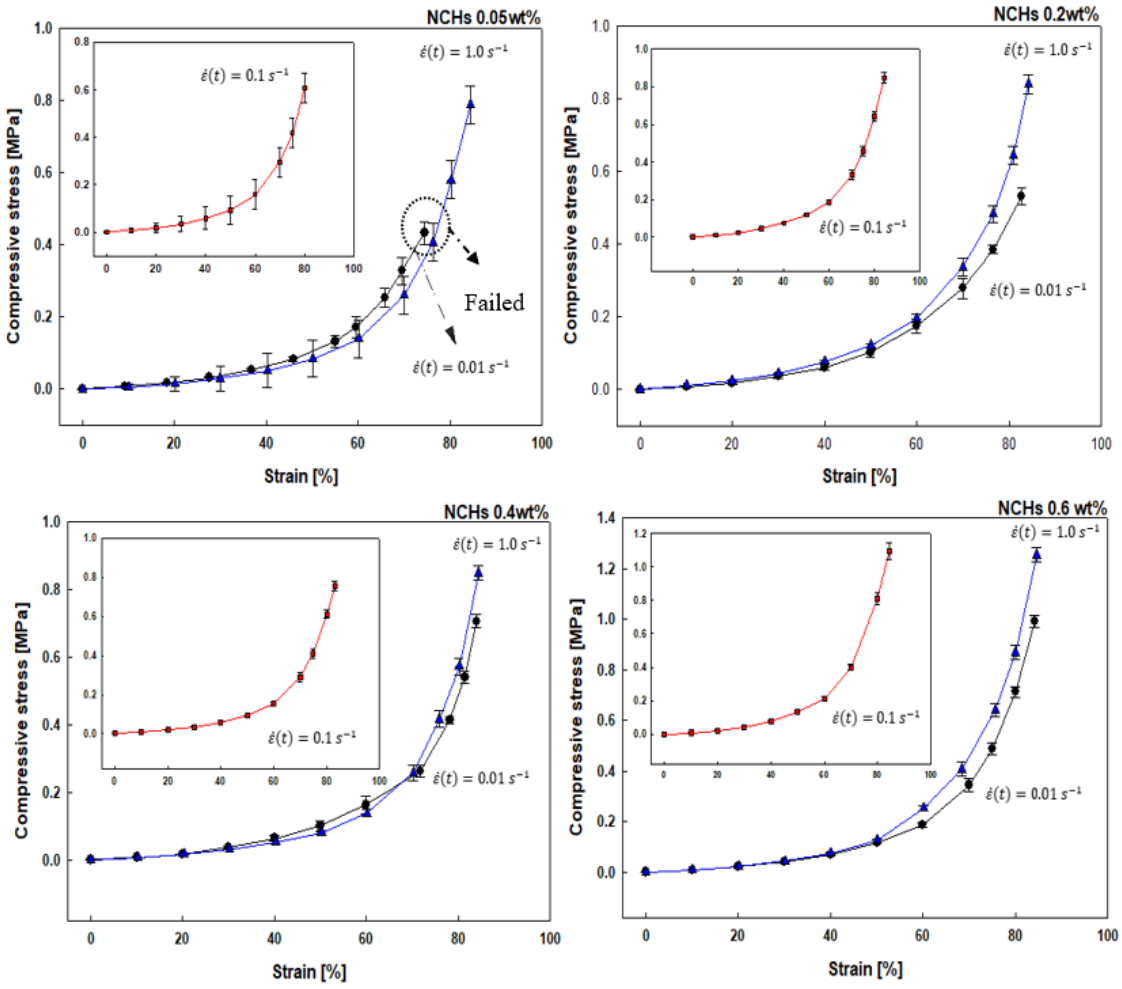

Figure 5. 3 Compressive stress-strain responses at different strain rates ($0.01s^{-1}$,$0.1s^{-1}$,$1.0s^{-1}$) (Mean (n=3) ± SD) for NCHs with 0.05wt% NPs, 0.2wt% NPs, 0.4wt% NPs and 0.6wt% NPs.

By increasing strain rates to $1.0s^{-1}$, all NCHs compressive stresses increase. The utmost compressive strength in the highest strain rate was attained by NCHs with 0.6wt% SNPs loading, reaching 1.4 MPa, which is in the range of AC compressive strength (0.26-1.37 MPa) [256]. AC responses under high strain rates ($0.01 \leq \dot{\varepsilon}(t)$) is shifted from consolidation-type deformation to hyper elastic deformation [63]. By hyper elastic deformation, fluid would not diffuse out of the cartilage structure and incorporation of fluid on dissipating energy reaches its maximum state. Distributed stresses over the fluid phase are gradually transmitted to the solid phase [35]. Therefore, the strain rate is inversely proportional to fluid rate diffusion; and by increasing strain rate, less fluid would diffuse out of the hydrogel. Fluid migration through the network under a

high strain rate is dependent on the mesh sizes. Therefore, the fluid trapped in the networks contributes to the tolerance of applied load [204]. In other words, stresses are mostly tolerated by the solid phase of the networks in the lower strain rate regime ($1.0 \geq \dot{\varepsilon}(t)$) when fluid has enough time to being diffused out. Therefore, hydrogel responses in hyper elastic deformation state, mimic the AC response in the same state. Hyper elastic deformation takes place when the elastic deformation is considerable.

In general, by increasing SNPs, extensive crosslinked chains result in smaller mesh size in the networks and consequently would uptake less volume of fluid. Therefore, most of the imposed load would be carried by the solid phase of the system, especially in the low strain rate regime. Due to this fact, a sample with the smallest mesh size (loaded by 0.6wt% SNPs) and under the lowest strain rate ($0.01s^{-1}$), exhibited the highest compressive strength compared to the rest of the samples is shown in Fig. 5.3 The interpretation of the results indicates that SNPs effectively enhance compressive strength when the solid phase of the structure carries the majority of the imposed loads.

As Table 2.6 was presented in the literature review chapter, lists of the recent studies on mechanical properties of AAm, AAc and Alg with $CaCl_2$ ionic crosslinked single layer hydrogels with and without using SNPs, similar to our proposed hydrogels. Mechanical properties of the studied hydrogels demonstrate that our developed hydrogel's elastic modulus is comparable to the best-performing hydrogels reported in the literature. Arjmandi et al. [257] used similar materials, but their hydrogel was synthesized in a bulk uni layer; however, our NCHs elastic modulus and compressive stress are 130% and 600% higher, respectively. Zhai et al. [196] used the same monomers, and different mixture and their elastic modulus reached 110 kPa, although they used a 10-fold greater amount of SNPs. The advantages of our proposed system are first, advancing our hydrogels with the lubricious layer that is useful in fluid diffusing rate and tribological applications. Secondly, we used one-tenth of SNPs compared to the SNPs amount that was reported in the previous study, and the elastic modulus was doubled without failure or

rupture under 85% compressive strain [196]. Thirdly, the presence of METAC as a hydrophilic monomer in our system that retains the fluid in the structure enhanced the viscoelastic and poroelastic relaxation.

5.3 COMPRESSIVE AND TANGENT MODULUS

Tangent modulus quantifies softening and hardening of the material and plastic deformation beyond yield stress. Softened materials can withstand more load before ultimate failure and are suitable for replacing tissues that undergo large deformations [257]. Two factors that have a considerable effect on tangent modulus are strain rate and strain point. Healthy knee cartilage typically experiences average strains under 10% [59] and a maximum of 17% [180]. However, we used a higher threshold (50%) to assess further tangent moduli response in our materials. It is reported that the tangent modulus [258] and strain-rate dependency [63] of AC decrease by ageing [258]. This obligates analyzing tangent modulus to quantify hydrogels' strain-magnitude and strain-rate dependency. The tangent moduli obtained are strain-magnitude dependent for all samples, and by increasing strain magnitude, tangent moduli increased. NCHs with 0.05 wt%, 0.2 wt% and 0.4 wt% SNPs have shown lower strain-magnitude dependency compared to NRHs. Especially, within the range of 30% - 40% strains, they have fallen in the same threshold. However, NCHs with 0.6 wt% SNPs revealed the most strain-magnitude dependency compared to other samples. Fig. 5.4 (a) shows that the tangent modulus of NCHs with 0.6wt% SNPs loading reached 7 MPa at its peak point. NRHs demonstrated the lowest tangent modulus with 4.8 MPa. The compressive modulus results presented in Fig. 5.4 (b) clearly show the strain-rate dependency of synthesized hydrogel samples which is highly desired in tissue engineering applications [186]. The articular joint under compressive loading pressurizes the interstitial fluid in the cartilage architecture and the fluid in the tissue carries the majority of the imposed loads until the fluid is exuded away at the beginning of the unloading. During the pressurized phase, the imposed load withstood by the fluid gradually transfers to cartilage [78]. Since hydrogels are incompressible with their high-water content [239], the higher compressive strain would result in greater compressive modulus. The samples in our experiments were compressed to 85% of their thickness

to investigate their response under very high strain and to obtain their compressive moduli at different strain rates. Since the developed NCHs didn't fail at this extremely high strain and pressure, it gives us confidence that they won't fail under pressure once implanted in the articular joint. NCHs with 0.4wt% and 0.6wt% SNP loadings demonstrated analogous results compared to the rest of the samples in all strain rates.

(a)

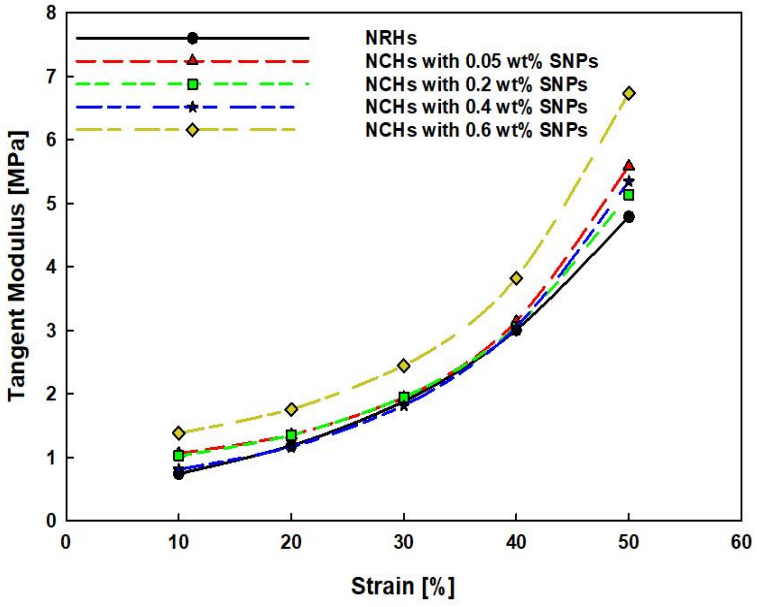

(b)

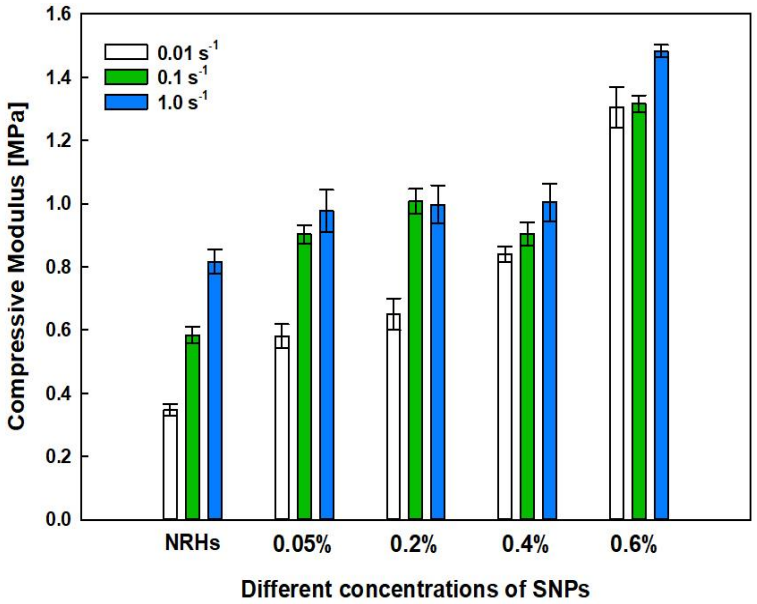

Figure 5. 4 (a) Tangent modulus at 0.01s^{-1} strain rate and (b) Compressive modulus of hydrogel samples (mean (n=3)) at different strain rates by 85% strain.

5.4 STRESS RELAXATION

Stress relaxation tests were performed by keeping the strain constant (compressed to half of the initial thickness) for one hour, and reaction stress versus time was recorded. Stress with respect to time is illustrated for all hydrogel samples in Fig.5.5. Immediately after loading, a sudden decrease in stress could be observed, followed by a further gradual decrease. A two-term exponential decay method was used to fit the stress relaxation data as described previously (3.7). The fitting curve parameters are listed in Table 5.1 The viscoelastic model provided a good correlation with experimental data and verified as a capable model to predict stress distribution over the network at any given time.

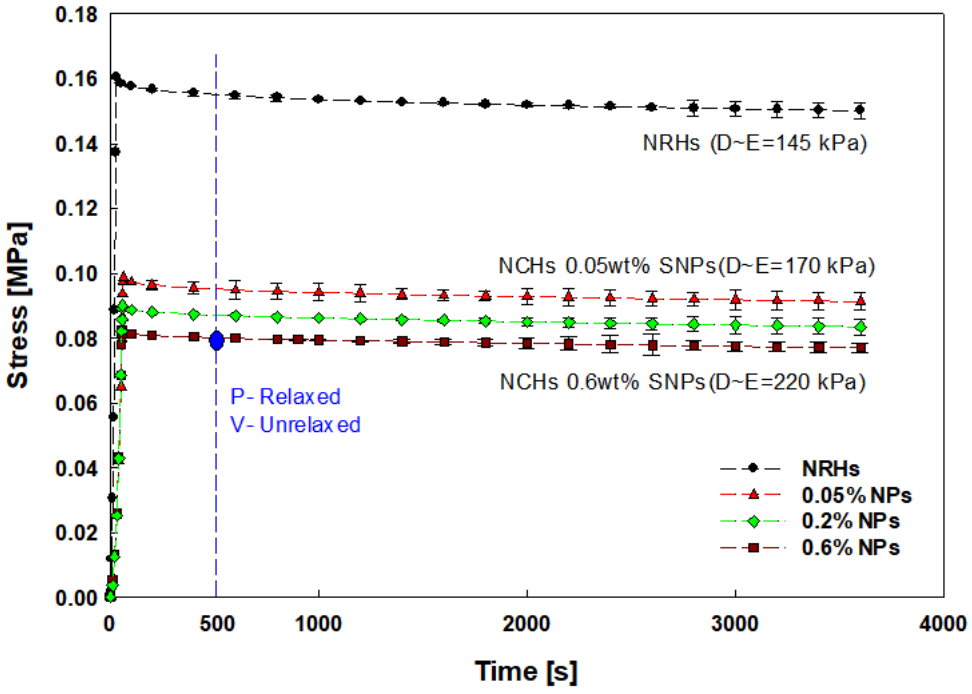

Figure 5. 5 Stress relaxation behaviour of NRHs compared with: NCHs with 0.05wt% SNPs, 0.2wt% SNPs and 0.6wt% SNPs at 50% strain (Mean (n=3) ± SD). D is the indication of diffusion rate, and E is the elastic modulus. P-relaxed is poroelastic relaxed, and V-Unrelaxed is viscoelastic unrelaxed.

Table 5. 1 Relaxation parameters for the NCHs and NRHs obtained from curve fitting.

Coefficient	NRHs	0.05wt% NPs	0.2wt% NPs	0.4wt% NPs	0.6wt% NPs
σ_f	0.154	0.095	0.086	0.085	0.079
a	-0.089	-0.059	-0.058	-0.058	-0.052
b	0.056	0.029	0.032	0.033	0.032
c	-0.080	-0.047	-0.044	-0.043	-0.041
d	0.056	0.029	0.032	0.033	0.032

A gradual decrease in stress level in the period of 1h demonstrates the amounts of stresses relaxed within the structure. Hydrogel with 0.6wt% SNPs showed the lowest peak stress and stress relaxation, as listed in Table 5.1 (σ_f = 0.079*)*. NRHs showed inferior stress relaxation compared to NCHs. Moreover, a sudden drop in stress relaxation within 3600s could indicate abrupt unzipping of covalently crosslinked chains, which was not observed in any of our samples. Cameron et al. [259] showed that a movement of loose ends of polymer chains takes place during stress relaxation tests; therefore, gels are considered viscoelastic and not viscoplastic. Minimal stress relaxation is observed in covalently crosslinked hydrogels, especially in PAAm-Alg hydrogels (similar to our formulation), compared to the soft tissues, where stress is extensively relaxed. Fitzgerald et al. [260] reported SNPs concentration has a proportional effect on stress relaxation. It was reported by Zhao et al. [199] that stress relaxation in ionically crosslinked hydrogels occurs in a short time compared to covalently crosslinked hydrogels. They proved that binding and unbinding of hydrogels' network that is ionically crosslinked is proportional to stress relaxation behavior. By exerting a force that causes unbinding ionically crosslinked networks, divalent cations detach from the anions of alginate chains and relocate (roughly by the size of the molecular units) and re-bond with another anion. In contrast, the covalently crosslinked network is not functioning similar to the ionically crosslinked networks; thus, instead of detaching, yields a longer time to relax the stress [200].

It is highlighted that an abundant amount of water in hydrogels also affects the viscoelastic responses. Fluid motion within the network would significantly impact dissipating energy from external loadings [199]. From a formulated theory of the coupled mass transport and large deformation within polymer hydrogel by Hong et al. [201], the motion of fluid inside the network and the resistance of the porous structure against the fluid migration yield macroscopic mechanical relaxation. This is different from relaxation resulting from structural deformation in the network. This phenomenon is called poroelasticity and is characterized by diffusion coefficient *D* of the fluid in the network [202] and can be obtained by the following equation:

$$D \sim Er^2/\eta \tag{5.1}$$

where *E* is the elastic modulus, *r* is the pore radius of the polymer network, and η is the fluid viscosity in the hydrogel. From the equation relation, the rate of relaxation depends on the poroelasticity. As mentioned previously, the smaller pore size results in slower fluid migration and thus slower stress relaxation. It is evident from the obtained results that a higher elastic modulus for samples loaded with 0.6wt% SNPs (215 kPa) yielded a higher diffusion rate with respect to Eq. 8 and, consequently, slower stress relaxation is shown in Table 5.1 and smaller coefficient of viscoelastic responses compared to other hydrogels. It is worth mentioning that the geometric scale *L*, of the sample, is inversely proportional to the time of stress relaxation. A smaller *L* yields faster stress relaxation due to the fluid migration in a shorter distance. However, the rate of deformations of a hydrogel is independent of the geometric scale [199]. In other words, when *L* is greater than *D*, it means that the sample scale is large enough that not let the fluid migrate to reach the end of the structure. In this state, viscoelastic relaxation occurs before poroelastic relaxation [203]. Huang et al. [198] showed this theory by using $\tau_v = L^2/D$, therefore, L>>$\sqrt{D\tau_v}$, where τ_v is the time of viscoelastic relaxation. On the other hand, L<<$\sqrt{D\tau_v}$ is the indication of poroelastic relaxation occurring before viscoelastic relaxation. From the diffusion rate theory and the achieved experimental data, the following calculations take

into account to figure out relaxation mechanism for 0.6wt% SNPs NCHs. Parameters of the Eq. (5.1) which are presented in Table 5.2, have been substitute and result in D ~ 0.009 m/s.

Table 5. 2 Diffusion rate parameters and values for NCHs with 0.6 wt% SNPs.

Parameters of NCHs (0.6 wt% NPs)	**Viscosity**	**Average Porosity Dia.**	**Elastic Modulus**
Values	20 mPa.s[261]	15 µm	215e3 Pa

By considering the thickness of our hydrogel L=14 mm, and following the diffusion theory, $\sqrt{D\tau_v}$, based on the stress relaxation test, stress relaxed and reached a plateau at 500 seconds in 0.6wt% SNPs. Therefore, 0.014 m<<$\sqrt{(0.009m/s) * (500s)}$, results in 0.014 m<< 2.12m. Thus, it verifies that poroelasticity occurred before viscoelasticity at 500 seconds. This shows that the fluid had sufficient time to migrate through the interconnected channels, while the chains conformation remained intact. In the design of bilayer hydrogels, this method can optimize the thickness of the implant. At different body-loading scenarios, fluid has enough time to migrate through the implant, or conversely, conformation takes place in chains similar to the load-withstanding mechanism in articular cartilage.

5.5 MORPHOLOGY AND EDS CHARACTERISTICS

SEM images of all hydrogel samples were used to characterize the bilayer features and mesh size of each sample with different SNPs concentrations. Uniform porosity, observed in the lubricious layer, is attributed to the interrupted polymerization process due to the excess of hydrogen molecules at the vicinity of the hydrophobic surface (polystyrene). The average diameter of pores is 10-12 µm, demonstrated in Fig. 5.6 (a). The interrupted polymerization extended to 235 µm from the hydrophobic surface, which is the lubricious layer thickness showed in Fig. 5.6 (b). The porous architecture of the lubricious layer depends on the propagation step at the polymerization process. Thus, the amount of crosslinking and excessive hydrogen at the

surface of the hydrophobic substrate results in pores of various shapes and sizes. We investigated how each concentration could affect the size of the pores and the thickness of the lubricious layer. Adding 0.05wt% SNPs resulted in larger pore sizes averaging 17-18 μm as shown in Fig. 5.6 (c). The pores gradually shrunk in size, transferring from the superficial layer through the thickness of the bilayer hydrogel. The thickness of the porous layer was enlarged to 300 μm, as is shown in Fig. 5.6 (d). Introducing more SNPs (0.2wt%) to the network that is functioning as a crosslinker promotes the polymerization process in a shorter time compared to the hydrogels with lower SNPs loading. As it is evident in Fig. 5.6 (e), the pore sizes increased to 20-39 μm, and the thickness of the porous layer increased to 452 μm, which is demonstrated in Fig. 5.6 (f). Increasing SNPs up to 0.4wt% to the network results in diminishing the size of the pores to 17 μm as a result of higher crosslinking density among the polymer chains, as shown in Fig. 5.6 (g), but an increase of the porous layer thickness up to nearly 760 μm in Fig. 5.6 (h).

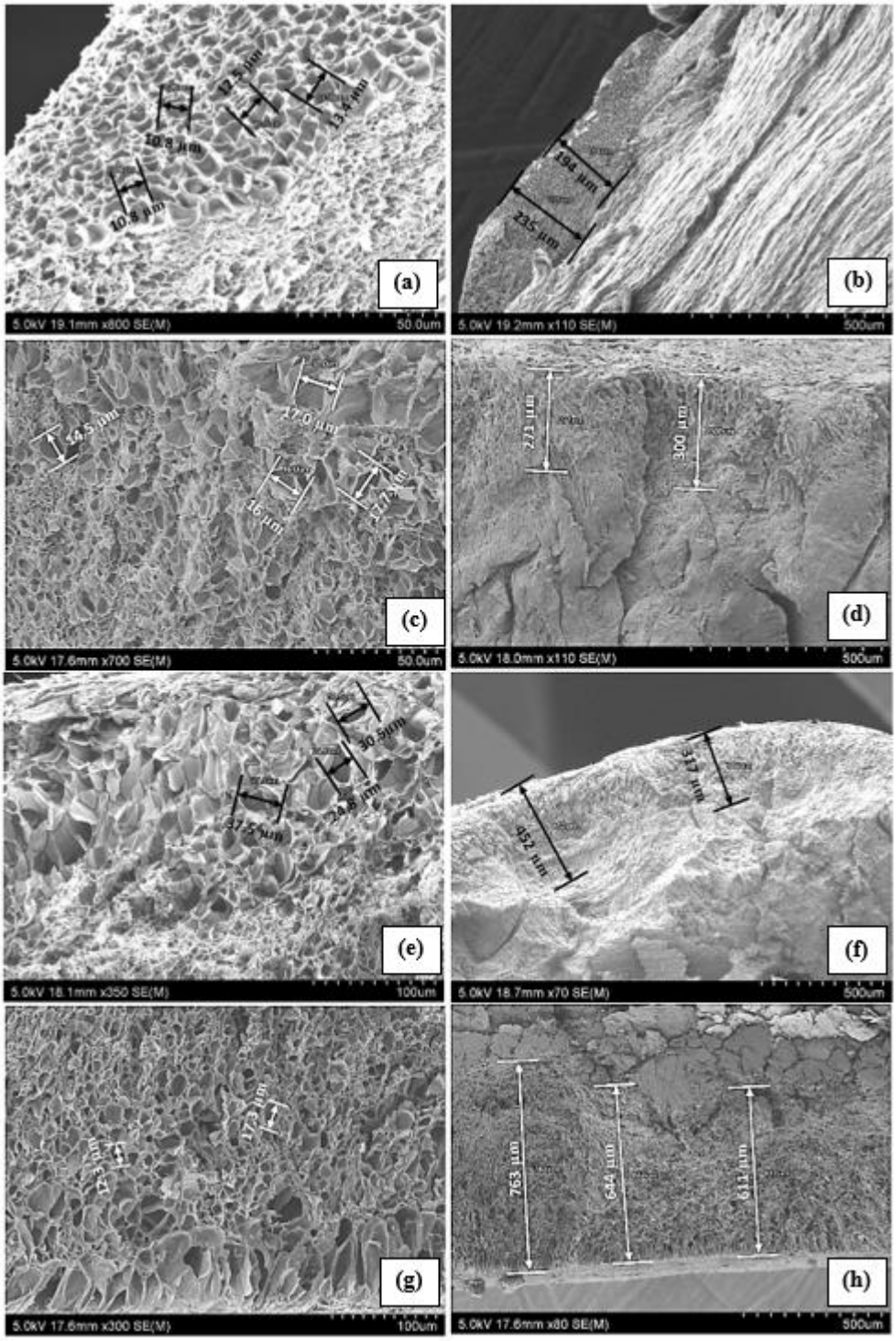

Figure 5. 6 The microstructure of the bilayer NRHs with local magnifications (a) 800x; (b) 110x, NCHs 0.05 wt% SNPs with local magnifications (c) 700x; (d) 110x, NCHs 0.2 wt% SNPs with local magnifications (e) 350x; (f) 70x and NCHs 0.4 wt% SNPs with local magnifications (g) 300x; (h) 80x.

Fig. 5.7 shows the hydrogels with 0.6wt% SNPs; however, the thickness of the lubricious layer remains intact compared to the samples with 0.4wt% SNPs. With 0.6wt% SNPs, uniform funnel-like pores were formed in the lubricious layer, as is shown in Fig. 5.7 (c,d). The average pore sizes are 13-15 μm as is shown in Fig. 5.7 (a). The uniform structure of the pores in this sample results in a higher water retention capacity and a lower coefficient of friction, the study of which is beyond the scope of this work.

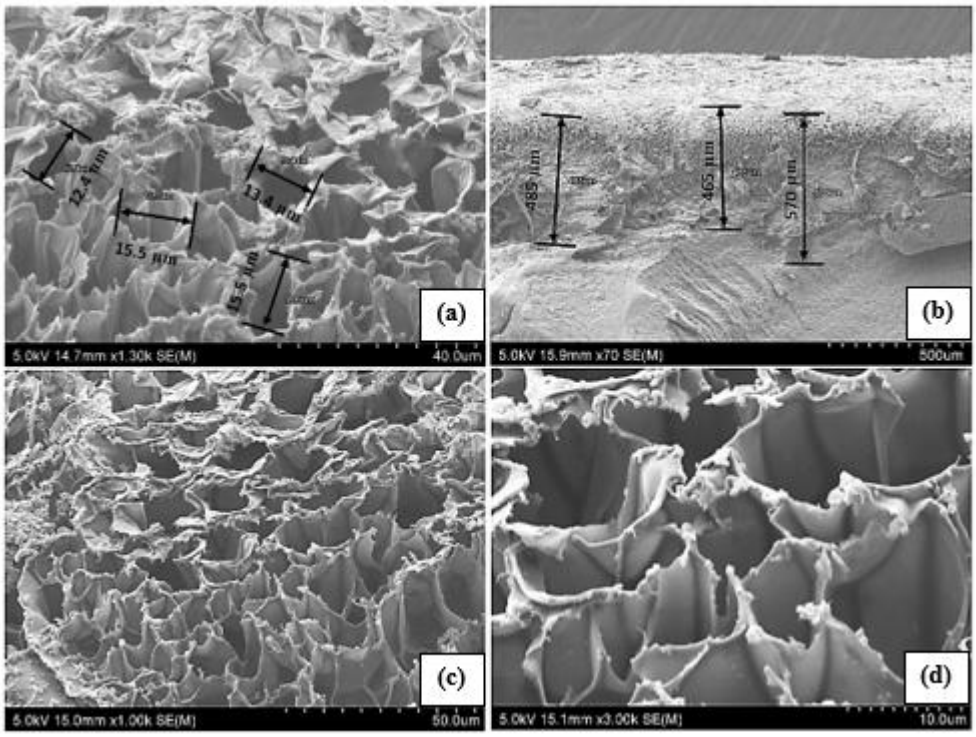

Figure 5. 7 The structure of the bilayer hydrogel strengthened by 0.6wt% SNPs with local magnifications (a) 1.30k; (b) 70x; (c) ×1.0k and (d) ×3.0k.

Fig. 5.8 illustrates EDS images with 4000x magnification and the chart of the chemical elements. SNPs and other elements were detected, and carbon counts were the highest compared to other elements, as carbon is the most abundant element in the ingredients of the hydrogels.

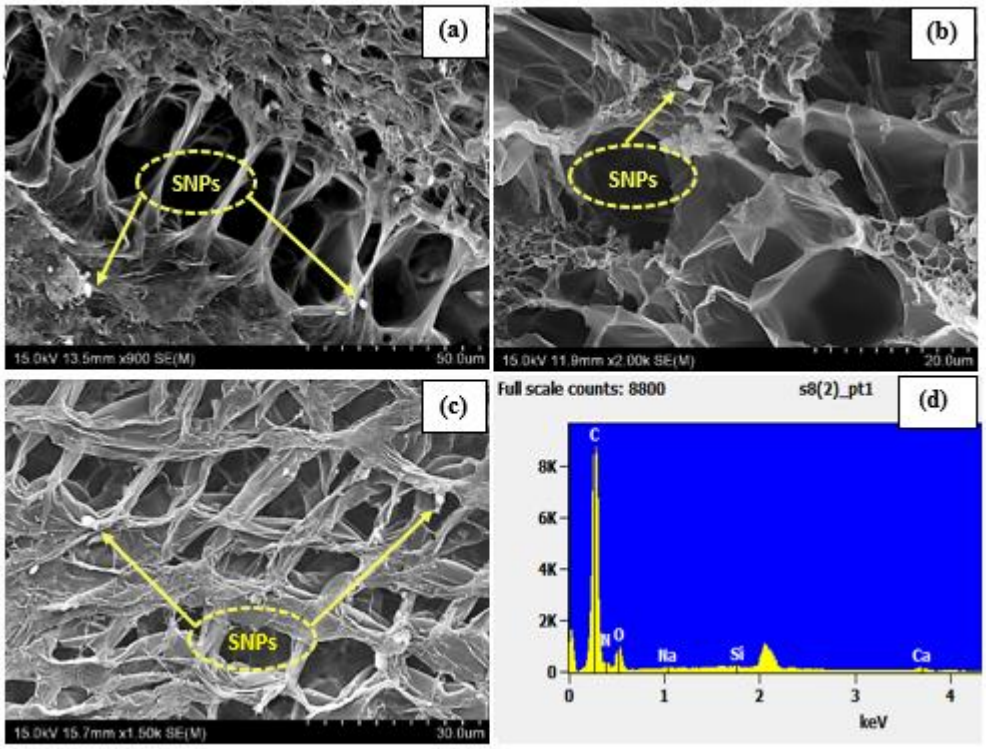

Figure 5. 8 SEM images of the hydrogel strengthened by 0.6wt% SNPs using 15.0kV power with different magnifications (a) 900x; (b) 2.0k; (c) 1.5k and (d) EDS spectra showing chemical elements count.

Monomers, crosslinkers, and initiators are the critical factors in the polymerization process. Adding SNPs would boost up interlocking and crosslinking processes in the propagation stage of polymerization. The rapid polymerization by the exacerbated SNPs at the vicinity of excessive hydrogens on the hydrophobic surface would be the reason for increasing the lubricious layer thickness [262]. The proposed NCHs with 0.6 wt% SNPs is a candidate material in the design of artificial cartilage due to its similar characteristics to the AC. The compressive stress and tangent modulus in our NCHs reached 1.4 MPa and 7 MPa, which is in the reported values of (0.1-2.0) MPa and 1.37 MPa, respectively, for native cartilage [263]. The maximum elastic modulus was 240 kPa, close to the 400 kPa elastic modulus of the native cartilage. The upper limit of the safe compressive loading regime for cartilage is 30% [264]; however, our NCHs with 0.6wt% SNPs could withstand up to 85% strain.

5.6 DISCUSSION

The mechanical characterizations showed a significant increase in compressive strength up to 1.4 MPa and doubled elastic modulus (240 kPa) by utilizing only 0.6wt% SNPs compared to the non-reinforced hydrogel. SNPs have promoted the degree of crosslinking in very weak chemically crosslinked PAAm hydrogels, which have interestingly presented the ability of SNPs to function as a crosslinker [25]. Arjmandi and Ramezani [257] reported that SNPs interact with PAAm chains resulting in network crosslinks through hydrogen bonds. Therefore, such interactions resulted in improved mechanical properties, and SNPs unlike titania NPs demonstrated the linear relationship of the crosslinking density and elastic modulus. In other words, by adding SNPs up to 0.6wt%, the elastic modulus would enhance relatively. However, from 0.6wt% to higher concentrations, the networks become brittle and stiffer. These analyses clarify that the mechanical properties of the NCHs using SNPs is the function of cross-linking density up to a certain amount of SNPs. However, SNPs saturation in the network transforms the linearity of the mechanical properties into non-linear properties.

The optimum amounts of monomers and SNPs resulted in the compression of samples up to 85% strain without failure. Strain-rate dependency is a critical consideration in the design of polymeric hydrogels. The compressive strength and tangent modulus of the knee joint cartilage has been reported in the range of 0.06-0.21 MPa and 0.26-1.37 MPa, respectively [263]. However, the cartilage solid-phase bears less pressure, and most of the energy on the joint is dissipated by the incompressible synovial fluid [35]. 0.6wt% NCHs demonstrated outstanding compressive strength higher than the mentioned threshold for the cartilage. This was the result of the bond between SNPs, alginate and AAm chains. In fact, unzipping of alginate and calcium chloride ions under the compressive load would not affect the strong bonds of AAm and SNPs since no rupture occurred at 85% strain and 1.4 MPa compressive stress. This was concluded from the compressive strength results since NRHs failed under strain-rate of $0.01s^{-1}$. Therefore, the presence of SNPs significantly attributes the compressibility, stretchability and strain-dependency responses in the

network. This improvement was found also in the recent studies by Yang et al. [265] as they showed the effect of SNPs concentrations on chemical and mechanical properties.

Viscoelastic responses improved as the stress relaxation lessened to half in all NCHs. These findings synchronized with the recent studies by Fitzgerald et al. [260] that demonstrated crosslinker variation has detrimental effects on the stress relaxation response; while total monomer concentration has a significant impact on the elastic modulus. As it was discussed in the previous section, the amount of SNPs concentrations affect the strain dependency. Also, mesh sizes vary proportionally due to more chains connections, and this could result in fluid and solid phase interaction within the network. This interaction directly impacts the energy dissipation by diffusion rate. Therefore, from the results, NCHs with 0.6wt% SNPs proved poroelastic relaxation occurred before viscoelastic relaxation. There are two hypotheses for this claim, which is the mathematical calculation from the diffusion rate theory and experimental observation from the network SEM images. An uninterrupted flow of the fluid inside the channel due to the uniform mesh results in poroelastic relaxation before viscoelastic relaxation. The balance of imposed pressure over the structure due to this uniform fluid distribution resulted in the poroelastic relaxation [203].

SEM images showed uniform funnel-like porosity with 570 µm thick lubricious layer, which is an important feature to retain interstitial fluid. Two hypotheses could be considered for this phenomenon. First, SNPs are hydrophilic and can disperse with the solution. This results in uniformity of cross-linkages, thus monotonous network architecture. Second, 0.6wt% SNPs is the very sufficient and optimum concentrations in the system by which the propagation step of the polymerization process could be accomplished promptly near the hydrophobic surface with the excessive hydrogen molecules. Therefore, there is no interruption of the polymerization process for the lubricious layer.

5.7 LIMITATIONS

It was very difficult to capture EDS images due to the high voltage of the SEM machine (15 kV). At the time of capturing images, some of the weak strings were subjected to shrink by the high voltage power. This issue resulted in re-shaping the architecture if extra time was spent on capturing images. That is why we tried to capture images as quickly as possible before reaching the polymer melting point.

5.8 CONCLUSIONS

In summary, AAm-Alg-AAc-METAC IPNs nanocomposite bilayer hydrogel, loaded with SNPs, were synthesized by the free radical polymerization method, and SEM images verified it. Silica particle elements on the polymer architecture were monitored under EDS images. Hydrogels with 0.6wt% SNPs showed uniform porosity with a funnel-like structure, which can be a promising candidate to retain interstitial fluid that is a critical function in the design of artificial cartilage. Mechanical and microscopical characteristics were investigated and compared with the non-reinforced hydrogel. The results showed SNPs entangled with polymer chains and reinforced the hydrogels enhancing load-bearing capacity, elastic and viscoelastic behavior. Hydrogels strengthened with 0.6wt% SNPs showed improved compressive strength (1.4 MPa) in the range of cartilage compressive strength. Tangent modulus was also improved using SNPs and reached 7 MPa compared to 1.37 MPa for the native cartilage. The elastic modulus reached 240 kPa, which is close to the elastic modulus of the cartilage. The tribological performance of the proposed bilayer NCHs needs to be assessed in terms of wear resistance, coefficient of friction and dominant wear mechanisms, which will be addressed in the later chapter.

CHAPTER 6

TRIBOLOGICAL ASSESSMENTS OF BILAYER NANOCOMPOSITE HYDROGELS WITH TiO_2 STRENGTHENING

6.1 COEFFICIENT OF FRICTION

Sliding wear tests were conducted on NRHs and NCHs with 0.2 wt% NPs loading. Fig. 6.1(a) illustrates mean CoF values for both NCHs and NRHs in lubricated conditions. CoF in both samples is a function of the applied load and decreases by increasing load. This behaviour is statistically significant ($p < 0.05$) for NCHs at all applied loads under lubrication. On the other hand, the effect of increasing load on the CoF was not obvious at 0.5N and 0.7N for NRH but a marked decrease was seen upon application of 0.9N. Moreover, the effect of the increasing load was not statistically significant at all loads for both samples in dry conditions. While the CoF of NRHs and NCHs did not differ significantly in dry conditions (Fig. 3(b)), this difference was statistically significant under lubrication ($p < 0.05$). This observation is of importance as articular cartilage operates under lubrication in real-life applications.

Since NCHs showed higher compression modulus (nearly three-fold) and stiffer network compared to NRHs, it experiences a higher contact pressure at a constant load. Although *Ra* and *Rq* values in NCHs are lower than NRHs, higher contact pressure in NCHs results in more asperity contacts under the boundary lubrication regime translating to higher CoF. At 0.9 N load, with the aid of bovine serum lubrication, the CoF was 0.005 in NRHs, which is close to that of the articular cartilage (0.001) [97]. The NCHs at the maximum load of 0.9 N experienced significantly lower CoF of 0.014 compared to the recently developed polyvinyl alcohol (PVA) hydrogels on natural

cartilage (CoF= 0.07) [138]. It is worth mentioning that the low CoF value in our NCHs is even attained by using an impermeable metallic ball interface, which detrimentally increases the CoF compared to those soft materials or native cartilage interface [243].

Fig. 6.1(b) shows mean CoF values for both NRHs and NCHs in dry conditions, however the differences in the mean CoF of both samples were not statistically significant. The CoF of NRHs and NCHs are distinguished clearly under lubrication. We hypothesized that modulating hydrogels with a lubricious layer and utilizing titania NPs, could effectively maximize fluid retention in the samples due to the porous layer and 'METAC's hydrophilicity nature. Generally, CoF values in NCHs are slightly higher than NRHs, and this could be because adding NPs to the system results in higher crosslinking density and a lower degree of freedom in chains. In the absence of lubricant, network mesh size and the lubricious layer fluid retention capacity control the CoF values. In dry contact, the highest CoF was observed for both samples at 0.7 N contact load. The variation of pore pressurization due to the diffusion rate resulted in a non-linear response of CoF as a function of load. At 0.5 N load, the pressure is not enough to push away the water under wear track in the lubricious layer, and pores retain the fluid. Once load increases to 0.7 N, the higher contact pressure yields fluid migrations through the interconnected channel, and the arid region would increase CoF, especially with smaller mesh size networks, which is the network of 0.2 wt% NCHs. However, increasing load to 0.9 N, the whole lubricous layer is deformed into conformal contact containing a highly hydrated region and decreases the CoF. The lesser difference between the decreased CoF in NCHs than NRHs from 0.7 N to 0.9 N is because the stiffer network of NCHs was conformed less than NRHs, and also due to the smaller mesh size, less water would be pumped to the conformed region. Therefore, increasing the contact interface temperature during dry sliding leads to water vaporization, and therefore, CoF would increase. Furthermore, the effect of sliding speed variations under a constant load was investigated and no meaningful correlation between the sliding speed and CoF was observed in both NRH and NCH samples.

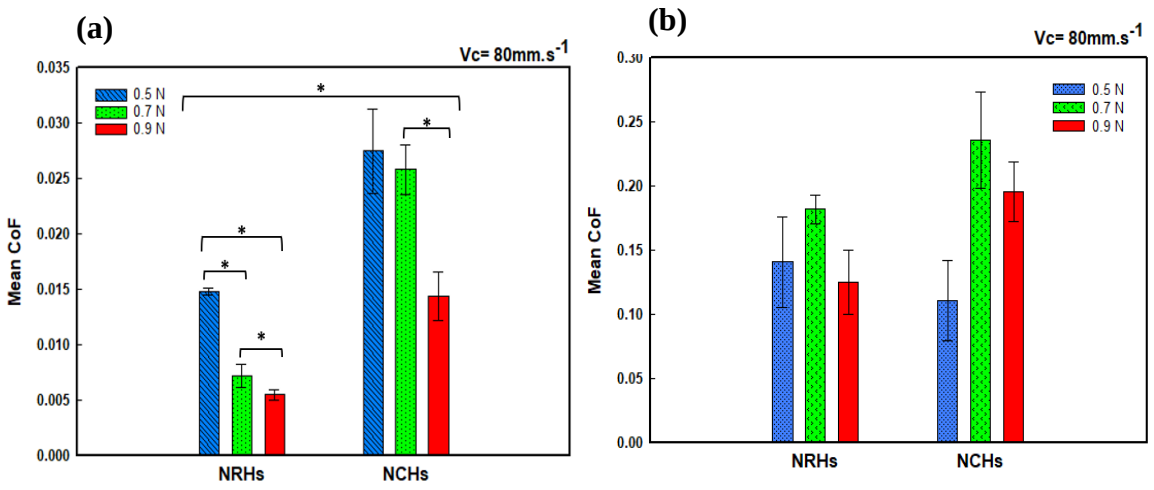

*Figure 6. 1 Mean friction coefficient values for NRHs and NCHs loaded by 0.2 wt% TiO2 NPs with respect to the applied loads with a constant sliding speed (80 mm/s), under (a) lubricated, and (b) dry conditions, (n= 3 ± SD). * Statistical significance performed using ANOVA and post-hoc Tukey test (p < 0.05).*

Variations of CoF with time for lubricated conditions are shown in Fig. 6.2. NRH under 0.5 N applied normal load, Fig. 6.2 (a), demonstrates severe fluctuations over time. The presence of hydrogen at the vicinity of the hydrophilic substrate resulted in heterogeneous density in the superficial region. Therefore, a gradual increase in density through the thickness upsurge the shear strength over time. Thus, a prolonged period of sliding motion could destroy the sparser network and reach the denser region. Consequently, the CoF increased by elapsed time while the lubricious layer is worn out. A few drops during tests indicate network flaws due to the propagation step of the polymerization process. A steadier variation of CoF with time at 0.9 N load is because of immense pressure on the spongy architecture that compressed it to the bulk layer. Hence, from 7500 seconds onward, the CoF reached a plateau, which shows the lubricious layer destroyed thoroughly, and the probe slides against the firm architecture of the bulk layer. However, in NCHs, an unwavering increase at 0.5 N load depicts a firm and stiff lubricious architecture compared to the NRHs, as shown in Fig. 6.2(b). When the load increased to 0.7 N in NCHs, slight drops in CoF can be interpreted as boundary lubrication transition to the mixed lubrication. This is because of the consistent CoF in the boundary lubrication regime, descent to another firm layer,

indicating the mixed lubrication regime due to some asperity contacts. By increasing the load to 0.9 N, conversely, a sudden drop can be explained by two reasons: firstly, plenty of regions with abundant preserved water and, secondly, thicker lubricious layer compared to NRHs.

Fig. 6.2(c) demonstrates variations of CoF with time in NRHs and NCHs, under 50 mm/s sliding speed with a constant load of 0.7 N. A steady trend represents the boundary lubrication regime with a thin fluid film that maintains shear stresses uniformly among asperity contacts. Under this condition, no severe destruction of lubricious layers was observed after sliding wear tests. In contrast, when sliding speed increased to 110 mm/s, extreme fluctuations in NRHs show the destruction of the lubricious layer, and as time passes, wear debris increases the viscosity of the fluid, and consequently, CoF increased gradually. A sharp increase at the end could be because of the destroyed lubricious layer and sliding mate in contact with bulk or denser network, which is shown in Fig. 6.2(d). NCHs, yet, show smooth fluctuations compared to NRHs. This is because of thicker bonds of chains and strengthened lubricious layer resisting against the high-speed sliding contact.

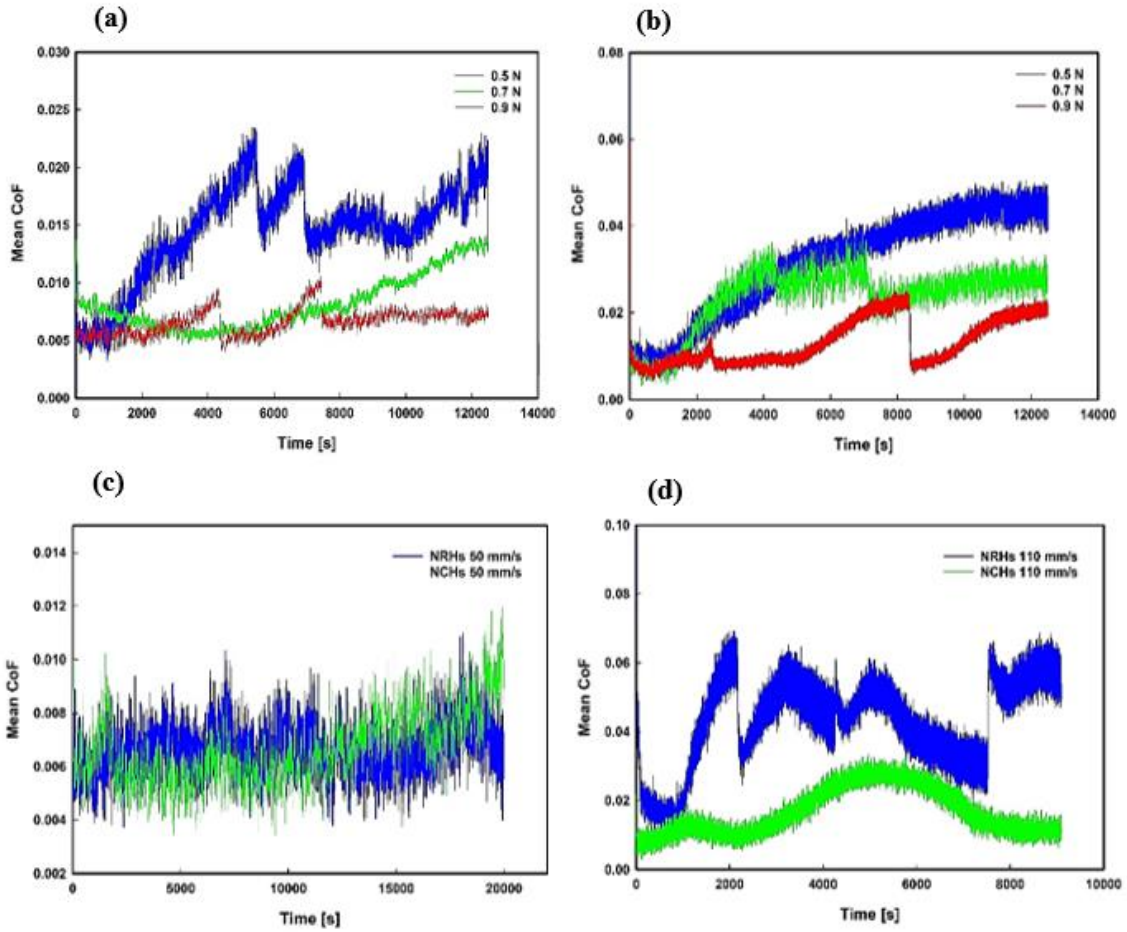

Figure 6. 2 Variation of CoF with time at different normal loads (constant speed 80 mm/s), in (a) NRHs, (b) NCHs samples, (c) sliding speed of 50 mm/s (constant load 0.7 N), and (d) sliding speed of 110 mm/s (constant load 0.7 N).

6.2 WEAR VOLUME

A stylus profilometer was used to map the wear profile and define the depth and width of wear tracks for different test conditions. Fig. 6.3 shows the effects of load and sliding speed on wear track profiles of NRH and NCH samples. From Fig. 6.3(a) and (b), at 0.5 N load, a chattered profile is observed in NRHs, compared to a smoother profile in NCHs. This has been discussed in the SEM images section. As expected, wear tracks are wider and deeper for samples tested under higher normal loads. It can also be seen that wear scars get bigger in both sets of samples by decreasing the sliding speed. By topping up 0.2 wt% NPs, wear depth and width decreased by increasing sliding speed. At low speed, polymer chains can be stretched because of their propensity to adhere to the sliding counterface. Nevertheless, at higher speeds, less adhesion

occurs between the sliding pair, and material loss would be minimized [266]. Therefore, NCHs demonstrated less adhesion tendency to the counterface because of its smaller mesh size with the lower conformational degree, as shown in Fig. 6.3 (c) and (d).

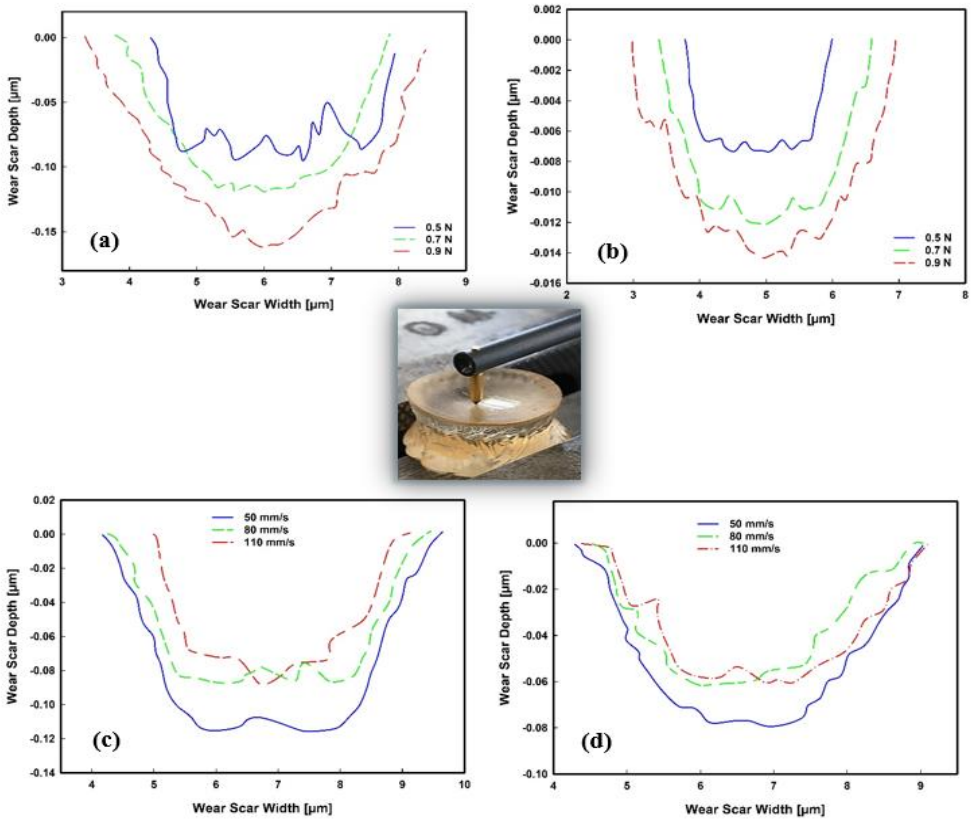

Figure 6. 3 Wear track profiles at different loads (constant sliding speed 80 mm/s) for a) NRHs, b) NCHs with 0.2 wt% NPs; and at different sliding speeds (constant load 0.7 N) for c) NRHs, d) NCHs with 0.2 wt% NPs. All tests were conducted under the lubricated condition.

Wear volumes were calculated from profiles with the procedure explained in section 2 and are shown in Fig. 6.4. By increasing load, wear volume increased in both NRHs and NCHs. however, no statistically significant changes in wear volume were observed above 0.7N. Moreover, the difference in wear volumes of NCHs compared to NRHs was statistically significant ($p < 0.05$). However, loading hydrogel samples with 0.2 wt% TiO_2 NPs promoted the polymer strength and significantly reduced wear volume. For example, under 0.9 N applied normal load, wear volume in NCHs is half of the wear volume observed in NRHs. This can be

attributed to the role of NPs on entangling strands that resist chain rupture. Wear volume is an indication of the rate of polymer chain disconnection [22]. This rate is lower in NCHs compared to NRHs, under increasing load. The wear volumes of samples tested in dry conditions are not presented in this paper because the wear volume values were significantly higher than the lubricated condition. The effect of sliding speed on the wear volume is more profound for NCHs compared to NRHs. While the difference in wear volumes between the two samples at different sliding speeds were statistically significant ($p < 0.05$), varying the sliding speed did not have a significant effect on the wear volume of NRHs. However, the wear volumes of NCH were similar at 50 and 80 mm/s and significantly higher at 110 mm/s. Due to the dominant boundary lubrication regime at 50 mm/s sliding speed, the duration of asperity contacts is long enough at each cycle to stretch the material and drag them away from its unit cell. Furthermore, a longer period of the test at 50 mm/s sliding speed, compared to 80 mm/s and 110 mm/s, results from inadequate time for adhesion of contacting mates and greater wear volume showed in Fig. 6.4(b). From 80 mm/s to 110 mm/s, the wear volumes decrease at a slower rate.

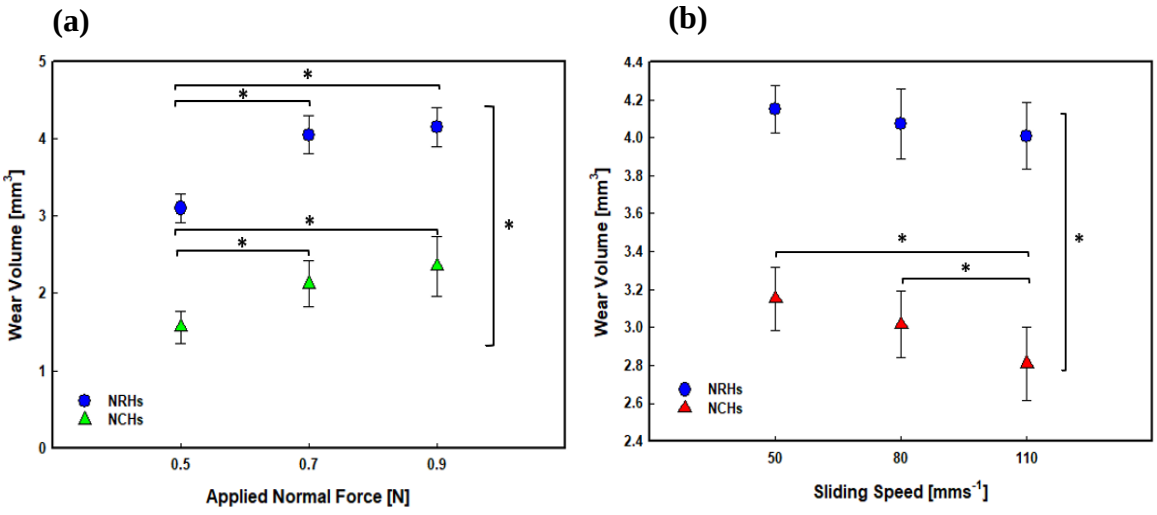

*Figure 6. 4 Wear volume in NRHs and NCHs samples in lubricated condition as a function of (a) load and (b) sliding speed (n=3 ± SD). * statistical significance performed using ANOVA and post-hoc Tukey test (p < 0.05).*

6.3 WEAR MECHANISMS

In lubricated conditions, under 0.5 N applied load, at the edge of the wear track in NRHs, large cracks were observed, as shown in Fig. 6.5(a). On the other hand, NCHs, exhibited short cracks as shown in Fig. 6.5(b). Li et al. [221] reported that under normal load, adhesion decreases at higher crosslinking degrees. NCHs with high crosslinking and low adhesion exhibited better wear resistance compared to NRHs. When the load increased to 0.7 N, the worn porous regions in NRHs resulted from the adhesive wear mechanism is shown in Fig. 6.5(c). Because of longer dangling polymer chains and their interweaving possibilities [267], sliding mate motion caused remarkable wear on NRHs surface. The debris generated from the surface wear and release of nanoparticles in NCHs caused shallow grooves due to abrasive wear [216], as shown in Fig. 6.5(d). It shows how the lubricious layer in NCHs, due to the shorter and sparser dangling polymer chains [191], reduced the wear rate.

Under 0.9 N applied load, several microcracks were observed in NRHs, and the superficial surface deteriorated thoroughly, as can be seen in Fig. 6.5(e). From 0.7 N to 0.9 N, cracks and wear debris indicate adhesive wear was transformed into fatigue wear mechanism, which shows that the PAAm-PAAc hydrogels' wear mechanism is load-dependent. The high contact pressure in NRHs resulted in substantial conformational normal and lateral forces. Such pressure on the lubricious architecture introduces greater conformational contact, and more fluid is retained in the concave-shape of the sliding track. Thus, the overall CoF value remained low, as shown in Fig.6.5(a), similar to the boundary lubrication regime in the Stribeck curve. In NCHs, an impregnated network with TiO_2 NPs with a bovine serum lubricant corporation demonstrated a very firm and stiff surface. Although the formation of the lateral grooves is sliding of one surface across another and can be described by referring to the modified Amontons' law [268] as below:

$$F_{LT} = S_c \pi a^2 + \mu F_N \quad (6.1)$$

where S_c is the shear strength, a is the contact surface radius, μ is the friction coefficient, and F_N is the normal force. The first term is adhesion-controlled, and the second term is load-controlled. When load increased to 0.9 N, the deformed lateral surface in NCHs is shown in Fig. 6.5(f). The increased lateral force would deform chains along the wear track, and as soon as it overcomes network shear strength, delamination occurs, and cracks are initiated. Therefore, at this stage, the first term of Amonton's law, which is adhesion-controlled, is dominant. Furthermore, we assume that cracks are not plastic deformation because a recent report shows that PAAm hydrogels have the elastic response and not time-dependent plasticity response [269]. An earlier study also found that wear increases surface stiffness [270]. PAAm shows elasticity-dominant toughening by interacting with the weak, noncovalent bonds between polymer chains and the strong covalent bonds along the polymer chains [271]. That is why deformed lines were observed along the wear track and not across them.

At 50 mm/s sliding speed with 0.7 N applied normal load, NRHs exhibited convex-shape debris stuck on the surface after the test. The adhesion strength between material and sliding mate deprived and chains were not debonded in lubricated condition, shown in Fig. 6.5(g). Thus, slowing down the sliding speed maintains the adhesion wear mechanism in NRHs. Nevertheless, due to the weak bonds between dangling chains and contacting mate asperities, they have enough time to debond with a significantly minimized rupture. In NCHs, due to the stronger bonds of strands, a very firm flattened surface with micro ploughing was observed in Fig. 6.5(h). Dunn and Sawyer [214] reported that at slower speeds, the mechanism of lubrication is ascribable to the mesh size and its capacity to confined-fluid within the contact. Therefore, fine mesh sizes of NCHs could confine more fluid than NRHs as tremendous energy is the essence of fluid migration beneath the mating contacts. By increasing the sliding speed to 110 mm/s, NRHs appeared with the flattened wear tracks and no wear debris was observed. Generally, wear volume decreased at the highest speed because of a shorter test period and less adhesion bonds between contacting mates. In NRHs, wear track can be distinguished by a few micro-grooves on its wear track, which is demonstrated in Fig 6.5(i), while micro-scratches could be observed on the NCHs wear track,

as illustrated in Fig. 6.5(j). In NCHs, some grains on the surface remained intact that could attribute to the repulsive interaction with the mating surface [272]. It is worth mentioning that at this sliding speed, the wear track was not detectable in NCHs by naked eyes. This is attributed to the improved wear resistance of NCHs compared to NRHs.

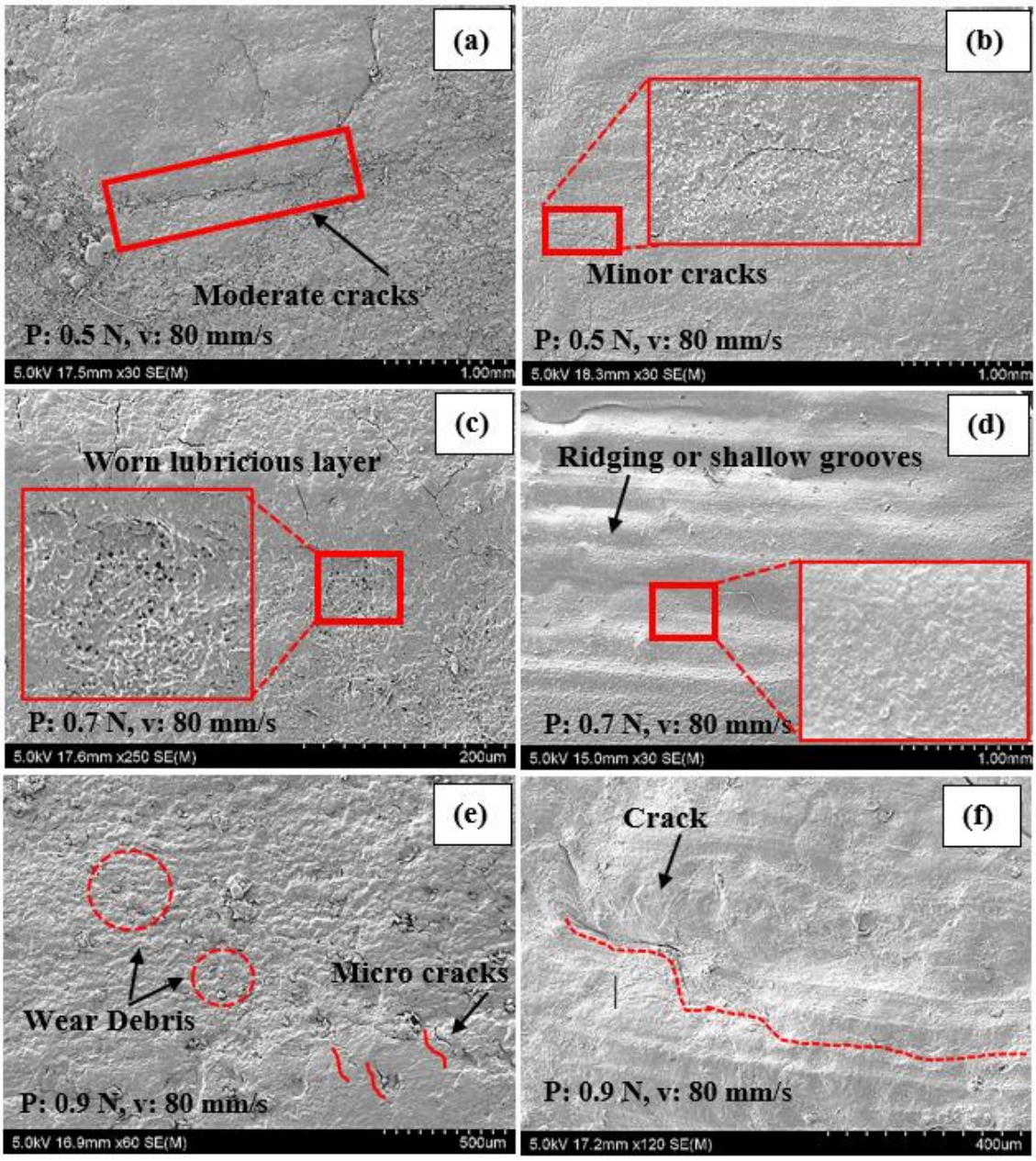

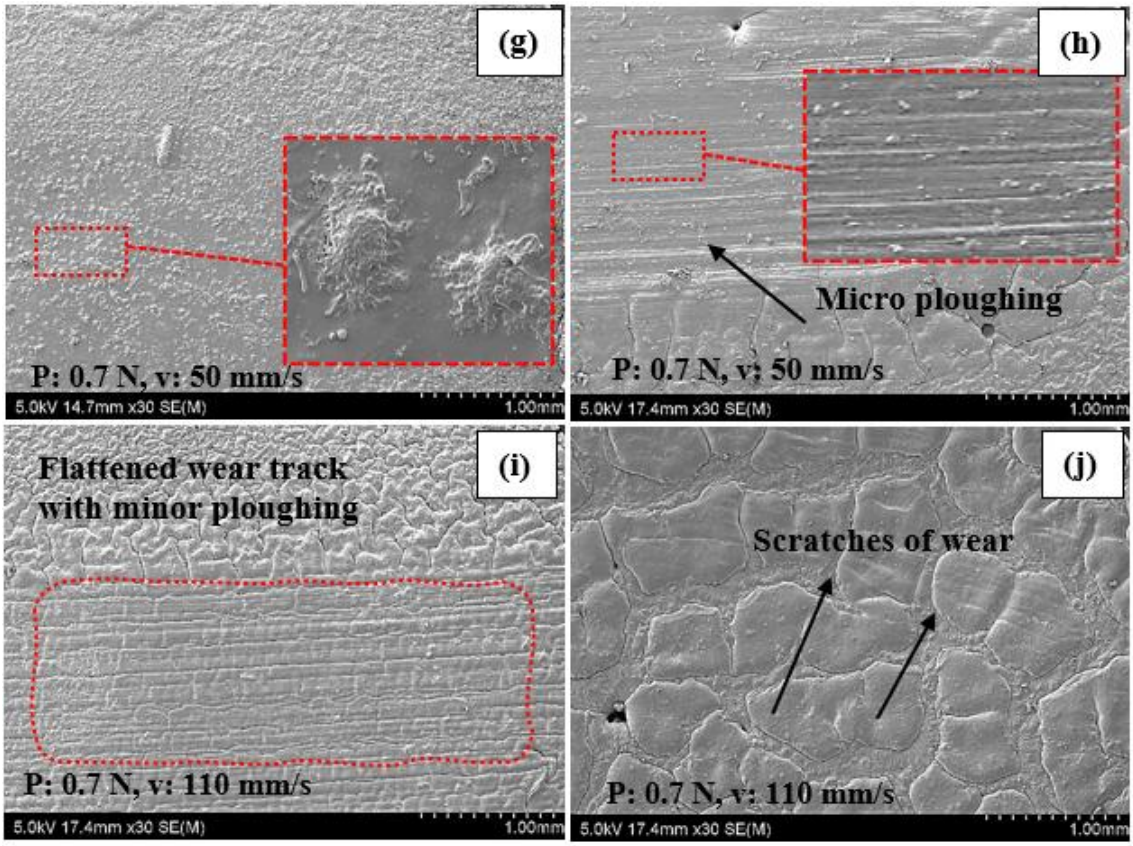

Figure 6. 5 SEM images of the wear tracks at different loads and sliding speed in the lubricated condition in NRH samples: (a), (c), (e), (g), (i); and NCH samples: (b), (d), (f), (h), (j).

6.4 LUBRICATION MECHANISMS

It is reported that hydrogels do not follow the classical engineering Stibeck curve [214]. Fig. 6.6 shows three different regimes by variation of load and speed in bilayer NCHs. Pore-pressurized lubrication is a regime that, due to high contact pressure and the lowest speed, hydrogel surfaces thoroughly deformed into conformal contact, which is obvious in Fig. 6.5(f). Moreover, high contact pressure would pump out fluid from the interconnected channels of the lubricious layer and provide a hydrated region for sliding contact. CoF value is the lowest, load-controlled (Fig. 6.1(a)) and increases gradually (Fig. 6.2(b)). By decreasing load and increasing speed, less conformal contact results in less fluid volume being diffused out of the lubricious layer and less hydrated. At this stage, disentangle of weak chains would yield free-end strands or chains engage with contacting mate asperities and increase the level of CoF. The ridging surface

observed in Fig. 6.5(d) is due to the stretched free-end chains along the sliding track that were woven together and formed the attained surface. Such a movement initiates dynamic shear and pressure-dependent viscosity [214] and is called elastoviscous transition. By increasing speed, CoF decreases because, at low load and high-speed, adhesion-control would take place. At this regime, fluid is preserved and confined in the network, and the lubricious layer is not worn because of minimum adhesion strength between asperities due to fast sliding mate movement. At this stage, mesh size and water retention play a vital role in wear and friction. It is worth mentioning that the lubrication mechanism in articular cartilage is the function of its permeability and the shear-thinning viscosity to originate a thin film of synovial fluid lubrication that detach the cartilage mates and minimize the imposed load [112].

Different lubrication regimes (boundary lubrication, mixed lubrication, Elastohydrodynamic lubrication (EHL), and fluid film lubrication) are illustrated in the Stribeck curve shown in Fig. 6.6. At high load and low speed (50 mm/s, which is equivalent to walking speed), due to the diffusion rate theory, pore pressurization occurred due to high contact pressure of sliding mate and conformational deformation. By decreasing load and increasing speed (in the region of 80 mm/s, which is the speed of jogging), the CoF is dependent on both load and speed factors with different responses. This regime is called elastoviscous transition because extended or disentangles polymer chains in the lubricious layer attach to contacting mate asperities and level up the CoF when speed is 80 mm/s. Due to the confined fluid in the lubricious layer at the high-speed region, a thoroughly hydrated regime could detrimentally decrease CoF, which is titled fluid-confined lubrication. f_p, f_v stands as the function of pressure and speed, respectively.

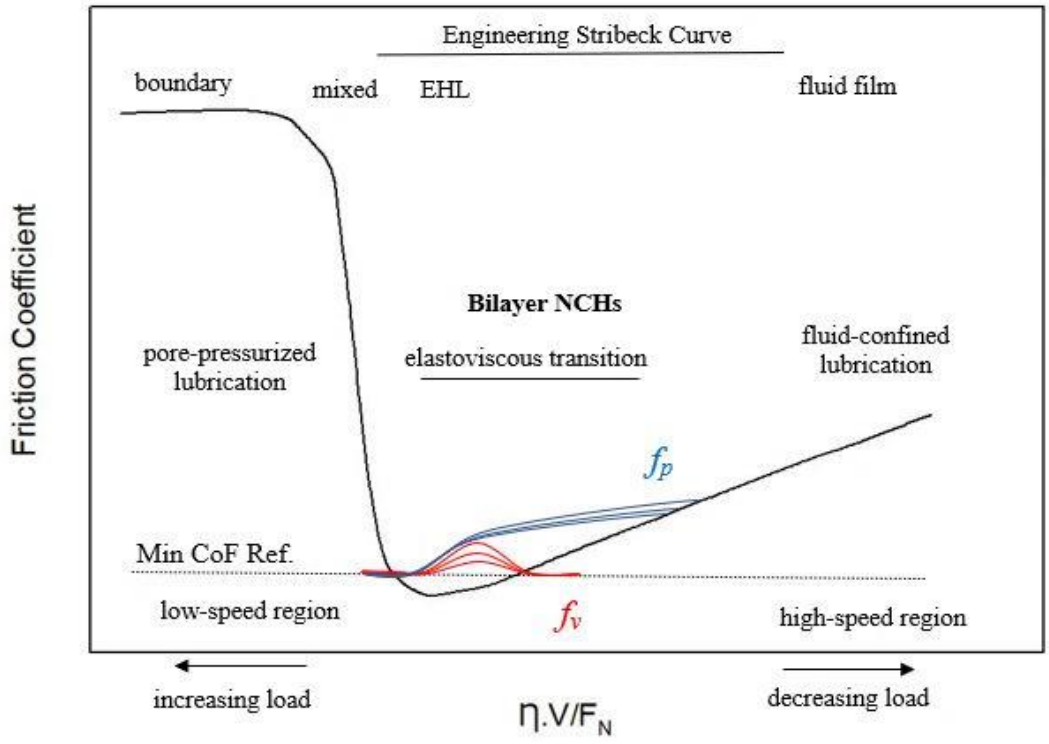

Figure 6. 6 Schematic illustration of the engineering Stribeck curve.

6.5 DISCUSSION

Tribological test results showed a low mean coefficient of friction values of 0.007 and 0.014 for non-reinforced hydrogels and NCHs, respectively. In this section, we discuss the overall tribological performance of the NRHs and NCHs from CoF results to wear mechanisms cohesively. The main reason to have lower CoF in NRHs compared to NCHs could be interpreted as the function of network stiffness. NRHs with lower stiffness and network density resulted in lower shear resistance compared to NCHs. Stiffer bonds of NCHs detrimentally withstood against the sliding movement and that was the reason for increased shear forces to the probe and consequently higher CoF [273]. Recent studies also showed that titania NPs interact with carboxyl groups and form complexes with TiO_2 NPs resulted in crosslink polymer chains [8]. Denser mesh, however, is the factor of fluid migration through the interconnected channel and therefore, impacting the sliding track lubrication. That is why by imposing low load (0.5N) in NCHs, less fluid could exude away and yield to maximum CoF at this stage. Results also proved NCHs subjected to maximum load (0.9N), demonstrated the lowest CoF due to concave-shape of

deformation and supplying a very hydrated track for the sliding mate, because this substantial load could diffuse out fluid that was trapped in the porosity. At this stage, it can be concluded that CoF variations are directly proportional to crosslinking density and network stiffness. This claim can be supported by analyzing wear scars profiles that mapped for NRHs and NCHs according to Fig. 6.3 in the previous section.

Wear scar profile of the NRHs under load variations showed not only inferior network stiffness, but also substantial network flaws compared to NCHs. This claim could be interpreted from Fig. 6.3 (a) when with low load, fluctuated profile was presented in NRHs. Wider wear width of NRHs compared to NCHs also is proof of chains disintegration by the increasing load. This phenomenon, however, was minimized overall in NCHs. It is worth mentioning that a minor variation of wear scar in NCHs from 0.7 N to 0.9 N is due to titania NPs properties in the improvement of load-independency characteristics. Speed factor was used to analyze the adhesive strength of the networks. Speed variations could be used to light up the path of chains tendency to adhere to the sliding mate which is a critical element in tribological studies [214]. Thus, the low load regime in NRHs showed a very wide wear width compared to NCHs. This finding proves that titania NPs minimize adhesive strength between sliding mate and polymer surface. This is an outstanding improvement in the design of any artificial cartilage, because less adhesive strength results in less shear forces and therefore, lower wear loss [274].

Continuing on this discussion, from SEM images it was clear that adhesive material dispatched from the surface of NRHs and caused a worn lubricious layer. Nevertheless, this case was never observed for NCHs. A very smooth track after sliding tests showed the strength of the network integration. Although we should remind that the hydrogel-steel contact used in this study could significantly increase adhesion and wear rates, compared to hydrogel-AC or hydrogel-hydrogel contact interfaces. It was reported that hydrogel-on-hydrogel could show a lower CoF threshold and wear loss volume according to recent studies [62, 243]. Moreover, the elimination of wear debris in NCHs proved the effect of titania NPs on shortening dangling chains in the

lubricious region. The presence of wear debris in long term sliding motions would increase the viscosity of the lubricant and that could be another factor for levelling up the CoF. In summary, the wear resistance of NCHs improved significantly, SEM images showed that wear mechanisms are a combination of adhesive wear and fatigue wear, although titania NPs enhance chains strength, minimize adhesive strength and improve wear loss volume compared to NRHs.

6.6 LIMITATIONS

The limitation of this part of the research was wear scar measurement by the stylus profiler. Since we used the stylus with the diamond tip, we could not measure the wear width and depth right after tribological tests. This is because hydrogel was hydrated and the wear track was soft, thus, the movement of the stylus across the wear track could have initiated cracks. Therefore, no accurate results for wear depth could be obtained. In this study, we placed the hydrogel in the incubator room at a constant temperature (35^{o}C) until it is dehydrated fully and dried thoroughly. Then samples were ready for wear scar measurements. Although after drying hydrogel samples, the wear track was subjected to a minor size variation and slightly shrunk. For a precise wear scar measurement, an optic profiler is required with a fast-capturing images feature (depending on the sliding stroke) that researchers can use right after the sliding test.

6.7 CONCLUSIONS

0.2 wt% NPs loading in modulated polymerized hydrogel enhanced elastic modulus, hardness, compressive modulus, and swelling ratio compared to non-reinforced counterpart. Over-utilized NPs (> 0.2 wt% NPs) weaken mechanical properties due to increased stress concentrations around interlaced chains and increase brittleness.

Utilizing 0.2 wt% NPs, as an optimum amount regarding mechanical responses resulted in a low CoF of 0.01 under the highest sliding speed in lubricated conditions. In dry conditions, CoF was reduced by 50% compared to NRHs at the highest sliding speed. CoF trends in NCHs showed

a firm and stable network with minimum fluctuations compared to NRHs. NCHs wear volumes were also significantly lower compared to NRHs.

SEM images illustrated NCHs lubricious surfaces strengthened, where shallow grooves and small micro-cracks and scratches were observed compared to NRHs with worn our lubricious layer and larger micro cracks.

Lubrication regimes mainly depend on the mesh size in the hydrogel network. NCHs, with a gradual decrease in mesh size through the lubricious layer thickness, showed the essence of NPs in water retention in a confined network and fluid migration. Their effects on pore pressurized lubrication, elastoviscous transition, and fluid-confined lubrication were discussed in section 6.4.

CHAPTER 7

TRIBOLOGICAL EVALUATION OF SILICA NANOPARTICLE ENHANCED BILAYER HYDROGELS

7.1 COEFFICIENT OF FRICTION

Sliding wear tests were conducted on NRHs and NCHs samples with 0.6 wt% NPs loading that resulted in superior mechanical properties. Fig. 7.1 demonstrates that CoF mean values in lubricated conditions decreased by increasing the applied load. In NCHs, the imposed load of 0.5 N resulted in contact pressure of 0.305MPa, close to the lower range of contact pressure experienced by AC (≈ 0.1MPa) [97, 178, 220]. Under this applied load, the mean CoF value was around 0.009, as can be seen in Fig. 7.1 (set 1). The attained CoF values are comparable to that of cartilage at 0.001 [97]. Under 0.7 N load, a 50% drop in CoF was observed in NRHs, which is because of the conformed region under the sliding probe due to its lower stiffness than NCHs. Therefore, the accumulated fluid reduces the shear forces of contacting asperities and lowers the CoF. In NCHs, due to a firmer lubricious network and smaller porosity sizes, insignificant fluid diffuses out. Then it boosts up asperity adhesion and maintains CoF at the same level. Geong and Osada [275] reported that CoF magnitude is highly contingent on the repulsion-adsorption friction. A high-water level is retained at a high-load regime due to its electrostatic repulsion and, therefore, yields to lower frictional forces between contacting asperities. Statistical analysis showed significant differences within groups and between NRHs and NCHs. Both 0.5 N and 0.7 N load demonstrated significant differences for the attained CoF.

The effect of sliding speed (at a constant load of 80 mm/s) on CoF for both NRHs and NCHs is shown in Fig. 7.1 (set 2).. It has been reported that SNPs in the lubricious layer affect polarity and surface tension, subsiding CoF [276]. Short strands at low sliding speeds result in lower CoF values [277], since SNPs enhance crosslinking density. SNPs also promoted abrasion resistance because they shortened the length of dangling chains and reduced residual stress and shrinkage [278]. Statistical analysis showed significant difference for all sliding speeds between NRHs and NCHs.

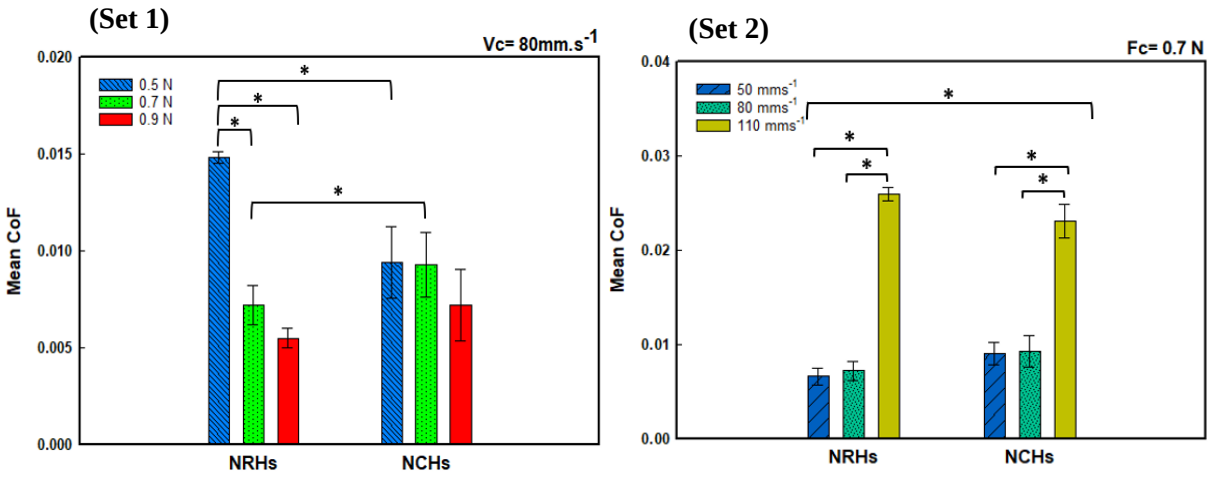

*Figure 7. 1 Mean coefficient of friction values for NRHs and NCHs in lubricated condition with respect to (set 1) applied load (Vc=80 mm/s), and (set 2) sliding speed (Fc=0.7 N) in lubricated condition, (n= 3 ± SD). * statistical significance performed using ANOVA and post-hoc Tukey test ($p < 0.05$).*

Fig. 7.2 illustrates mean CoF values for both NRHs and NCHs in dry contact conditions. We hypothesized that advancing hydrogels with lubricious layer incorporation with METAC monomer would retain water and significantly impact CoF. Hence, tribology tests were conducted in dry conditions to test this hypothesis. NRHs showed different patterns compared to NCHs. By increasing load to 0.7 N, matrix stiffness in NRHs conformed, and due to loose mesh sizes, network destructions resulted in weaving dangling chains; thus, CoF values increased. At 0.9 N load, CoF decreased in NRHs due to the entire compression of the lubricious layer by the contacting mate, which promptly deteriorated it. Therefore, the sliding probe mainly slides over

the bulk region with a firmer matrix and lower CoF. In NCHs, continuous decrease by increasing load is because of a firmer stiffness through the thickness in the lubricious layer and its sufficient resistance against a higher contact pressure. In set 2, sliding speed variations highlight the adhesion between counterparts. From 50 mm/s to 110 mm/s, a lower CoF threshold in NCHs shows SNPs effect in reducing the adhesive strength of dangling chains.

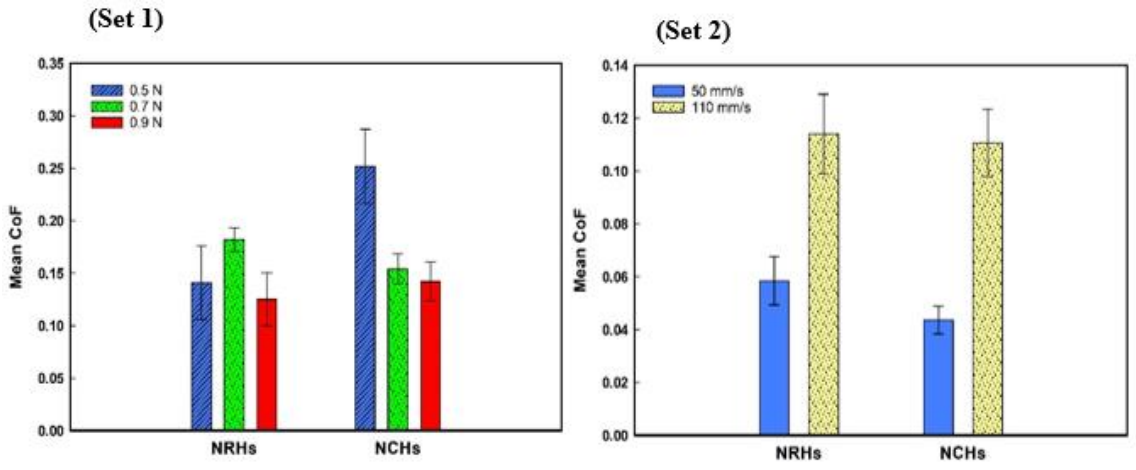

Figure 7. 2 Mean coefficient of friction values for NRHs and NCHs with respect to (set 1) applied load (Vc=80 mm/s), and (set 2) sliding speed (Fc=0.7 N) in dry condition, (n= 3 ± SD).

In dry conditions, the hydrogel matrix stiffness depends on SNPs, mesh size, the conformational volume of the wear track, and fluid loss due to generated heat. Furthermore, elastic force and its distribution on surface energy are correlated to the adhesion variations and CoF. Robert and Kendall used rubber and glass contact in their experiments and reported that at a low-load regime, strong adhesion was found when the surfaces were dry. Therefore, the Johnson–Kendall–Roberts (JKR) model was used to estimate surface energy, adhesion, and contact area to address friction values, especially in the absence of lubricant in our proposed bilayer system [279]. We assumed, due to different crosslinking densities, dangling polymer chains, and porosity architecture presented in NRHs and NCHs, stored elastic energy and lost surface energy between asperities contact. Therefore, consideration of the contact equilibrium from elastic matings requires considering total energy U_T as the function of the contact radius. In

the system, total energy U_T is the summation of the stored elastic energy U_E, the mechanical energy associated with the applied load U_M, and the surface energy U_S.

$$U_T = U_E + U_M + U_S \tag{7.1}$$

The surface energy U_s is defined as below:

$$U_S = -\pi {a_1}^2 \gamma \tag{7.2}$$

where a is the radius of the circle of contact area, γ is the energy per unit contact area that is obtained by:

$$\gamma = \frac{P_0(R_1+R_2)}{\pi R_1 R_2} \tag{7.3}$$

where P_0 is the normal load imposed on the hydrogel, R_1 is the radius of the contacting indenter, and R_2 is the radius of the deformed hydrogel under the contacting load.

$${a_1}^3 = RP_1/K \tag{7.4}$$

Elastic contacts of indenter and hydrogel are calculated as below:

$$k_1 = \frac{1-v_1^2}{\pi E_1} \qquad k_2 = \frac{1-v_2^2}{\pi E_2} \tag{7.5}$$

where v is the Poisson's ratio and E the Young's modulus of each material. All of the mentioned terms are presented in Table 7.2 at the end of this section. From Eq. 7.3, R and K can be obtained by $R = R_1R_2/(R_1 + R_2)$ and $K = 4/3\pi(k_1 + k_2)$. Thus, in Eq. 7.2, the surface energy is obtained as below:

$$U_S = -\pi\gamma\left(\frac{RP_1}{K}\right)^{\frac{2}{3}} \tag{7.6}$$

The elastic energy U_E is the difference between imposing energy to the system U_1 and releasing energy from the system U_2. The attained graphs for both NRHs and NCHs are shown in Fig.7.3.

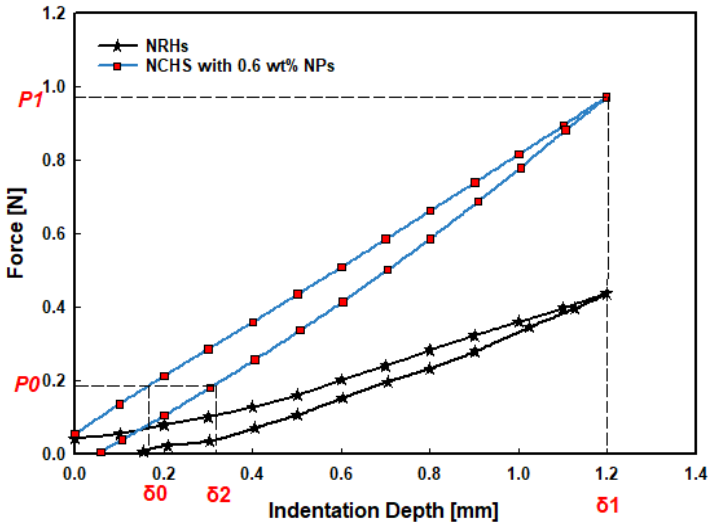

Figure 7. 3 Load-displacement graphs for NRHs and 0.6 wt% loaded NCHs.

Therefore, stored elastic energy is:

$$U_E = U_1 - U_2 \tag{7.7}$$

Neglecting surface forces, load P_1 was imposed to form the contact radius of a_1, which requires energy U_1.

$$U_1 = \int_0^{P_1} \frac{2}{3} \frac{P^{\frac{2}{3}}}{K^{\frac{2}{3}} R^{\frac{1}{3}}} dP = \frac{2}{5} \frac{P_1^{\frac{5}{3}}}{K^{\frac{2}{3}} R^{\frac{1}{3}}} \tag{7.8}$$

Keeping the contact radius at a_1, the load then decreased to P_0 to give the system's final state, releasing energy U_2.

$$U_2 = \int_{P_0}^{P_1} \frac{2}{3} \frac{P}{K a_1} \, dP = \frac{1}{3K^{\frac{2}{3}} R^{\frac{1}{3}}} \left[\frac{P_1^2 - P_0^2}{P_1^{\frac{1}{3}}} \right] \tag{7.9}$$

Therefore, substituting Eq. 9 and Eq. 10 into Eq.8, the elastic energy equation is attained as follows:

$$U_E = \frac{1}{K^{\frac{2}{3}} R^{\frac{1}{3}}} \left[\frac{1}{15} P_1^{\frac{5}{3}} + \frac{1}{3} P_0^2 P_1^{-\frac{1}{3}} \right] \quad (7.10)$$

The mechanical potential energy U_M of the applied load P_0 is:

$$U_M = -P_0 \delta_2 \quad (7.11)$$

where δ is the elastic displacement and can be obtained by:

$$\delta = \frac{2}{3} P / K a_1 \quad (7.12)$$

Thus, the final mechanical energy U_M is:

$$U_M = -P_0 \left[\delta_1 - \frac{2}{3} \frac{(P_1 - P_0)}{K a_1} \right] = \frac{-P_0}{K^{\frac{2}{3}} R^{\frac{1}{3}}} \left[\frac{1}{3} P_1^{\frac{2}{3}} + \frac{2}{3} P_0 P_1^{-\frac{1}{3}} \right] \quad (7.13)$$

Substituting Eq. 7, Eq. 11 and Eq.14 into Eq. 2 results in total energy U_T

$$U_T = \frac{1}{K^{\frac{2}{3}} R^{\frac{1}{3}}} \left[\frac{1}{15} P_1^{\frac{5}{3}} + \frac{1}{3} P_0^2 P_1^{-\frac{1}{3}} \right] - \frac{1}{K^{\frac{2}{3}} R^{\frac{1}{3}}} \left[\frac{P_0 P_1^{\frac{2}{3}}}{3} + \frac{2}{3} P_0 P_1^{-\frac{1}{3}} \right] - \gamma \pi \frac{R^{\frac{2}{3}} P_1^{\frac{2}{3}}}{K^{\frac{2}{3}}} \quad (7.14)$$

Table 7.1 presents variables used to calculate interfacial surface energy for samples. The total energy in NCHs increased by up to four-fold compared to NRHs. Results showed that even by a higher amount of surface, mechanical and stored elastic energies in NCHs, which indicates enhanced adhesion strength, CoF values in dry conditions were reduced compared to NRHs. It presents that NCHs strengthened with SNPs significantly improved mechanical and tribological performances compared to NRHs.

Table 7. 1 Variables used for total energy calculations of hydrogel samples.

Variables	***NRHs***	***NCHs***
Elastic modulus (E)	150 kPa	240 kPa
Poisson's ratio (v)	0.5	0.5
R	0.7 mm	0.5 mm
P_0	0.1 N	0.2 N
P_1	0.4 N	1.0 N
δ_1	1.2 mm	1.2 mm
δ_2	0.4 mm	0.35 mm
δ_0	0.2 mm	0.18 mm
U_S	34.22	170.88
U_E	11.28	62.34
U_M	0.035	0.164
$\boldsymbol{U_T}$	**22.97**	**108.71**

The variation of CoF versus time for both NRHs and NCHs are shown in Fig. 7.4 CoF in NRHs, under 0.5 N load, fluctuated during the sliding wear tests. It indicates the instability of the network resistance against shear forces. A continuous increase up to 5500s and a sudden fall demonstrate shear stresses overcome the network strength. The SEM image of the lubricious layer for NRHs shows irregular and weak bonding that yields unstable resistance showed in Fig. 7.4(a). In contrast, Fig. 7.4(b) illustrates reasonable stability in network resistance after topped up by 0.6 wt% SNPs. The SEM image of NCHs in Fig. 7.4(d) presents a very regular and firm mesh network, which averts the lubricious layer destruction in the early stages. It is worth mentioning that lines for NCHs in Fig. 7.4(b) for both 0.7 N and 0.9 N loads were smoothed to a single line for the better graph presentation since all results fall in the minimum CoF threshold. SEM images, along with CoF trends, ascertain the prominence of the size of the linkages and meshes. It is clear

that the optimum size of crosslinked chains detrimentally minimizes the network destruction rate. It is because of the improvement in chains transverse micromotions. A sudden fall in CoF could be due to the unlinked spaces in meshes present in NRHs. It has been reported that transverse micromotions of linkages steadily increase the CoF until the breaking point due to their material loss [221].

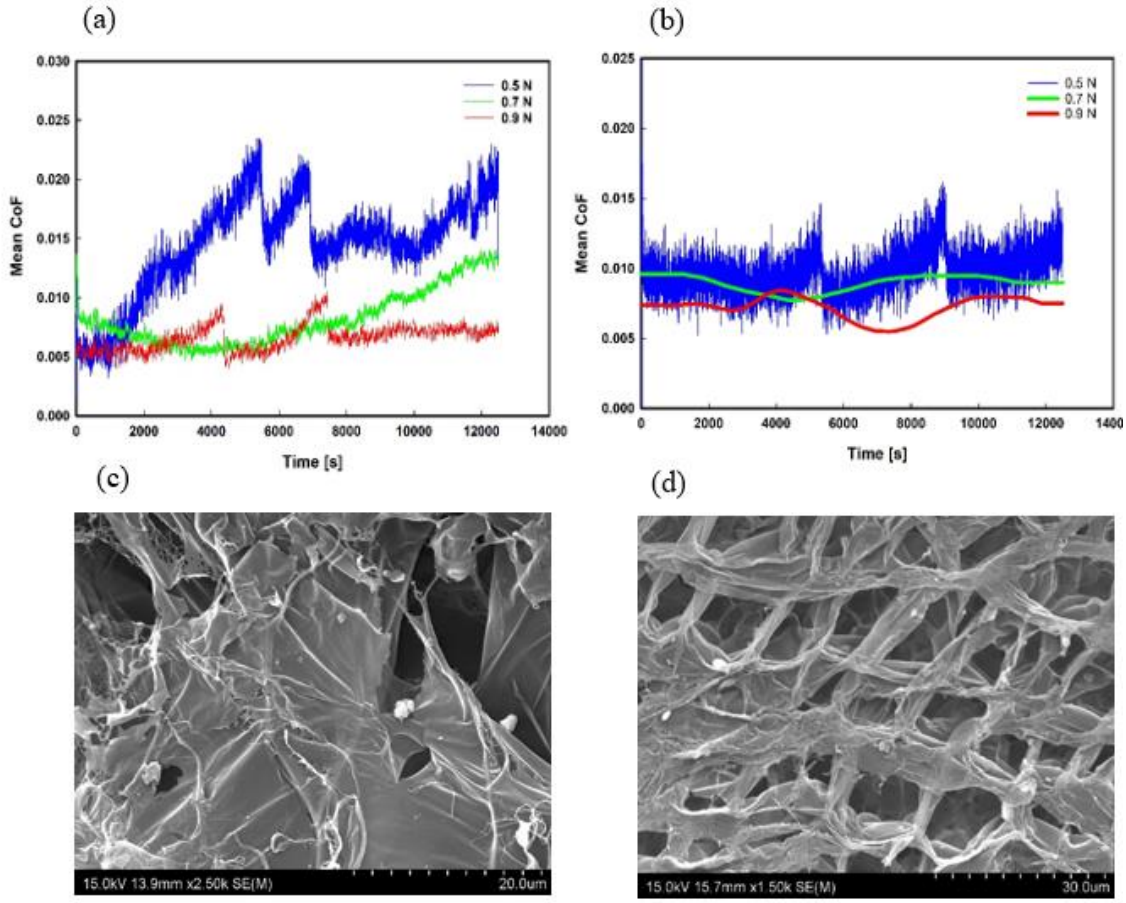

Figure 7. 4 Variations of CoF versus time for 1000 m sliding wear tests at 0.5 N, 0.7 N and 0.9 N; in (a) NRHs and (b) NCHs. SEM images of the superficial layer in (c) NRHs and (d) NCHs.

7.2 WEAR VOLUME

The stylus profiler was used to map the depth and width of the wear scars. The variations of wear profiles under different loads and sliding speeds are shown in Fig. 7.5. At 0.5 N load in NRHs, a severely chattered profile was obtained compared to NCHs, indicating unlinked porosity

through the lubricious layer's thickness in NRHs. However, a flatter and narrower profile in NCHs shows well-distributed crosslinking, illustrated in Fig. 7.5 (b).

Overall, the wear profiles in NRHs tested under 0.7 N and 0.9 N applied loads are more sweeping than NCHs. This phenomenon is because of the network elastic energy absorbed by the pressure from the contacting ball. The greater elastic energy in NCHs resulted in a lower transverse deformation imposed by contacting mate. By increasing speed, the worn area decreased because of the adhesion tendency between contacting mates. At higher speeds, less adhesion strikes between contacting asperities and, therefore, less material loss, reported by Kim et al. [266]. This phenomenon becomes prominent with the abundance of long-length dangling chains in the superficial layer in NRHs.

In NCHs, the worn profile gradually decreased by increasing sliding speed; however, in NRHs, wear depth remains intact from 80 mm/s to 110 mm/s. This shows that wear in NRHs is independent at higher sliding speeds by which adhesion strength would not decrease. In both samples, wear depth did not exceed 15 µm, which is much lower than the thickness of the lubricious layer (235 µm in NRHs and 485 µm in NCHs).

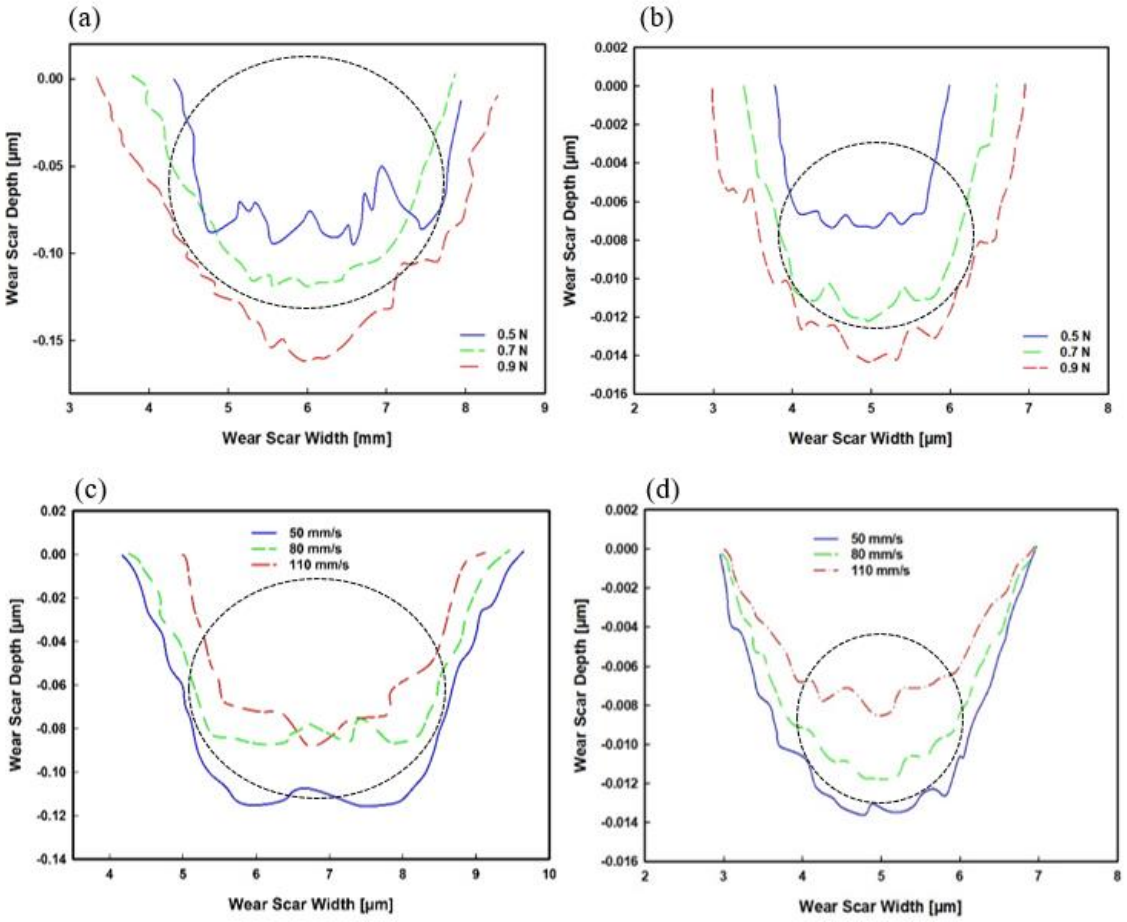

Figure 7. 5 Wear scar depth and width at different loads under a constant sliding speed of 80 mm/s for a) NRHs, b) NCHs samples; and at different sliding speeds under a constant load of 0.7 N for c) NRHs, d) NCHs samples.

The wear volume of samples are presented in Fig. 7.6. Increasing load resulted in increased wear volume in both NRHs and NCHs, as shown in Fig. 7.6 (a). However, introducing 0.6 wt % SNPs strengthened up the wear resistance of the NCHs and its wear volume is less than one-third of the wear volume in NRHs. By increasing sliding speed, wear volume overall decreased in both NRHs and NCHs. Significantly improved wear resistance in NCHs was due to lessening adhesion tendency and higher elastic energy, as described in the previous section. Our formulation shows significant wear loss reduction by utilizing additional monomers (AAc, METAC) and SNPs. AAc incorporation with SNPs reported excellent tensile properties and elongation at break up to 900% [280] and also showed SNPs were encapsulated by polymer chains and formed core-shell structure [281], which supply a firmer structure for sliding contacts. Both NRHs and NCHs

showed significant difference statistically under applied load and sliding speed. Also two-factors ANOVA analysis showed significant difference with each group of controlled and treated samples.

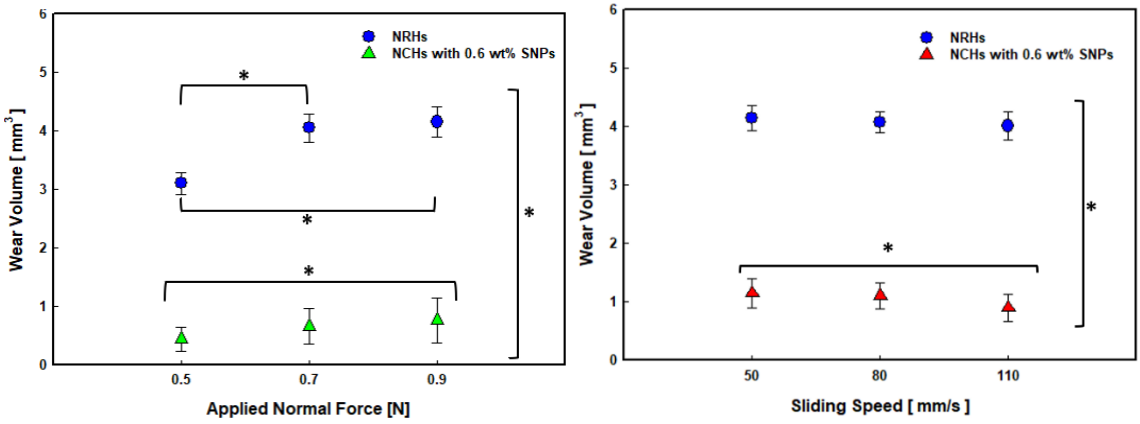

*Figure 7. 6 Wear volume of NRHs and NCHs in lubricated conditions at different (a) loads and (b) sliding speeds (n=3 ± SD). * statistical significance performed using ANOVA and post-hoc Tukey test ($p < 0.05$).*

7.3 WEAR MECHANISMS

In lubricated conditions, at 0.5 N load in NRHs, minor scoring was observed in Fig. 7.7(a), and this is due to network flaws or loops associated with self-bonding or crosslinking deficiency. Fig. 7.7(b), presents NCHs, showing an integrated and connective surface. Minor plowing improved polymer plastic deformation with the same experiment set compared to NRHs. By increasing the load to 0.7 N, significant distinctions are elucidated in the wear mechanisms of NRHs and NCHs. NRHs showed the worn lubricious layer due to the moderate adhesive wear mechanism in Fig. 7.7(c). It indicates the brittle fracture of dangling chains and disconnectivity of the network, as also discussed in the recent research study [216]. In contrast, a minor adhesive patch and moderate depression in NCHs occurred due to the enhanced plastic deformation in strands in Fig. 7.7(d). It is evident that by increasing the applied load from 0.5 N to 0.7 N, in NRHs samples, the wear mechanism transformed from abrasive to adhesive phase. In contrast, in NCHs, the accumulative plastic rate only increased without evidence of disintegrated tissues. At

0.9 N load, as illustrated in Fig. 7.7(e), microcracks and wear debris were observed in NRHs, and the superficial surface deteriorated. From 0.7 N to 0.9 N, cracks and wear debris indicate adhesive wear was transformed to fatigue wear mechanism showed in Fig. 7.7(e). This shows that the PAAm-PAAc hydrogels' wear mechanism is load-dependent. However, in NCHs, moderate accumulative plastic deformation was observed, which shows wear mechanism remains mostly intact compared to lower load magnitudes in Fig. 7.7(f). Utilizing SNPs leads to the load-independent wear mechanism of the NCHs network.

By maintaining load constant and slowing down the sliding speed to 50 mm/s, convex-shape debris on the surface of NRHs appeared, and rubble-shape particles on the surface of NCHs illustrated in Fig. 7.7(f) and (g), respectively. In NCHs, shorter strands were debonded, rolled under the sliding ball, and formed rubble-shape particles. Comparing NCHs with the same applied normal load and higher sliding speed (*p=0.7, v=80 mm/s*) in Fig. 7.7(d), the adhesive patches contain tiny spheres on the surface. When sliding speed is 80mm/s, adhesion between asperities stuck them up in sparser zones. On the other hand, when the speed decreased to 50 mm/s, contacting asperities had sufficient time to detach spheres, roll them over, and distribute them randomly due to a longer test period. Increasing sliding speed to 110 mm/s resulted in a flattened superficial layer in NRHs with laminated layers along the sliding direction. Conversely, in NCHs, the wear track is barely recognized since the prompt movement of the sliding ball and lessened adhesion minimized asperities engagements and the wear loss.

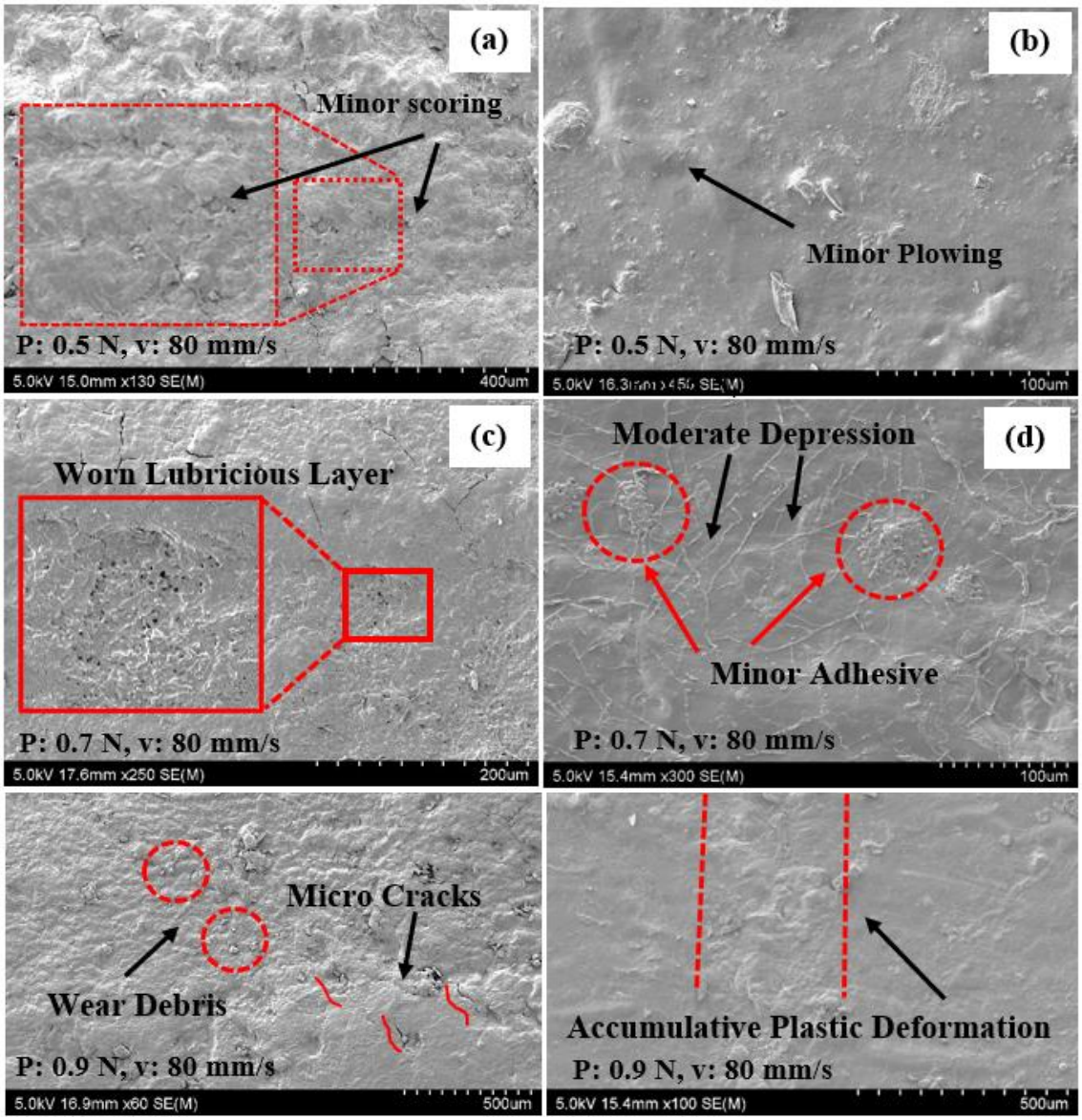
(a)
Minor scoring
P: 0.5 N, v: 80 mm/s
5.0kV 15.0mm x130 SE(M)
400um
(b)
Minor Plowing
P: 0.5 N, v: 80 mm/s
100um
(c)
Worn Lubricious Layer
P: 0.7 N, v: 80 mm/s
5.0kV 17.6mm x250 SE(M)
200um
(d)
Moderate Depression
Minor Adhesive
P: 0.7 N, v: 80 mm/s
5.0kV 15.4mm x300 SE(M)
100um
Micro Cracks
Wear Debris
P: 0.9 N, v: 80 mm/s
5.0kV 16.9mm x60 SE(M)
500um
Accumulative Plastic Deformation
P: 0.9 N, v: 80 mm/s
5.0kV 15.4mm x100 SE(M)
500um

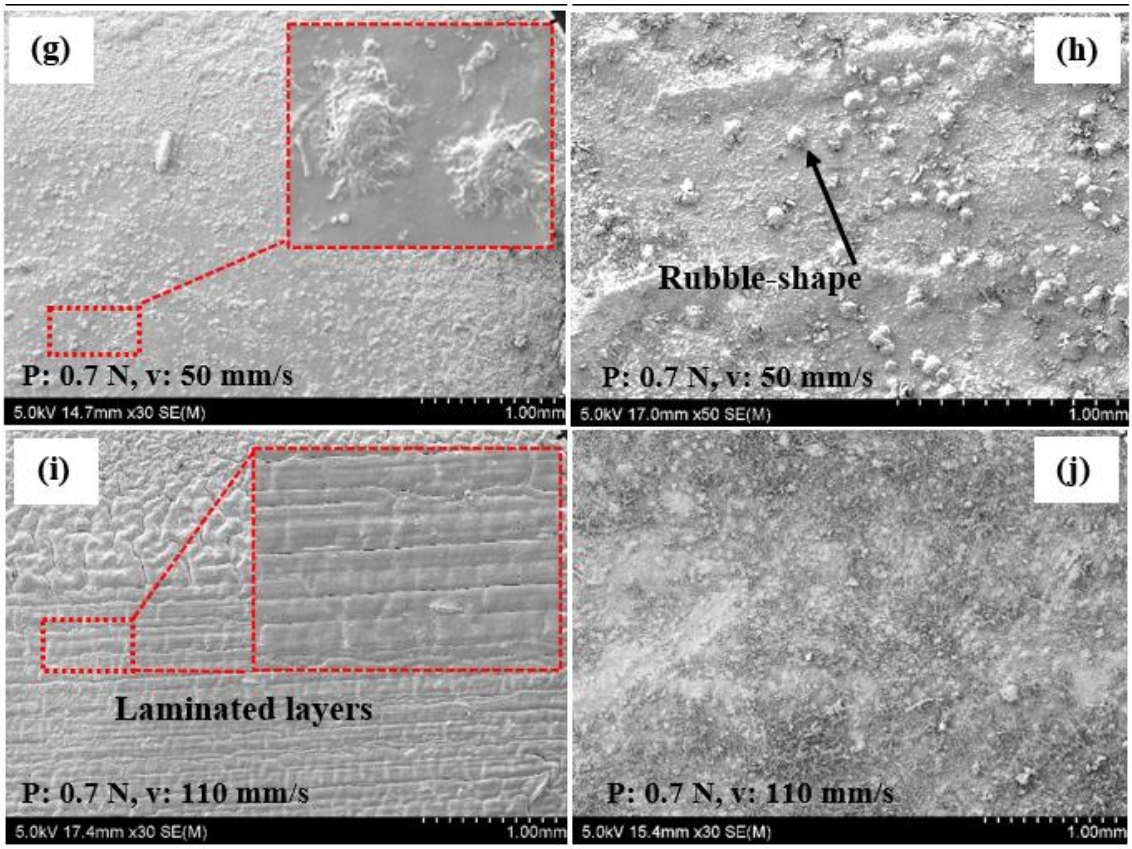

Figure 7. 7 SEM images of the wear tracks at different loads and sliding speeds in lubricated condition in NRHs by (a), (c), (e), (g), (i) and NCHs samples by (b), (d), (f), (h), (j).

7.4 LUBRICATION MECHANISMS

Hydrogel materials do not follow the Stribeck engineering curve [214]. Because hydrogels are viscoelastic and constant pressure was maintained during the sliding wear tests; therefore, boundary lubrication and fluid film lubrication regimes are not relevant. Thus, three main regimes have been developed for hydrogels: pore-pressurized lubrication, elastoviscous transition, and fluid-confined lubrication, as shown in Fig. 7.8. According to our experimental setup, the elastoviscous regime has been focused and models were developed with the aid of load and sliding speed factors. By increasing speed, CoF decreases because, at low load and high-speed, adhesion-control would take place. At this regime, fluid was preserved and confined in the network, and the lubricious layer was not worn because of minimum adhesion between asperities due to fast

sliding-mate movements. At this stage, mesh size and water retention play a vital role in wear and friction mechanisms. At maximum contact pressure (4.25 MPa), a large amount of water would pump out due to high conformal contact, which results in less adhesion between contacting asperities in NCHs observed in Fig. 7.7(f). This phenomenon results in lower shear stress and CoF, especially for NCHs with shorter strands.

In contrast, in NRHs, long dangling chains could be woven during the reciprocating movement, resulting in a sudden-detached region, as shown in Fig. 7.7(e). Because of the described phenomenon, reciprocating movement initiates dynamic shear, and also due to the fluid viscosity alteration by mixing with polymer debris, elastoviscous transition (EVT) occurs [214]. Furthermore, by decreasing load, a large amount of water traps in the interconnected channel and does not diffuse out, which results in less conformal-hydrated region with an increased CoF. This regime in hydrogels is called fluid-confined lubrication (FCL). That is why, by moving from EVT to FCL regime, CoF increases. SNPs detrimentally play a crucial role in the transition of EVT to FCL regime, since a gradual increase in CoF was drawn in NCHs compared to NRHs. By considering the speed factor (F_v), less CoF magnitude variation was mapped for NCHs. F_v and f_p stand for speed and load factors, respectively. It is worth mentioning that the lubrication mechanism in articular cartilage is a function of its permeability and the shear-thinning viscosity to originate a thin film of synovial fluid lubrication that detaches the cartilage mates and minimizes the imposed load [112].

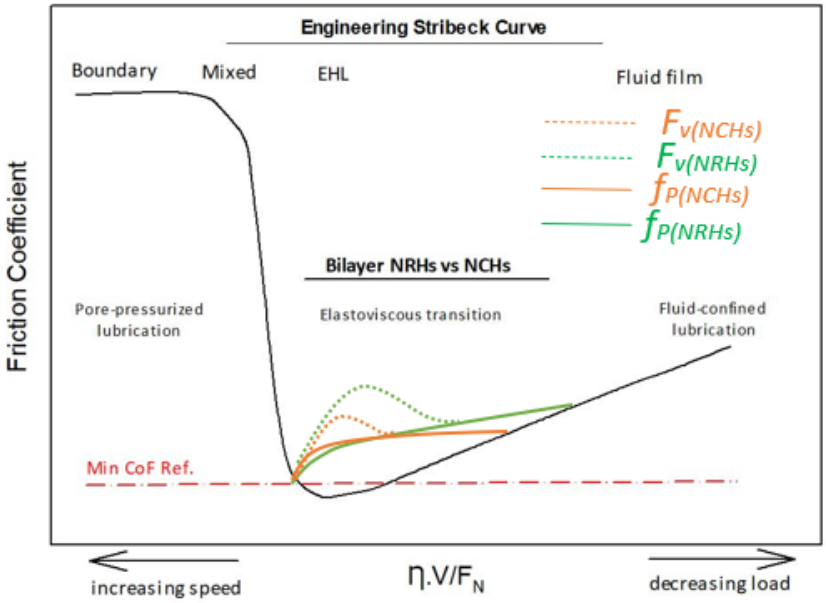

Figure 7. 8 Schematic illustration of developed lubrication regimes in hydrogels in the frame of the engineering Stribeck curve.

7.5 DISCUSSION

Results from the previous section showed that CoF of both NRH and NCH at maximum contact pressure ranged from 0.006 to 0.008, which is in the order of the CoF of healthy articular cartilage. Interestingly, NCHs strengthened with 0.6wt% SNPs showed superior tribological properties compared to NRHs. Unlike other NPs, SNPs showed a significant impact on initial shear modulus and viscoelastic properties, since they could immobilize the polymer chains and form NPs-polymer interphases [20]. SNPs also enhance slower chain kinetics and relaxation due to tough NPs-polymer bonds [22]. Polymer bonds relax promptly when NPs are located far from chains [23]. This is clarifying that chains kinetics play a vital role under sliding motions, in the sense that if chains kinetics are loose due to the long length of strands, after a certain period, chains rupture occur. This yields an incremental shear stresses rate through the network due to unzipped loops within the network. Cameron et al. [259] proved this claim in their study and demonstrated that a movement of loose ends of polymer chains takes place during stress relaxation tests. In fact, the energy dissipation capacity is affected by the imposed shear stresses under the sliding movements. NCHs showed lower CoF compared to NRHs under 0.5N load,

because the imposed shear stresses energy was dissipated with the network more than what occurred for NRHs. However, when the load increased to 0.7N and 0.9N, higher CoF (compared to NRHs) showed this energy absorption was diminished due to the rigidity of the strands and tighter network. Fitzgerald et al. [260] reported SNPs concentration has a proportional effect on the network stress relaxation. It was reported by Zhao et al. [199] that stress relaxation in ionically crosslinked hydrogels occurs in a short time compared to covalently crosslinked hydrogels.

The comparison of the total surface energy of NRHs and NCHs data demonstrated that the elastic modulus and mechanical energy of NCHs were considerably greater than NRHs. This was due to different crosslinking densities, dangling polymer chains, and porosity architecture factors [279]. Stored elastic energy and lost surface energy between asperities contact highlighted the measurement of contact equilibrium from elastic matings and how they absorb energies. Loose chains and loops in NRHs were deficient under shear stresses and energy absorption. Therefore, the imposed energy could release to the entire architecture and disconnect crosslinked chains. This phenomenon, moreover, results in an unstable network over the period of continuous sliding motions. Consequently, SNPs showed an effective contribution in absorbing release energy and maintaining the structure under its performance. This conclusion can be proved also by analysing the mean CoF trends illustrated in Fig. 7.4. The very fluctuated and unstable data for NRHs compared to the smoother trend in NCHs prove that the bilayer hydrogel becomes stable by using SNPs.

Further to discussed results, wear scar profiles also showed superior performance for NCHs compared to NRHs. Narrower wear width and lower wear depth is due to regular mesh and tie points in the NCHs network. The smaller circle diameter that was shown in Fig. 7.5 clarifies the fact that wear loss volume detrimentally decreased in NCHs. A recent study also showed that SNPs affect mesh patterns, and therefore, are strongly correlated with wear volume loss [233]. This is also attributed to the amount of fluid diffusion through the interconnect channels. Therefore, continues pumping out of the lubrication through the smaller mesh would provide a

very lubricated region for the reciprocating sliding mate. That is why wear loss volume significantly decreased in NCHs.

SEM images showed the dominant wear mechanisms for NRHs and NCHs. It was observed that NRHs disintegrated on its surface when it was subjected to the sliding wear tests. Furthermore, not just dispatched lesions, but also minor scoring and wear debris could be observed in the wear track. All these elements are indicating that NRHs network was not adhesion-control. Since AC is a function of permeability and shear-thinning viscosity to originate a thin film of synovial fluid lubrication that support detaching process between cartilage mates [112], however, in our study sliding mate was an impermeable steel ball that could defiantly affect the adhesion process. Considering this phenomenon, NCHs still performed much better than NRHs, with minimized tissue disconnectivity. This was due to a strong interfacial NPs-polymer bonding in the hydrogel matrix [233].

Finally, the comparison of SNPs and titania NPs proved that NCHs topped up with SNPs could perform with superior tribological properties, lower wear loss volume and minimized wear scar profile. The mean CoF of this product is significantly lower and close to the order of AC's CoF. It also proved the network integrity and shear resistance under sliding movements in the developed NCHs. Therefore, NCHs loaded with 0.6wt% SNPs exhibits better tribological performance compared to NCHs with titania NPs. Although NCHs loaded with titania NPs showed superior mechanical properties compared to SNPs strengthened NCHs. In the next chapter, we summarize these two proposed systems and recommendations of the NPs suitability according to the age grouping.

7.8 LIMITATIONS

The limitation of this tribological study of NCHs loaded SNPs was stylus profiler apparatus and measurement of wear scar as discussed in chapter 6, section 6.6.

7.5 CONCLUSIONS

In summary, a 0.6 wt% maximum SNPs loading of the bilayer hydrogel boosted up elastic modulus, hardness, compressive modulus, and strength significantly compared to the same formulation without SNPs. Regarding tribological properties, wear resistance in NCHs improved significantly and lower CoF was observed compared to NRHs.

With respect to the lubricious layer topography and its worn surfaces, in the control sample, by increasing the load, wear mechanisms were transformed from abrasive and adhesive to fatigue phase. However, in NCHs, wear mechanisms remained intact and mostly accumulative plastic deformation was observed. By adding SNPs, a four-fold increase in calculated total surface energy of NCHs was achieved compared to NRHs, which remarkably affected the improvement of tribological properties.

CHAPTER 8

CONCLUSIONS AND FUTURE WORKS

8.1 SUMMARY

An artificial material that can be implanted for localized cartilage lesions and postpone total joint replacement was proposed and investigated in this study. The whole structure of the implant was proposed, and the most critical part of it, which is bilayer hydrogel, was the target of this study to carry out the research. The bilayer hydrogels were formulated at the first stage by conducting an assortment of monomers mixture to enhance mechanical and tribological properties. After achieving the right formulation, a series of titania and silica NPs were utilized separately to enhance both the mechanical and tribological properties of the proposed bilayer hydrogels. Then, mechanical and tribological tests according to FDA and ICRS were conducted to study the properties of the manufactured samples and nominate the best NCHs resembling the properties and performance of native cartilage.

Most of the previous studies focused on developing single-layer hydrogels and assessed either their mechanical or tribological properties. Having considered this gap, strengthened bilayer hydrogels were developed, and both mechanical and tribological properties were assessed to find the suitable candidate for cartilage replacement. To the best of our knowledge, this research is the first attempt to enhance the lubricious layer's mechanical and tribological properties by titania and silica NPs. The lubricious layer was also analyzed for total surface energy and diffusion rate theory was applied to investigate the effect of the lubricious and bulk layers in poroelastic or viscoelastic relaxation, which is essential in the design of artificial tissues.

8.2 CONCLUSIONS

According to the experimental results, the following conclusions can be drawn:

1. Mechanical improvements of NCHs strengthened with titania NPs:

    - 0.2 wt% topping of TiO_2 NPs in our formula showed significant enhancement of elastic modulus, hardness, compressive strength, and tangent modulus compared to NRHs. Higher concentration resulted in a higher degree of chain entanglement and stiffer material which was very brittle.
    - Stress relaxation study on the effects of TiO_2 NPs on the molecular displacement of polymer chains by imposing 0.2wt%, 0.4wt%, and 0.6wt% NPs concentrations showed lower stress and reached a constant modulus in a shorter time.
    - Bilayer hydrogels strengthened by 0.2 wt% TiO_2 NPs demonstrated gradual shrinking of pore sizes from the top layer to the bulk layer, and this could be beneficial for developing cartilage implants with stiffness gradient through the thickness.

2. Mechanical improvements of NCHs strengthened with silica NPs:

    - 0.6 wt% SNPs in the developed bilayer hydrogel exhibited excellent viscoelastic and material properties compared to other samples.
    - Elastic modulus and hardness of the NCHs with 0.6 wt% SNPs improved by 155% and 165%, respectively, compared to NRHs. The elastic modulus reached 240 kPa, which is close to the elastic modulus of the cartilage.
    - Compressive strength in 0.6 wt% NCHs reached 1.3 MPa compared to 0.8 MPa in NRHs.
    - Diffusion rate theory showed poroelasticity occurred before viscoelasticity in the first 500 seconds. This shows that the fluid had sufficient time to migrate through the interconnected channels, while chain conformation remained intact.

- SEM images from 0.6 wt% NCHs cross-section showed very uniform linkages in the lubricious layer were formed.

By comparing the mechanical properties of both proposed NCHs, titania NPs demonstrated superior mechanical properties compared to SNPs. Elastic modulus of the proposed NCHs loaded with 0.2wt% titania NPs was 350 kPa compared to that of 240 kPa by NCHs with SNPs. Hardness, also attained 215 kPa for titania NPs compared with 140 kPa performed by SNPs. Both NCHs' elastic modulus fall in the range of AC's elastic modulus (160 kPa to 500 kPa)[33].

Compressive strength results by using titania NPs also was superior to SNPs and acquired 1.4 MPa and 1.3 MPa respectively, considering the medium strain rate. This achieved improvement by NPs fall within the range of compressive modulus to that of AC, 0.1 – 2.0 MPa [179] showed the optimum loaded amount of NPs for both hydrogels. The tangent modulus of both NCHs showed the maximum strain-rate dependency at each strain point. This is an essential requirement for biomimetic tissues like artificial cartilage. 0.2wt% titania NPs and 0.6wt% SNPs were superior to other counterparts.

SEM images of the lubricious layer for both proposed NCHs showed distinguished patterns of porosity sizes through the thickness. The thickness of the lubricious layer in NCHs loaded with 0.2wt% titania NPs reached 721 μm compared to 570 μm in NCHs loaded with 0.6wt% SNPs. This premier thickness could result in a higher capacity of water retention in its lubricious layer.

Therefore titania NPs can be used for mostly load-bearing applications. For instance, young adults with sufficient interstitial fluid and subject to substantial daily activities with cyclic high contact pressure on joints would preferably use NCHs strengthened with 0.2wt% titania NPs.

3. Tribological improvements of NCHs strengthened with titania NPs:

- CoF variations with respect to time for NCHs exhibited minimized fluctuations due to lesser network flaws. This was the result of toughened polymer bond in NCHs compared to NRHs.

- CoF of NCHs was higher compared to NRHs due to greater network density that resists against sliding probe in the lubricious layer.
- CoF at 0.9 N load, with the aid of bovine serum lubrication in NRHs, was around 0.005, which is close to that of the articular cartilage (0.001).
- NCHs wear track showed smaller wear depth and width compared to NRHs, which indicates the effect of titania NPs in the enhancement of wear resistance of the lubricious layer.
- SEM images proved that NPs strengthened the lubricious layer, where shallow grooves and small micro-cracks were observed compared to NRHs with worn lubricious layers and larger micro cracks.
- Lubrication regimes were developed, and it was described that disentangled polymer chains in the lubricious layer attach to the sliding mate asperities and results in increasing CoF. Also, Due to the confined fluid in the lubricious layer at the high-speed region, a thoroughly hydrated regime could decrease CoF, which was described as fluid-confined lubrication.

4. Tribological improvements of NCHs strengthened with silica NPs:

- SNPs boost up wear resistance significantly, and lower CoF was observed compared to NRHs.
- The wear mechanism was found to be a function of applied load and sliding speed and transforms from abrasive and adhesive to fatigue phase in NRHs. However, topping 0.6wt% SNPs, results in consistent wear mechanisms in the form of accumulative plastic deformation. This achievement proved that NCHs strengthened by SNPs are not subject to wear mechanism transformation with variations of contact pressure and sliding speed.

- 0.6 wt% SNPs in the proposed bilayer hydrogels significantly improved the total surface energy in NCHs compared to NRHs. Improved surface energy remarkably affected the improvement of tribological properties according to JKR model.
- SNPs play a crucial role in the transition of EVT to FCL regime since a gradual increase in CoF was drawn in NCHs compared to NRHs.
- NCHs showed relatively lower CoF under dry sliding test compared to NRHs, which indicates shorted branched strands in the lubricious layer and less adhesion to the sliding probe.

By comparing the tribological properties of both proposed NCHs, SNPs performed excellent compared to titania NPs under all tribological experiments. The mean CoF of NCHs loaded with SNPs at the maximum contact pressure reached 0.007 compared to 0.015 for NCHS with titania NPs. The attained CoF values for SNPs are comparable to that of healthy cartilage at 0.001 [97]. Moreover, the CoF trend over time, showed moderate fluctuation compared to titania NPs loaded NCHs, and that was due to a neater mesh and crosslinked network in SNPs loaded NCHs.

Wear scar and wear volume of NCHs loaded with SNPs also proved the proficiency of this NPs compared to titania NPs in tribological properties enhancement. SNPs loaded NCHs demonstrated lower wear volume in comparison with titania NCHs, under both load and sliding speed control factors.

Wear mechanisms in both NCHs was found to be different compared to NRHs; however, SNPs was considerably distinct from the titania effects. By titania NPs, abrasive and adhesive fatigue wear minimized and transformed to the accumulated plastic deformation with minor cracks. However, SNPs loaded NCHs showed a similar improvement without the presence of cracks on their sliding bed. These findings prove SNPs dominant efficiency on the wear resistance compared to titania NPs.

It is therefore recommended that SNPs be used by the proposed NCHs for the elderly group since their knee joints may be subject to depleted interstitial fluid and the NCH with superior tribological performances is required rather than load-bearing NCHs.

8.3 FUTURE WORKS

This thesis covers a comprehensive preliminary study on material selection, synthesis, and mechanical and tribological testing of the bilayer hydrogels strengthened with NPs; however, further research needs to be conducted to develop and optimize the complete cartilage implant. From the proposed implant in the introduction chapter, only bilayer hydrogels were manufactured and assessed in this thesis, which is the most critical part of the cartilage implant. However, in the next phase of the study, the entire implant with the proposed materials should be developed and analyzed. Comprehensive mechanical, structural and tribological tests must be conducted on the entire implant and its osteointegration with bone and cartilage should be investigated. The finalized design should then be implanted in animal joints for clinical study and in vivo interactions.

The bilayer hydrogel can be examined in more realistic test conditions, and especially sliding wear tests can be conducted in a controlled environment in terms of temperature and humidity with synovial fluid lubrication and native cartilage as a sliding mate. Also, a wider range of contact pressures and sliding speeds can be used in the experiments to simulate the exact condition of joint movements.

A future study should also focus on impact and fatigue tests to improve the stability of the entire hydrogel implant. Dynamic loading, shear force analysis on the lubricious layer and integration point of hydrogel with the scaffold should be thoroughly investigated. It is very important to optimize the design of the scaffold to minimize micro shear forces exerted on the bulk layer. In order to enhance this research in future, biocompatibility and toxicity tests should take into consideration for better results at the stage of clinical follow-up.

REFERENCES

[1] Gabriela Espinosa, Gaston Otarola, Jerry C Hu, Prof. Kyriacos A Athanasiou, *Cartilage assessment requires a surface characterization protocol: roughness, friction, and function.* Tissue Engineering Part C: Methods, 2021.

[2] Mow Van C., Ratcliffe Anthony, Poole Robin A., *Cartilage and diarthrodial joints as paradigms for hierarchical materials and structures.* Biomaterials, 1992. **13**(2): p. 67-97.

[3] Soltz Michael, Ateshian Gerard A., *A Conewise Linear Elasticity Mixture Model for the Analysis of Tension-Compression Nonlinearity in Articular Cartilage.* Journal of Biomechanical Engineering, 2000. **122**(6): p. 576-586.

[4] Fergusson C.M., *The aetiology of osteoarthritis.* Postgrad Med J, 1987. **63**(740): p. 439-445.

[5] Mostakhdemin Mohammad, Sadegh Amiri Iraj, Syahrom Ardiyansyah, *Multi-axial Fatigue of trabecular Bone with Respect to Normal Walking*. Forensic and Medical Bioinformatic. 2016, Singapore: Springer.

[6] Ronken S., Wirz D., Daniels A. U., Kurokawa T., Gong J. P., Arnold M. P., *Double-network acrylamide hydrogel compositions adapted to achieve cartilage-like dynamic stiffness.* Biomechanics and Modeling in Mechanobiology, 2013. **12**(2): p. 243-248.

[7] Higa Kotaro, Kitamura Nobuto, Goto Keiko, Kurokawa Takayuki, Gong Jian Ping, Kanaya Fuminori, Yasuda Kazunori, *Effects of osteochondral defect size on cartilage regeneration using a double-network hydrogel.* BMC Musculoskeletal Disorders, 2017. **18**(1): p. 210.

[8] Mostakhdemin Mohammad, Nand Ashveen, Arjmandi Mohammadreza, Ramezani Maziar, *Mechanical and microscopical characterisation of bilayer hydrogels strengthened by TiO_2 nanoparticles as a cartilage replacement candidate.* Materials Today Communications, 2020. **25**: p. 101279.

[9] Asik Mehmet, Ciftci Feyyaz, Sen Cengiz, Erdil Mehmet, Atalar Atacan, *The Microfracture Technique for the Treatment of Full-Thickness Articular Cartilage Lesions of the Knee: Midterm Results.* Arthroscopy: The Journal of Arthroscopic & Related Surgery, 2008. **24**(11): p. 1214-1220.

[10] Kreuz P. C., Steinwachs M. R., Erggelet C., Krause S. J., Konrad G., Uhl M., Südkamp N, *Results after microfracture of full-thickness chondral defects in different compartments in the knee.* Osteoarthritis and Cartilage, 2006. **14**(11): p. 1119-1125.

[11] Benthien J. P., Behrens P., *Autologous Matrix-Induced Chondrogenesis (AMIC): Combining Microfracturing and a Collagen I/III Matrix for Articular Cartilage Resurfacing.* CARTILAGE, 2010. **1**(1): p. 65-68.

[12] Harris Joshua D., Siston Robert A., Pan Xueliang, Flanigan David C., *Autologous Chondrocyte Implantation: A Systematic Review.* JBJS, 2010. **92**(12): p. 2220-2233.

[13] Solheim Eirik, Hegna Janne, Inderhaug Eivind, Øyen Jannike, Harlem Thomas, Strand Torbjørn, *Results at 10–14 years after microfracture treatment of articular cartilage defects in the knee.* Knee Surgery, Sports Traumatology, Arthroscopy, 2016. **24**(5): p. 1587-1593.

[14] M. B. Hurtig, M. D. Buschmann, L. A. Fortier, C. D. Hoemann, E. B. Hunziker, J. S. Jurvelin, P. Mainil-Varlet, C. W. McIlwraith, R. L. Sah, R. A. Whiteside, *Preclinical studies for cartilage repair: recommendations from the International Cartilage Repair Society*. 2011. **2**(2): p. 137–152.

[15] Redaelli F., Sorbona M., Rossi F., *10 - Synthesis and processing of hydrogels for medical applications*, in *Bioresorbable Polymers for Biomedical Applications*, G. Perale and J. Hilborn, Editors. 2017, Woodhead Publishing. p. 205-228.

[16] Li Lan, Yu Fei, Zheng Liming, Wang Rongliang, Yan Wenqiang, Wang Zixu, Xu Jia, Wu Jianxiang, Shi Dongquan, Zhu Liya, Wang Xingsong, Jiang Qing, *Natural hydrogels for cartilage regeneration: Modification, preparation and application.* Journal of Orthopaedic Translation, 2019. **17**: p. 26-41.

[17] Abdurrahmanoglu Suzan, Can Volkan, Okay Oguz, *Equilibrium swelling behavior and elastic properties of polymer–clay nanocomposite hydrogels.* Journal of Applied Polymer Science, 2008. **109**(6): p. 3714-3724.

[18] Toledo Leandro, Racine Lisa, Pérez Viviana, Henríquez Juan P, Auzely-Velty Rachel, Urbano Bruno F, *Physical nanocomposite hydrogels filled with low concentrations of TiO_2 nanoparticles: Swelling, networks parameters and cell retention studies.* Materials Science and Engineering: C, 2018. **92**: p. 769-778.

[19] Jaiswal Manish K., Xavier Janet R., Carrow James K., Desai Prachi, Alge Daniel, Gaharwar Akhilesh K., *Mechanically Stiff Nanocomposite Hydrogels at Ultralow Nanoparticle Content.* ACS Nano, 2016. **10**(1): p. 246-256.

[20] Janet D., Pearl MD,. *diagram-of-osteoarthritis-in-knee-joint*. Available from: https://www.completepaincare.com/patient-education/conditions-treated/elbow-pain/diagram-of-osteoarthritis-in-knee-joint/.

[21] Zareie Camellia, Bahramian Ahmad Reza, Sefti Mohsen Vafaie, Salehi Mahsa Baghban, *Network-gel strength relationship and performance improvement of polyacrylamide hydrogel using nano-silica; with regards to application in oil wells conditions.* Journal of Molecular Liquids, 2019. **278**: p. 512-520.

[22] Arjmandi Mohammadreza, Ramezani Maziar, *Mechanical and tribological assessment of silica nanoparticle-alginate-polyacrylamide nanocomposite hydrogels as a cartilage replacement.* Journal of the Mechanical Behavior of Biomedical Materials, 2019. **95**: p. 196-204.

[23] Zhan Yuexing, Pan Yihui, Chen Bing, Lu Jian, Zhong Zheng, Niu Xinrui, *Strain rate dependent hyperelastic stress-stretch behavior of a silica nanoparticle reinforced poly (ethylene glycol) diacrylate nanocomposite hydrogel.* Journal of the Mechanical Behavior of Biomedical Materials, 2017. **75**: p. 236-243.

[24] Mao Yunwei, Lin Shaoting, Zhao Xuanhe, Anand Lallit, *A large deformation viscoelastic model for double-network hydrogels.* Journal of the Mechanics and Physics of Solids, 2017. **100**: p. 103-130.

[25] Adibnia Vahid, Hill Reghan J., *Viscoelasticity of near-critical silica-polyacrylamide hydrogel nanocomposites.* Polymer, 2017. **112**: p. 457-465.

[26] Hooper G., Lee A. J., Rothwell A., and Frampton C., *Current trends and projections in the utilisation rates of hip and knee replacement in New Zealand from 2001 to 2026.* N Z Med J, 2014. **127**(1401): p. 82-93.

[27] Roos Ewa M., *Joint injury causes knee osteoarthritis in young adults.* Rehabilitation medicine in rheumatic diseases, 2005. **17**(2): p. 5.

[28] H Roos, Harald Adalberth, Torsten Dahlberg, Leif Lohmander, L. Stefan, *Osteoarthritis of the knee after injury to the anterior cruciate ligament or meniscus: the influence of time and age.* Osteoarthritis and Cartilage, 1995. **3**(4): p. 261-267.

[29] Peter Maitland, *Institute of Gender and Health: A Portrait of Innovation and Health Research Growth.* Canadian Institutes of Health Research ottawa, 2001.

[30] Bossley C.J., Miles, K.B. *Musculo-skeletal conditions in New Zealand, "the crippling burden".* 2009; Available from: https://nzoa.org.nz//system/files/The%20Crippling%20Burden.pdf.

[31] King, D., Hume, Patria, Milburn, Peter, Gianotti, Simon, *Rugby league injuries in New Zealand: Variations in injury claims and costs by ethnicity, gender, age, district, body site, injury type and occupation.* New Zealand Journal of Sports Medicine, 2009.

[32] Knecht Sven, Vanwanseele Benedicte, Stüssi Edgar, *A review on the mechanical quality of articular cartilage – Implications for the diagnosis of osteoarthritis.* Clinical Biomechanics, 2006. **21**(10): p. 999-1012.

[33] Hunziker E. B., *Articular cartilage repair: basic science and clinical progress. A review of the current status and prospects.* Osteoarthritis and Cartilage, 2002. **10**(6): p. 432-463.

[34] Maroudas A., Wachtel E., Grushko G., Katz E. P., Weinberg, P., *The effect of osmotic and mechanical pressures on water partitioning in articular cartilage.* Biochimica et Biophysica Acta (BBA) - General Subjects, 1991. **1073**(2): p. 285-294.

[35] Ateshian Gerard A., *The role of interstitial fluid pressurization in articular cartilage lubrication.* Journal of Biomechanics, 2009. **42**(9): p. 1163-1176.

[36] Sardinha V. M., Lima L. L., Belangero W. D., Zavaglia C. A., Bavaresco V. P., Gomes, J. R., *Tribological characterization of polyvinyl alcohol hydrogel as substitute of articular cartilage.* Wear, 2013. **301**(1): p. 218-225.

[37] Martin Nicholas, Youssef George, *Dynamic properties of hydrogels and fiber-reinforced hydrogels.* Journal of the Mechanical Behavior of Biomedical Materials, 2018. **85**: p. 194-200.

[38] Travis J. Klein, Jos Malda, Robert L. Sah, and Dietmar W. Hutmacher, *Tissue Engineering of Articular Cartilage with Biomimetic Zones.* Tissue Engineering Part B: Reviews, 2009. **15**(2): p. 143-157.

[39] Daniela Anahí Sánchez-Téllez, Lucía Téllez-Jurado, Luís María Rodríguez-Lorenzo, *Hydrogels for Cartilage Regeneration, from Polysaccharides to Hybrids.* Polymers, 2017. **9**(12): p. 671.

[40] Buckwalter J.A., Mow V.C., Mankin H.J., *Articular Cartilage: Structure, Function, Metabolism, Injury and Pathogenesis of Osteoarthritis*. 2003, Philadelphia: London: Lippincott Williams & Wilkins.

[41] C. A. Poole, H. Flint, W. Beaumont, *Morphological and functional interrelationships of articular cartilage matrices.* J Anat, 1984. **138(Pt 1)**: p. 113–138.

[42] Askew M. J., Mow V. C., *The Biomechanical Function of the Collagen Fibril Ultrastructure of Articular Cartilage.* Journal of Biomechanical Engineering, 1978. **100**(3): p. 105-115.

[43] Lipshitz H., Etheredge R., Glimcher M. J., *Changes in the hexosamine content and swelling ratio of articular cartilage as functions of depth from the surface.* The Journal of bone and joint surgery. American volume, 1976. **58**(8): p. 1149-1153.

[44] Kumar P., Oka M., Toguchida J., Kobayashi M., Uchida E., Nakamura T., Tanaka K., *Role of uppermost superficial surface layer of articular cartilage in the lubrication mechanism of joints.* Journal of Anatomy, 2001. **199**(3): p. 241-250.

[45] Mow Van C., Guo X. Edward, *Mechano-Electrochemical Properties Of Articular Cartilage: Their Inhomogeneities and Anisotropies.* Annual Review of Biomedical Engineering, 2002. **4**(1): p. 175-209.

[46] Graindorge S., Ferrandez W., Ingham E., Jin Z., Twigg P., Fisher J., *The role of the surface amorphous layer of articular cartilage in joint lubrication.* Proc Inst Mech Eng H, 2006. **220**(5): p. 597-607.

[47] Stockwell R. A., *The interrelationship of cell density and cartilage thickness in mammalian articular cartilage.* Journal of anatomy, 1971. **109**(Pt 3): p. 411-421.

[48] Vega Sebastián L., Kwon Mi Y., Burdick Jason A., *Recent advances in hydrogels for cartilage tissue engineering.* European Cells and Materials, 2017. **33**: p. 59-75.

[49] Kiviranta I., Tammi M., Jurvelin J., Arokoski J., Säämänen A. M., Helminen H. J., *Articular cartilage thickness and glycosaminoglycan distribution in the canine knee joint after strenuous running exercise.* Clin Orthop Relat Res., 1992. **283**: p. 302-308.

[50] Vanwanseele B., Lucchinetti E., Stüssi E., *The effects of immobilization on the characteristics of articular cartilage: current concepts and future directions.* Osteoarthritis and Cartilage, 2002. **10**(5): p. 408-419.

[51] Buckwalter Joseph A., Martin James A., *Osteoarthritis.* Advanced Drug Delivery Reviews, 2006. **58**(2): p. 150-167.

[52] Brown CR Jr., *The Adult Knee. Lippincott Williams & Wilkins*, ed. R.A. Callaghan JJ, Rubash HE, Simonian PT, Wickiewicz TL. 2003: Lippincott Williams & Wilkins.

[53] Arjmandi M., Ramezani M., Nand A., Neitzert T., *Experimental study on friction and wear properties of interpenetrating polymer network alginate-polyacrylamide hydrogels for use in minimally-invasive joint implants.* Wear, 2018. **406-407**: p. 194-204.

[54] Clouet Johann, Vinatier Claire, Merceron Christophe, Pot-vaucel Marianne, Maugars Yves, Weiss Pierre, Grimandi Gaël, Guicheux Jérôme, *From osteoarthritis treatments to future regenerative therapies for cartilage.* Drug Discovery Today, 2009. **14**(19): p. 913-925.

[55] Han H. S., Kang S.B.,Yoon K. S., *High incidence of loosening of the femoral component in legacy posterior stabilised-flex total knee replacement.* The Journal of Bone and Joint Surgery. British volume, 2007. **89-B**(11): p. 1457-1461.

[56] Arakaki K., Kitamura N., Fujiki H., Kurokawa T., Iwamoto M., Ueno M., Kanaya F., Osada Y., Gong J. P., and Yasuda K., *Artificial cartilage made from a novel double-network hydrogel: In vivo effects on the normal cartilage and ex vivo evaluation of the friction property.* J Biomed Mater Res A, 2010. **93**(3): p. 1160-8.

[57] Sutter Leo, Sindermann Andrew, Wyse Jackson Thomas, Bartell Lena, Bonassar Lawrence, Cohen Itai, Das Moumita, *Mechanical structure function properties and fracture toughness of Articular Cartilage modeled as a biopolymer double network*. 2019. p. X59.007.

[58] Setton Lori A., Zhu Wenbo, Mow Van C., *The biphasic poroviscoelastic behavior of articular cartilage: Role of the surface zone in governing the compressive behavior.* Journal of Biomechanics, 1993. **26**(4): p. 581-592.

[59] Deva D. Chan, Luyao Cai, Kent D. Butz, Stephen B. Trippel, Eric A. Nauman, Corey P. Neu, *In vivo articular cartilage deformation: noninvasive quantification of intratissue strain during joint contact in the human knee.* Scientific Reports, 2016. **6**(1): p. 19220.

[60] Woo S. L. Y., Simon B. R., Kuei S. C., Akeson W. H., *Quasi-Linear Viscoelastic Properties of Normal Articular Cartilage.* Journal of Biomechanical Engineering, 1980. **102**(2): p. 85-90.

[61] Kazunobu Arakaki, Nobuto Kitamura, Hiroyuki Fujiki, Takayuki Kurokawa ,Mikio Iwamoto, Masaru Ueno, Fuminori Kanaya, Yoshihito Osada, Jian Ping Gong, Kazunori Yasuda, *Artificial cartilage made from a novel double-network hydrogel: In vivo effects on the normal cartilage and ex vivo evaluation of the friction property.* J. Biomed. Mater., 2010: p. 1160-1168. .

[62] Zevenbergen L., Gsell W., Cai L., Chan D. D., Famaey N., Vander Sloten J., Himmelreich U., Neu C. P., and Jonkers I., *Cartilage-on-cartilage contact: effect of compressive loading on tissue deformations and structural integrity of bovine articular cartilage.* Osteoarthritis and Cartilage, 2018. **26**(12): p. 1699-1709.

[63] Oloyede Adekunle, Flachsmann Rene, Broom Neil D., *The Dramatic Influence of Loading Velocity on the Compressive Response of Articular Cartilage.* Connective Tissue Research, 1992. **27**(4): p. 211-224.

[64] Eric L., Radin M.D., Igor L., Paul SC.D, Martin Lowy, *A comparison of the dynamic force transmitting properties of subchondral bone and articular cartilage.* The Journal of Bone and Joint Surgery, 1970. **52-A**(3): p. 444-456.

[65] Wahlquist Joseph A, DelRio Frank W., Randolph Mark A., Aziz Aaron H., Heveran Chelsea M., Bryant Stephanie J., Neu Corey P., Ferguson Virginia L, *Indentation mapping revealed poroelastic, but not viscoelastic, properties spanning native zonal articular cartilage.* Acta Biomaterialia, 2017. **64**: p. 41-49.

[66] Katz E. P., Wachtel E. J., Maroudas A., *Extrafibrillar proteoglycans osmotically regulate the molecular packing of collagen in cartilage.* Biochimica et Biophysica Acta (BBA) - General Subjects, 1986. **882**(1): p. 136-139.

[67] Y.C. Fung, P. Tong, *Classical and Computational Solid Mechanics.* World Scientific Publishing Co Inc., 2001.

[68] Nam Sungmin, Hu Kenneth H., Butte Manish J., Chaudhuri Ovijit, *Strain-enhanced stress relaxation impacts nonlinear elasticity in collagen gels.* Proceedings of the National Academy of Sciences, 2016. **113**(20): p. 5492-5497.

[69] Li L. P., Buschmann M. D., Shirazi-Adl A., *A fibril reinforced nonhomogeneous poroelastic model for articular cartilage: inhomogeneous response in unconfined compression.* Journal of Biomechanics, 2000. **33**(12): p. 1533-1541.

[70] Han Guebum, Hess Cole, Eriten Melih, Henak Corinne R., *Uncoupled poroelastic and intrinsic viscoelastic dissipation in cartilage.* Journal of the Mechanical Behavior of Biomedical Materials, 2018. **84**: p. 28-34.

[71] Wilson W., Huyghe J.M., Van Donkelaar C.C, *Depth-dependent compressive equilibrium properties of articular cartilage explained by its composition.* Biomechanics and Modeling in Mechanobiology, 2007. **6**(1-2): p. 43-53.

[72] Kurkijärvi J.E., Nissi M.J., Kiviranta I., Jurvelin J.S., Nieminen M.T., *Delayed gadolinium-enhanced MRI of cartilage (dGEMRIC) and T2 characteristics of human knee articular cartilage: Topographical variation and relationships to mechanical properties.* Magnetic Resonance in Medicine, 2004. **52**(1): p. 41-46.

[73] Amin Komeili, Ziad Abusara, Salvatore Federico, Walter Herzog, *Effect of strain rate on transient local strain variations in articular cartilage.* Journal of the Mechanical Behavior of Biomedical Materials, 2019. **95**: p. 60-66.

[74] Arabshahi Zohreh, Afara Isaac Oluwaseun, Moody Hayley Ruscoe, Schrobback Karsten, Kashani Jamal, Fischer Nadine, Oloyede Adekunle, and K.T. Jacob, *A new mechanical indentation framework for functional assessment of articular cartilage.* Journal of the Mechanical Behavior of Biomedical Materials, 2018. **81**: p. 83-94.

[75] Deng Yaling, Sun Jianjun, Ni Xingya, Yu Bo, *Tribological properties of hierarchical structure artificial joints with poly acrylic acid (AA) - poly acrylamide (AAm) hydrogel and Ti6Al4V substrate.* Journal of Polymer Research, 2020. **27**(6): p. 157.

[76] Lohmander L. Stefan, Englund P. Martin, Dahl Ludvig L., and R.E. M., *The Long-term Consequence of Anterior Cruciate Ligament and Meniscus Injuries:Osteoarthritis.* The American Journal of Sports Medicine, 2007. **35**(10): p. 1756-1769.

[77] A.M. Bendele, *Animal models of osteoarthritis.* J Musculoskel Neuron Interact, 2001. **1**(4): p. 363-376.

[78] Katta Jayanth, Jin Zhongmin, Ingham Eileen, Fisher John, *Biotribology of articular cartilage—A review of the recent advances.* Medical Engineering & Physics, 2008. **30**(10): p. 1349-1363.

[79] Link Jarrett M, Salinas Evelia Y, Hu Jerry C, Athanasiou Kyriacos A, *The tribology of cartilage: Mechanisms, experimental techniques, and relevance to translational tissue engineering.* Clinical Biomechanics, 2019.

[80] A.C. Moore, D.L. Burris, *Tribological and material properties for cartilage of and throughout the bovine stifle: support for the altered joint kinematics hypothesis of osteoarthritis.* Osteoarthritis and Cartilage, 2017. **23**(1): p. 161-169.

[81] Oungoulian Sevan R., Chang Stephany, Bortz Orian, Hehir Kristin E., Zhu Kaicen, Willis Callen E., Hung Clark T., Ateshian Gerard A., *Articular cartilage wear characterization with a particle sizing and counting analyzer.* Journal of biomechanical engineering, 2013. **135**(2): p. 024501-024501.

[82] Mankin H. J., *Workshop on etiopathogenesis of osteoarthritis. Proceedings and Recommendations*, in *J Rheumatol.* 1986. p. 1130-1160.

[83] Jae Hyun Jung, *Knee osteoarthritis and menopausal hormone therapy in postmenopausal women: a nationwide cross-sectional study.* Medicine, 2018.

[84] VC Mow, LJ Soslowsky, *Friction, lubrication and wear of diarthrodial joints.* Basic orthopaedic biomechanics, 1991.

[85] Wu Pei-Jung, Masouleh Maryam Imani, Dini Daniele, Paterson Carl, Török Peter, Darryl R., Kabakova Irina V., *Detection of proteoglycan loss from articular cartilage using Brillouin microscopy, with applications to osteoarthritis.* Biomedical Optics Express, 2019. **10**(5): p. 2457-2466.

[86] Burris D. L., Ramsey L., Graham B. T., Price C., Moore A. C., *How Sliding and Hydrodynamics Contribute to Articular Cartilage Fluid and Lubrication Recovery.* Tribology Letters, 2019. **67**(2): p. 46.

[87] Graindorge Simon L., Stachowiak Gwidon W., *Changes occurring in the surface morphology of articular cartilage during wear.* Wear, 2000. **241**(2): p. 143-150.

[88] Lipshitz H., Etheredge R., Glimcher M. J., *In vitro wear of articular cartilage.* The Journal of bone and joint surgery. American volume, 1975. **57**(4): p. 527-534.

[89] H. Lipshitz, R. Etheredge, M. J. Glimcher, *Changes in the hexosamine content and swelling ratio of articular cartilage as functions of depth from the surface.* The Journal of bone and joint surgery. American volume, 1976. **58**(8): p. 1149-1153.

[90] Hossain M. Jayed, Noori-Dokht Hessam, Karnik Sonali, Alyafei Naomi, Joukar Amin, Trippel Stephen B., Wagner Diane R., *Anisotropic properties of articular cartilage in an accelerated in vitro wear test.* Journal of the Mechanical Behavior of Biomedical Materials, 2020. **109**: p. 103834.

[91] Jay Gregory D., Torres Jahn R., Rhee David K., Helminen Heikki J., Hytinnen Mika M., Cha Chung-Ja, Elsaid Khaled, Kim Kyung-Suk, Cui Yajun, and Warman Matthew L., *Association between friction and wear in diarthrodial joints lacking lubricin.* Arthritis & Rheumatism, 2007. **56**(11): p. 3662-3669.

[92] Jurvelin J. S., Müller D. J., Wong M., Studer D., Engel A., Hunziker E. B., *Surface and Subsurface Morphology of Bovine Humeral Articular Cartilage as Assessed by Atomic Force and Transmission Electron Microscopy.* Journal of Structural Biology, 1996. **117**(1): p. 45-54.

[93] McCutchen C. W., *Mechanism of Animal Joints: Sponge-hydrostatic and Weeping Bearings.* Nature, 1959. **184**(4695): p. 1284-1285.

[94] Mow V. C., Kuei S. C., Lai W. M., and A.C. G., *Biphasic Creep and Stress Relaxation of Articular Cartilage in Compression: Theory and Experiments.* Journal of Biomechanical Engineering, 1980. **102**(1): p. 73-84.

[95] W.M. Lai, J.S. Hou, V.C. Mow, *A Triphasic Theory for the Swelling and Deformation Behaviors of Articular Cartilage.* Journal of Biomechanical Engineering, 1991. **113**(3).

[96] Caligaris M. and A.G. A., *Effects of sustained interstitial fluid pressurization under migrating contact area, and boundary lubrication by synovial fluid, on cartilage friction.* Osteoarthritis and Cartilage, 2008. **16**(10): p. 1220-1227.

[97] Covert Rebeccah J., Ott R. D., Ku David N., *Friction characteristics of a potential articular cartilage biomaterial.* Wear, 2003. **255**(7): p. 1064-1068.

[98] Forster H., Fisher J., *The Influence of Loading Time and Lubricant on the Friction of Articular Cartilage.* Proceedings of the Institution of Mechanical Engineers, Part H: Journal of Engineering in Medicine, 1996. **210**(2): p. 109-119.

[99] Katta J., Pawaskar S. S., Jin Z. M., Ingham E., Fisher J., *Effect of load variation on the friction properties of articular cartilage.* Proceedings of the Institution of Mechanical Engineers, Part J: Journal of Engineering Tribology, 2007. **221**(3): p. 175-181.

[100] Krishnan Ramaswamy, Mariner Elise N., Ateshian Gerard A., *Effect of dynamic loading on the frictional response of bovine articular cartilage.* Journal of Biomechanics, 2005. **38**(8): p. 1665-1673.

[101] Northwood Ewen and F. John, *A multi-directional in vitro investigation into friction, damage and wear of innovative chondroplasty materials against articular cartilage.* Clinical Biomechanics, 2007. **22**(7): p. 834-842.

[102] Gleghorn Jason P., Jones Aled R. C., Flannery Carl R., and Bonassar Lawrence J., *Boundary mode lubrication of articular cartilage by recombinant human lubricin.* Journal of Orthopaedic Research, 2009. **27**(6): p. 771-777.

[103] Farnham Margot S., Larson Riley E., Burris David L., Price Christopher, *Effects of mechanical injury on the tribological rehydration and lubrication of articular cartilage.* Journal of the Mechanical Behavior of Biomedical Materials, 2020. **101**: p. 103422.

[104] Santarella Francesco, Simpson Christopher R., Lemoine Mark, McGrath Sean, Cavanagh Brenton, Smith Avi, Murphy Ciara M., Garlick Jonathan A., O'Brien Fergal J., Kearney Cathal J., *The lubricating effect of iPS-reprogrammed fibroblasts on collagen-GAG scaffolds for cartilage repair applications.* Journal of the Mechanical Behavior of Biomedical Materials, 2021. **114**: p. 104174.

[105] Naka M. H., Morita Y., Ikeuchi K., *Influence of proteoglycan contents and of tissue hydration on the frictional characteristics of articular cartilage.* Proceedings of the Institution of Mechanical Engineers, Part H: Journal of Engineering in Medicine, 2005. **219**(3): p. 175-182.

[106] Thompson R. C., Oegema T. R., *Metabolic activity of articular cartilage in osteoarthritis. An in vitro study.* The Journal of bone and joint surgery. American volume, 1979. **61**(3): p. 407-416.

[107] Basalo Ines M., Raj David, Krishnan Ramaswamy, Chen Faye H., Hung Clark T., Ateshian Gerard A., *Effects of enzymatic degradation on the frictional response of articular cartilage in stress relaxation.* Journal of Biomechanics, 2005. **38**(6): p. 1343-1349.

[108] Katta J., Jin Z., Ingham E., and F. J., *Chondroitin sulphate: an effective joint lubricant?* Osteoarthritis and Cartilage, 2009. **17**(8): p. 1001-1008.

[109] Bell C. J., Ingham E., Fisher J., *Influence of hyaluronic acid on the time-dependent friction response of articular cartilage under different conditions.* Proceedings of the Institution of Mechanical Engineers, Part H: Journal of Engineering in Medicine, 2006. **220**(1): p. 23-31.

[110] Naka Marco Hiroshi, Hattori Koji, Ohashi Tetsuo, Ikeuchi Ken, *Evaluation of the effect of collagen network degradation on the frictional characteristics of articular cartilage using a simultaneous analysis of the contact condition.* Clinical Biomechanics, 2005. **20**(10): p. 1111-1118.

[111] Sun Zhexun, Feeney Elizabeth, Guan Ya, Cook Sierra G., Gourdon Delphine, Bonassar Lawrence J., Putnam David, *Boundary mode lubrication of articular cartilage with a biomimetic diblock copolymer.* Proceedings of the National Academy of Sciences, 2019. **116**(25): p. 12437-12441.

[112] Schmidt Tannin A., Gastelum Nicholas S., Nguyen Quynhhoa T., Schumacher Barbara L., Sah Robert L., *Boundary lubrication of articular cartilage: Role of synovial fluid constituents.* Arthritis & Rheumatism, 2007. **56**(3): p. 882-891.

[113] T.A. Schmidt, R.L. Sah, *Effect of synovial fluid on boundary lubrication of articular cartilage.* Osteoarthritis and Cartilage, 2007. **15**(1): p. 35-47.

[114] Radin Eric L., Swann David A., Weisser Paul A., *Separation of a Hyaluronate-free Lubricating Fraction from Synovial Fluid.* Nature, 1970. **228**(5269): p. 377-378.

[115] Obara T., Mabuchi K., Iso T., Yamaguchi T., *Increased friction of animal joints by experimental degeneration and recovery by addition of hyaluronic acid.* Clinical Biomechanics, 1997. **12**(4): p. 246-252.

[116] Forsey Richard W., Fisher John, Thompson Jonathan, Stone Martin H., Bell Carol, Ingham Eileen, *The effect of hyaluronic acid and phospholipid based lubricants on friction within a human cartilage damage model.* Biomaterials, 2006. **27**(26): p. 4581-4590.

[117] Chen Yi, Crawford Ross W., and O. Adekunle, *Unsaturated phosphatidylcholines lining on the surface of cartilage and its possible physiological roles.* Journal of Orthopaedic Surgery and Research, 2007. **2**(1): p. 14.

[118] Hills B. A., Crawford R. W., *Normal and prosthetic synovial joints are lubricated by surface-active phospholipid: a hypothesis.* The Journal of Arthroplasty, 2003. **18**(4): p. 499-505.

[119] Pickard J, Ingham E, Egan J, Fisher J, *Investigation into the effect of proteoglycan molecules on the tribological properties of cartilage joint tissues.* Proceedings of the Institution of Mechanical Engineers, Part H: Journal of Engineering in Medicine, 1998. **212**(3): p. 177-182.

[120] Caló Enrica, Khutoryanskiy Vitaliy V., *Biomedical applications of hydrogels: A review of patents and commercial products.* European Polymer Journal, 2015. **65**: p. 252-267.

[121] Ahmed Enas M., *Hydrogel: Preparation, characterization, and applications: A review.* Journal of Advanced Research, 2015. **6**(2): p. 105-121.

[122] Pretzel David, Linss Stefanie, Ahrem Hannes, Endres Michaela, Kaps Christian, Klemm Dieter, and Kinne Raimund W., *A novel in vitro bovine cartilage punch model for assessing the regeneration of focal cartilage defects with biocompatible bacterial nanocellulose.* Arthritis Research & Therapy, 2013. **15**(3): p. R59.

[123] Shimon A. Unterman, Matthew Gibson, Janice H. Lee, Joshua Crist, Thanissara Chansakul, Elaine C. Yang, Jennifer H. Elisseeff, *Hyaluronic Acid-Binding Scaffold for Articular Cartilage Repair.* Tissue Engineering Part A, 2012. **18**(23-24): p. 2497-2506.

[124] Sartori M., Pagani S., Ferrari A., Costa V., Carina V., Figallo E., Maltarello M. C., Martini L., Fini M., and Giavaresi G., *A new bi-layered scaffold for osteochondral tissue regeneration: In vitro and in vivo preclinical investigations.* Materials Science and Engineering: C, 2017. **70**: p. 101-111.

[125] Kon Elizaveta, Filardo Giuseppe, Shani Jonathan, Altschuler Nir, Levy Andrew, Zaslav Ken, Eisman John E., and Robinson Dror, *Osteochondral regeneration with a novel aragonite-hyaluronate biphasic scaffold: up to 12-month follow-up study in a goat model.* Journal of Orthopaedic Surgery and Research, 2015. **10**(1): p. 81.

[126] Erggelet Christoph, Endres Michaela, Neumann Katja, Morawietz Lars, Ringe Jochen, Haberstroh Kathrin, Sittinger Michael, and Kaps Christian, *Formation of cartilage repair tissue in articular cartilage defects pretreated with microfracture and covered with cell-free polymer-based implants.* Journal of Orthopaedic Research, 2009. **27**(10): p. 1353-1360.

[127] Schagemann Jan C., Rudert Nicola, Taylor Michelle E., Sim Sotcheadt, Quenneville Eric, Garon Martin, Klinger Mathias, Buschmann Michael D., and H. Mittelstaed, *Bilayer Implants: Electromechanical Assessment of Regenerated Articular Cartilage in a Sheep Model.* CARTILAGE, 2016. **7**(4): p. 346-360.

[128] Desireé Alesa Gyles, Lorena Diniz Castro, José Otávio Carréra Silva Jr., Roseane Maria Ribeiro-Costa, *A review of the designs and prominent biomedical advances of natural and synthetic hydrogel formulations.* European Polymer Journal, 2017. **88**: p. 373-392.

[129] Peppas Nikolaos A., Merrill Edward W., *Development of semicrystalline poly(vinyl alcohol) hydrogels for biomedical applications.* Journal of Biomedical Materials Research, 1977. **11**(3): p. 423-434.

[130] Okay Oguz, *Semicrystalline physical hydrogels with shape-memory and self-healing properties.* Journal of Materials Chemistry B, 2019. **7**(10): p. 1581-1596.

[131] Yuan Jian-Jun, Jin Ren-Hua, *Fibrous Crystalline Hydrogels Formed from Polymers Possessing A Linear Poly(ethyleneimine) Backbone.* Langmuir, 2005. **21**(7): p. 3136-3145.

[132] Zhang Hongbin, Zhang Fei, Wu Juan, *Physically crosslinked hydrogels from polysaccharides prepared by freeze–thaw technique.* Reactive and Functional Polymers, 2013. **73**(7): p. 923-928.

[133] N. A. Peppas, Y. Huang, M. Torres-Lugo, J. H. Ward, J. Zhang, *Physicochemical Foundations and Structural Design of Hydrogels in Medicine and Biology.* Annual Review of Biomedical Engineering, 2000. **2**(1): p. 9-29.

[134] Hou Wenwen, Sheng Nannan, Zhang Xiaohui, Luan Zhaohui, Qi Pengfei, Lin Min, Tan Yeqiang, Xia Yanzhi, Li Yanhui, and Sui Kunyan, *Design of injectable*

agar/NaCl/polyacrylamide ionic hydrogels for high performance strain sensors. Carbohydrate Polymers, 2019. **211**: p. 322-328.

[135] Zhang Tao, Silverstein Michael S, *Highly porous, emulsion-templated, zwitterionic hydrogels: amplified and accelerated uptakes with enhanced environmental sensitivity.* Polymer Chemistry, 2018. **9**(25): p. 3479-3487.

[136] Yasuda Kazunori, Ping Gong Jian, Katsuyama Yoshinori, Nakayama Atsushi, Tanabe Yoshie, Kondo Eiji, Ueno Masaru, Osada Yoshihito, *Biomechanical properties of high-toughness double network hydrogels.* Biomaterials, 2005. **26**(21): p. 4468-4475.

[137] Faturechi Rahim, Karimi Alireza, Hashemi Ata, Yousefi Hossein, Navidbakhsh Mahdi, *Influence of Poly(acrylic acid) on the Mechanical Properties of Composite Hydrogels.* Advances in Polymer Technology, 2015. **34**(2).

[138] Zhang Ran, Lin Peng, Yang Wufang, Cai Meirong, Yu Bo, Zhou Feng, *Simultaneous superior lubrication and high load bearing by the dynamic weak interaction of a lubricant with mechanically strong bilayer porous hydrogels.* Polymer Chemistry, 2017. **8**(46): p. 7102-7107.

[139] Burdick Jason A., Prestwich Glenn D., *Hyaluronic Acid Hydrogels for Biomedical Applications.* Advanced Materials, 2011. **23**(12): p. H41-H56.

[140] Czaja Wojciech K., Young David J., Kawecki Marek, Brown R. Malcolm, *The Future Prospects of Microbial Cellulose in Biomedical Applications.* Biomacromolecules, 2007. **8**(1): p. 1-12.

[141] Wang Zheng, Zhu Xiaolu, Zhang Ruiyuan, *Characterization and Analysis of Collective Cellular Behaviors in 3D Dextran Hydrogels with Homogenous and Clustered RGD Compositions.* Materials, 2019. **12**(20): p. 3391.

[142] Pawar Siddhesh N., Edgar Kevin J., *Alginate derivatization: A review of chemistry, properties and applications.* Biomaterials, 2012. **33**(11): p. 3279-3305.

[143] Luca Gasperini, João F. Mano, Rui L. Reis, *Natural polymers for the microencapsulation of cells.* NCBI, 2014. **6**(11): p. 100.

[144] Toh Wei Seong, Loh Xian Jun, *Advances in hydrogel delivery systems for tissue regeneration.* Materials Science and Engineering: C, 2014. **45**: p. 690-697.

[145] Zhang Dekun, Duan Junjie, Wang Dagang, Ge Shirong, *Effect of Preparation Methods on Mechanical Properties of PVA/HA Composite Hydrogel.* Journal of Bionic Engineering, 2010. **7**(3): p. 235-243.

[146] Chuang E. Y., Chiang C. W., Wong P. C., Chen C. H., *Hydrogels for the Application of Articular Cartilage Tissue Engineering: A Review of Hydrogels.* Advances in Materials Science and Engineering, 2018. **2018**.

[147] Hennink W. E., van Nostrum C. F., *Novel crosslinking methods to design hydrogels.* Advanced Drug Delivery Reviews, 2012. **64**: p. 223-236.

[148] van Dijk-Wolthuis W. N. E., Franssen O., Talsma H., van Steenbergen M. J., Kettenes-van den Bosch J. J., Hennink W. E., *Synthesis, Characterization, and Polymerization of Glycidyl Methacrylate Derivatized Dextran.* Macromolecules, 1995. **28**(18): p. 6317-6322.

[149] Stenekes Robert, J. H. De Smedt, Stefaan C. Demeester, Joseph Sun, Guangzhi Zhang, Zhibing Hennink, Wim E., *Pore Sizes in Hydrated Dextran Microspheres.* Biomacromolecules, 2000. **1**(4): p. 696-703.

[150] Sperinde Jeffrey J., Griffith Linda G., *Synthesis and Characterization of Enzymatically-Cross-Linked Poly(ethylene glycol) Hydrogels.* Macromolecules, 1997. **30**(18): p. 5255-5264.

[151] Lin Peng, Ma Shuanhong, Wang Xiaolong, Zhou Feng, *Molecularly engineered dual-crosslinked hydrogel with ultrahigh mechanical strength, toughness, and good self-recovery.* Adv Mater, 2015. **27**(12): p. 2054-9.

[152] Seddiki Nesrinne, Djamel Aliouche, *Synthesis, characterization and rheological behavior of pH sensitive poly(acrylamide-co-acrylic acid) hydrogels.* Arabian Journal of Chemistry, 2017. **10**(4): p. 539-547.

[153] Yoshikawa Masakazu, Wano Takashi, Kitao Toshio, *Specialty polymeric membranes 2. Pervaporation separation of aqueous lower alcohol solutions throuh modified polybutadiene membranes.* Journal of Membrane Science, 1994. **89**(1): p. 23-36.

[154] Sennakesavan Gangadevi, Mostakhdemin Mohammad, Dkhar L. K., Seyfoddin Ali, Fatihhi S.J., *Acrylic acid/acrylamide based hydrogels and its properties - A review.* Polymer Degradation and Stability, 2020. **180**: p. 109308.

[155] Hawker C. J., Piotti M. E., and Saldívar-Guerra E., *Nitroxide-Mediated Free Radical Polymerization*, in *Reference Module in Materials Science and Materials Engineering*. 2016, Elsevier.

[156] Kunlun Hong, Hongwei Zhang, Jimmy W. Mays, Ann E. Visser, Christopher S. Brazel, John D. Holbrey, W. Matthew Reichert and Robin D. Rogers *Conventional free radical polymerization in room temperature ionic liquids: a green approach to commodity polymers with practical advantages.* Royal Society of Chemistry, 2002: p. 1368-1369.

[157] Rizzardo Ezio, Chiefari John, Chong Bill Y.K., Ercole Frances, Krstina Julia, Jeffery Justine, Le Tam P.T., Mayadunne Roshan T.A., Meijs Gordon F., Moad Catherine L., Moad Graeme, Thang San H., *Tailored polymers by free radical processes.* Macromolecular Symposia, 1999. **143**(1): p. 291-307.

[158] AkzoNobel, *Free radical polymerization*, in *Science & Technology*. 2016, AkzoNobel Polymer Chemistry.

[159] Gong Jian Ping, Kurokawa Takayuki, Narita Tetsuharu, Kagata Go, Osada Yoshihito, Nishimura Goro, Kinjo Masataka, *Synthesis of Hydrogels with Extremely Low Surface Friction.* Journal of the American Chemical Society, 2001. **123**(23): p. 5582-5583.

[160] Gong Jian, Ping Kurokawa,Takayuki Narita,Tetsuharu Kagata, Go Osada,Yoshihito Nishimura, Goro Kinjo Masataka, *Synthesis of Hydrogels with Extremely Low Surface Friction.* Journal of the American Chemical Society, 2001. **123**(23): p. 5582-5583.

[161] Azuma Chinatsu, Yasuda Kazunori, Tanabe Yoshie,Taniguro Hiroko, Kanaya Fuminori, Nakayama Atsushi, Chen Yong Mei, Gong Jian Ping, Osada Yoshihito, *Biodegradation of high-toughness double network hydrogels as potential materials for artificial cartilage.* Journal of Biomedical Materials Research Part A, 2007. **81A**(2): p. 373-380.

[162] Kim Dukjoon, Park Kinam, *Swelling and mechanical properties of superporous hydrogels of poly(acrylamide-co-acrylic acid)/polyethylenimine interpenetrating polymer networks.* Polymer, 2004. **45**(1): p. 189-196.

[163] Hoare Todd R., Kohane Daniel S., *Hydrogels in drug delivery: Progress and challenges.* Polymer, 2008. **49**(8): p. 1993-2007.

[164] Zahra Bahrami, Ali Akbari, Bagher Eftekhari-Sis, *Double network hydrogel of sodium alginate/polyacrylamide cross-linked with POSS: Swelling, dye removal and mechanical properties.* International Journal of Biological Macromolecules, 2019. **129**: p. 187-197.

[165] Gong J. P., Katsuyama Y., Kurokawa T., Osada Y., *Double-Network Hydrogels with Extremely High Mechanical Strength.* Advanced Materials, 2003. **15**(14): p. 1155-1158.

[166] Na Yang-Ho, Kurokawa Takayuki, Katsuyama Yoshinori, Tsukeshiba Hiroyuki, Gong Jian Ping, Osada Yoshihito, Okabe Satoshi, Karino Takeshi, Shibayama Mitsuhiro, *Structural Characteristics of Double Network Gels with Extremely High Mechanical Strength.* Macromolecules, 2004. **37**(14): p. 5370-5374.

[167] Ahmed Saika, Nakajima Tasuku, Kurokawa Takayuki, Haque Md. Anamul, Gong Jian Ping, *Brittle–ductile transition of double network hydrogels: Mechanical balance of two networks as the key factor.* Polymer, 2014. **55**(3): p. 914-923.

[168] Fajardo André R., Fávaro Silvia L., Rubira Adley F., and M.E. C., *Dual-network hydrogels based on chemically and physically crosslinked chitosan/chondroitin sulfate.* Reactive and Functional Polymers, 2013. **73**(12): p. 1662-1671.

[169] Brandon J. DeKosky, Nathan H. Dormer, Ganesh C. Ingavle, Christopher H. Roatch, Joseph Lomakin, Michael S. Detamore, and S.H. Gehrke, *Hierarchically Designed Agarose and Poly(Ethylene Glycol) Interpenetrating Network Hydrogels for Cartilage Tissue Engineering.* Tissue Engineering Part C: Methods, 2010. **16**(6): p. 1533-1542.

[170] Sun Jeong-Yun, Zhao Xuanhe, Illeperuma Widusha R. K., Chaudhuri Ovijit, Oh Kyu Hwan, Mooney David J., Vlassak Joost J., Suo Zhigang, *Highly stretchable and tough hydrogels.* Nature, 2012. **489**: p. 133.

[171] Moutos Franklin T., Estes Bradley T., and G. Farshid, *Multifunctional Hybrid Three-dimensionally Woven Scaffolds for Cartilage Tissue Engineering.* Macromolecular Bioscience, 2010. **10**(11): p. 1355-1364.

[172] Moutos Franklin T., Freed Lisa E., Guilak Farshid, *A biomimetic three-dimensional woven composite scaffold for functional tissue engineering of cartilage.* Nature Materials, 2007. **6**: p. 162.

[173] Chen Hong, Chen Qiang, Hu Rundong, Wang Hua, Newby Bi-min Zhang, Chang Yung, and Z. Jie, *Mechanically strong hybrid double network hydrogels with antifouling properties.* Journal of Materials Chemistry B, 2015. **3**(27): p. 5426-5435.

[174] Wang Huiqun, Ateshian Gerard A., *The normal stress effect and equilibrium friction coefficient of articular cartilage under steady frictional shear.* Journal of Biomechanics, 1997. **30**(8): p. 771-776.

[175] Sophia Fox Alice, *The Basic Science of Articular Cartilage: Structure, Composition, and Function.* Sports Health: A Multidisciplinary Approach, 2009. **1**(6).

[176] Mow V. C., Kuei S. C., Lai W. M., Armstrong C. G, *Biphasic Creep and Stress Relaxation of Articular Cartilage in Compression: Theory and Experiments.* Journal of Biomechanical Engineering, 1980. **102**(1): p. 73-84.

[177] Jay M. Patel, Brian C. Wise, Edward D. Bonnevie, Robert L. Mauck, *A Systematic Review and Guide to Mechanical Testing for Articular Cartilage Tissue Engineering.* Tissue Engineering Part C: Methods, 2019. **25**(10): p. 593-608.

[178] Brand Richard A., *Joint contact stress: a reasonable surrogate for biological processes?* The Iowa orthopaedic journal, 2005. **25**: p. 82-94.

[179] Kleemann R. U., Krocker D., Cedraro A., Tuischer J., Duda G. N., *Altered cartilage mechanics and histology in knee osteoarthritis: relation to clinical assessment (ICRS Grade).* Osteoarthritis and Cartilage, 2005. **13**(11): p. 958-963.

[180] Carter Teralyn E., Taylor Kevin A., Spritzer Charles E., Utturkar Gangadhar M., Taylor Dean C., Moorman Claude T., Garrett William E., Guilak Farshid, McNulty Amy L., and DeFrate Louis E., *In vivo cartilage strain increases following medial meniscal tear and correlates with synovial fluid matrix metalloproteinase activity.* Journal of Biomechanics, 2015. **48**(8): p. 1461-1468.

[181] Alexander R. M., *Energy-saving mechanisms in walking and running.* Journal of Experimental Biology, 1991. **160**(1): p. 55-69.

[182] Soltz Michael A., Ateshian Gerard A., *Experimental verification and theoretical prediction of cartilage interstitial fluid pressurization at an impermeable contact interface in confined compression.* Journal of Biomechanics, 1998. **31**(10): p. 927-934.

[183] Tuncaboylu Deniz C., Sari Murat, Oppermann Wilhelm, and O. Oguz, *Tough and Self-Healing Hydrogels Formed via Hydrophobic Interactions.* Macromolecules, 2011. **44**(12): p. 4997-5005.

[184] Rockville MD, *Guidance for Industry: preparation of IDEs and INDs for products intended to repair or replace knee cartilage*. 2001.

[185] International ASTM, *Standard Guide for In Vivo Assessment of Implantable Devices Intended to Repair or Regenerate Articular Cartilage*, in *ASTM F2451-05(2010)*. 2010.

[186] Liao I. C., Moutos F. T., Estes B. T., Zhao X., Guilak F., *Composite three-dimensional woven scaffolds with interpenetrating network hydrogels to create functional synthetic articular cartilage.* Adv Funct Mater, 2013. **23**(47): p. 5833-5839.

[187] Lin Peng, Zhang Ran, Wang Xiaolong, Cai Meirong, Yang Jun, Yu Bo, Zhou Feng, *Articular Cartilage Inspired Bilayer Tough Hydrogel Prepared by Interfacial Modulated Polymerization Showing Excellent Combination of High Load-Bearing and Low Friction Performance.* ACS Macro Letters, 2016. **5**(11): p. 1191-1195.

[188] Xu, B., H. Li, Y. Wang, G. Zhang, and Q. Zhang, *Nanocomposite hydrogels with high strength cross-linked by titania.* RSC Advances, 2013. **3**(20): p. 7233-7236.

[189] Gong, J.P., T. Kurokawa, T. Narita, G. Kagata, Y. Osada, G. Nishimura, and M. Kinjo, *Synthesis of Hydrogels with Extremely Low Surface Friction.* Journal of the American Chemical Society, 2001. **123**(23): p. 5582-5583.

[190] Gong Jian Ping, *Why are double network hydrogels so tough?* ROYAL SOCIETY OF CHEMISTRY, 2010. **6**: p. 2583-2590.

[191] Xu Bo, Li Huanjun,Wang Yuyang,Zhang Gongzheng,Zhang Qingshan, *Nanocomposite hydrogels with high strength cross-linked by titania.* RSC Advances, 2013. **3**(20): p. 7233-7236.

[192] Yang Can Hui, Wang Mei Xiang, Haider Hussain, Yang Jian Hai, Sun Jeong-Yun, Chen Yong Mei, Zhou Jinxiong, and S. Zhigang, *Strengthening Alginate/Polyacrylamide Hydrogels Using Various Multivalent Cations.* ACS Applied Materials & Interfaces, 2013. **5**(21): p. 10418-10422.

[193] Amanda N. Buxton, Junmin Zhu, Roger Marchant, Jennifer L. West, Jung U. Yoo, Brian Johnstone, *Design and Characterization of Poly(Ethylene Glycol) Photopolymerizable Semi-Interpenetrating Networks for Chondrogenesis of Human Mesenchymal Stem Cells.* Tissue Engineering, 2007. **13**(10): p. 2549-2560.

[194] Hadi Doulabi, Azadehsadat Hashemi Mequanint, Kibret Mohammadi, *Blends and Nanocomposite Biomaterials for Articular Cartilage Tissue Engineering.* Materials, 2014. **7**(7): p. 5327-5355.

[195] Puppi D., Chiellini F., Piras A. M., Chiellini E., *Polymeric materials for bone and cartilage repair*. Progress in Polymer Science, 2010. **35**(4): p. 403-440.

[196] Yunge Zhai, Hongdong Duan, Xia Meng, Kun Cai, Yu Liu, Lucian Lucia, *Reinforcement Effects of Inorganic Nanoparticles for Double-Network Hydrogels.* Macromolecular Materials and Engineering, 2015. **300**(12): p. 1290-1299.

[197] Yue Yiying, Wang Xianhui, Han Jingquan, Yu Lei, Chen Jianqiang, Wu Qinglin, Jiang Jianchun, *Effects of nanocellulose on sodium alginate/polyacrylamide hydrogel: Mechanical properties and adsorption-desorption capacities.* Carbohydrate Polymers, 2019. **206**: p. 289-301.

[198] Danyang Huang, Yong Huang, Yun Xiao, Hai Lin, Ganjun Feng, Xiangdong Zhu, Xingdong Zhang, *Viscoelasticity in natural tissues and engineered scaffolds for tissue reconstruction.* Acta Biomaterialia, 2019. **97**: p. 74-92.

[199] Zhao Xuanhe, Huebsch Nathaniel, Mooney David J., Suo Zhigang, *Stress-relaxation behavior in gels with ionic and covalent crosslinks.* Journal of Applied Physics, 2010. **107**(6): p. 063509.

[200] Ovijit Chaudhuri, Luo Gu, Max Darnell, Darinka Klumpers, Sidi A. Bencherif, James C. Weaver, Nathaniel Huebsch, David J. Mooney, *Substrate stress relaxation regulates cell spreading.* Nature Communications, 2015. **6**(1): p. 6365.

[201] Wei Hong, Xuanhe Zhao, Jinxiong Zhou, Zhigang Suo, *A theory of coupled diffusion and large deformation in polymeric gels.* Journal of the Mechanics and Physics of Solids, 2008. **56**(5): p. 1779-1793.

[202] Emad Moeendarbary, Léo Valon, Marco Fritzsche, Andrew R. Harris, Dale A. Moulding, Adrian J. Thrasher, Eleanor Stride, L. Mahadevan, Guillaume T. Charras, *The cytoplasm of living cells behaves as a poroelastic material.* Nature Materials, 2013. **12**(3): p. 253-261.

[203] Qi-Ming Wang, Anirudh C. Mohan, Michelle L. Oyen, Xuan-HeZhao, *Separating viscoelasticity and poroelasticity of gels with different length and time scales.* Acta Mechanica Sinica, 2014. **30**(1): p. 20-27.

[204] Hu Yuhang, Suo Zhigang, *Viscoelasticity and Poroelasticity in Elastomeric Gels.* Acta Mechanica Solida Sinica, 2012. **25**(5): p. 441-458.

[205] J. F. Archard, W. Hirst, Thomas Edward Allibone, *The wear of metals under unlubricated conditions.* Proceedings of the Royal Society of London. Series A. Mathematical and Physical Sciences, 1956. **236**(1206): p. 397-410.

[206] Czichos H., K.H. Habig,, *Tribologie-Handbuch.* . 2010, GWV Fachverlage GmbH, Wiesbaden: Tribologie-Handbuch: Tribometrie, Tribomaterialien, Tribotechnik.

[207] Stachowiak G., A.W. Batchelor, *Engineering tribology*. 2013: Butterworth-Heinemann.

[208] Hamrock B.J., S.R. Schmid, B.O. Jacobson, *Fundamentals of fluid film lubrication*. 2004: CRC press.

[209] Podsiadlo P., Kuster M., Stachowiak G. W., *Numerical analysis of wear particles from non-arthritic and osteoarthritic human knee joints.* Wear, 1997. **210**(1): p. 318-325.

[210] Peng Z., *Osteoarthritis diagnosis using wear particle analysis technique: Investigation of correlation between particle and cartilage surface in walking process.* Wear, 2007. **262**(5): p. 630-640.

[211] Urueña Juan Manuel, Pitenis Angela A., Nixon Ryan M., Schulze Kyle D., Angelini Thomas E., and Gregory Sawyer W., *Mesh Size Control of Polymer Fluctuation Lubrication in Gemini Hydrogels.* Biotribology, 2015. **1-2**: p. 24-29.

[212] Thoniyot Praveen, Tan Mein Jin , Abdul Karim Anis, Young David James, Jun Loh Xian, *Nanoparticle–Hydrogel Composites: Concept, Design, and Applications of These Promising, Multi-Functional Materials.* Advanced Science, 2015. **2**(1-2): p. 1400010.

[213] Katta J., Jin Z., Ingham E., Fisher J., *Friction and wear of native and GAG deficient articular cartilage.* World Biomaterials Congress, 2008: p. 1191.

[214] Dunn Alison C., Sawyer W. Gregory, Angelini Thomas E., *Gemini Interfaces in Aqueous Lubrication with Hydrogels.* Tribology Letters, 2014. **54**(1): p. 59-66.

[215] Penskiy I., Gerratt A. P., Bergbreiter S., *Friction, adhesion and wear properties of PDMS films on silicon sidewalls.* Journal of Micromechanics and Microengineering, 2011. **21**(10): p. 105013.

[216] Bonyadi Shabnam Z., Dunn Alison C., *Brittle or Ductile? Abrasive Wear of Polyacrylamide Hydrogels Reveals Load-Dependent Wear Mechanisms.* Tribology Letters, 2020. **68**(1): p. 16.

[217] Schey J.A., *Systems view of optimizing metal on metal bearings.* Clinical orthopaedics and related research, 1996. **329**: p. S115-S127.

[218] Lin Hong-Ru, Ling Ming-Hung, Lin Yiu-Jiuan, *High Strength and Low Friction of a PAA-Alginate-Silica Hydrogel as Potential Material for Artificial Soft Tissues.* Journal of Biomaterials Science, Polymer Edition, 2009. **20**(5-6): p. 637-652.

[219] Arakaki Kazunobu, Kitamura Nobuto, Fujiki Hiroyuki, Kurokawa Takayuki, Iwamoto Mikio, Ueno Masaru, Kanaya Fuminori, Osada Yoshihito, Gong Jian Ping, Yasuda Kazunori, *Artificial cartilage made from a novel double-network hydrogel: In vivo effects on the normal cartilage and ex vivo evaluation of the friction property.* Journal of Biomedical Materials Research Part A, 2010. **93A**(3): p. 1160-1168.

[220] Feng Li, Anmin Wang, Chengtao Wang, *Analysis of friction between articular cartilage and polyvinyl alcohol hydrogel artificial cartilage.* Journal of Materials Science: Materials in Medicine, 2016. **27**(5): p. 87.

[221] Li Hua, Choi Yu Suk, Rutland Mark W. Atkin Rob, *Nanotribology of hydrogels with similar stiffness but different polymer and crosslinker concentrations.* Journal of Colloid and Interface Science, 2020. **563**: p. 347-353.

[222] Maliheh Hasan Nia, Mostafa Rezaei-Tavirani, Ali Reza Nikoofar, Hamed Masoumi, Reza Nasr, Hadi Hasanzadeh*, Majid Jadidi, Mahdi Shadnush, *Stabilizing and dispersing methods of TiO2 nanoparticles in biological studies.* Journal of Paramedical Sciences (JPS), 2015. **6**.

[223] Tso Chih-ping, Zhung Cheng-min, Shih Yang-hsin, Tseng Young-Ming, Wu Shian-chee, and Doong Ruey-an, *Stability of metal oxide nanoparticles in aqueous solutions.* Water Science and Technology, 2010. **61**(1): p. 127-133.

[224] Jiang Jingkun, Oberdörster Günter, Biswas Pratim, *Characterization of size, surface charge, and agglomeration state of nanoparticle dispersions for toxicological studies.* Journal of Nanoparticle Research, 2009. **11**(1): p. 77-89.

[225] Mandzy N., Grulke E., Druffel T., *Breakage of TiO_2 agglomerates in electrostatically stabilized aqueous dispersions.* Powder Technology, 2005. **160**(2): p. 121-126.

[226] Ian D. Morrison, Sydney Ross, *Colloidal Dispersions: Suspensions, Emulsions, and Foams.* Surface & Colloid Chemistry, 2002: p. 656.

[227] Bo Xu, Haoyang Jiang, Huanjun Li, Gongzheng Zhang, Qingshan Zhang, *High strength nanocomposite hydrogel bilayer with bidirectional bending and shape switching behaviors for soft actuators.* RSC Advances, 2015. **5**(17): p. 13167-13170.

[228] Deiss J. L., Anizan P., El Hadigui S., Wecker C., *Steric stability of TiO_2 nanoparticles in aqueous dispersions.* Colloids and Surfaces A: Physicochemical and Engineering Aspects, 1996. **106**(1): p. 59-62.

[229] Memic Adnan, Alhadrami Hani A., Hussain M. Asif, Aldhahri Musab, Al Nowaiser Fozia, Al-Hazmi Faten, Oklu Rahmi, Khademhosseini Ali, *Hydrogels 2.0: improved properties with nanomaterial composites for biomedical applications.* Biomedical Materials, 2015. **11**(1): p. 014104.

[230] Mostakhdemin Mohammad, Nand Ashveen, Ramezani Maziar, *A novel assessment of microstructural and mechanical behaviour of bilayer silica-reinforced nanocomposite hydrogels as a candidate for artificial cartilage.* Journal of the Mechanical Behavior of Biomedical Materials, 2021. **116**: p. 104333.

[231] Shin Heungsoo, Jo Seongbong, Mikos Antonios G., *Modulation of marrow stromal osteoblast adhesion on biomimetic oligo[poly(ethylene glycol) fumarate] hydrogels modified with Arg-Gly-Asp peptides and a poly(ethylene glycol) spacer.* Journal of Biomedical Materials Research, 2002. **61**(2): p. 169-179.

[232] Taffetani M., Gottardi R., Gastaldi D., Raiteri R., Vena P., *Poroelastic response of articular cartilage by nanoindentation creep tests at different characteristic lengths.* Medical Engineering & Physics, 2014. **36**(7): p. 850-858.

[233] Arjmandi Mohammadreza, Ramezani Maziar, *Effect of Silica Nanoparticles on Wear Mechanism of Alginate-Polyacrylamide Hydrogel Matrix as a Load-Bearing Biomaterial.* Materials Science and Engineering, 2019. **823**: p. 15-20.

[234] Arjmandi Mohammadreza, Ramezani Maziar, Bolle Tim, Köppe Gesine, Gries Thomas, Neitzert Thomas, *Mechanical and tribological properties of a novel hydrogel composite reinforced by three-dimensional woven textiles as a functional synthetic cartilage.* Composites Part A: Applied Science and Manufacturing, 2018. **115**: p. 123-133.

[235] Tsioptsias C., Paraskevopoulos M. K., Christofilos D. Andrieux P., Panayiotou C., *Polymeric hydrogels and supercritical fluids: The mechanism of hydrogel foaming.* Polymer, 2011. **52**(13): p. 2819-2826.

[236] Masiak Michal, Hyk Wojciech, Stojek Zbigniew, Ciszkowska Malgorzata, *Structural Changes of Polyacids Initiated by Their Neutralization with Various Alkali Metal Hydroxides. Diffusion Studies in Poly(acrylic acid)s.* The Journal of Physical Chemistry B, 2007. **111**(38): p. 11194-11200.

[237] Kango Sarita, Kalia Susheel, Celli Annamaria, Njuguna James, Habibi Youssef, Kumar Rajesh, *Surface modification of inorganic nanoparticles for development of organic–inorganic nanocomposites—A review*. Progress in Polymer Science, 2013. **38**(8): p. 1232-1261.

[238] ASTM, *Standard Practice for Instrumented Indentation Testing*, in *ASTM E2546*. 2015, ASTM International: USA.

[239] Dimitriadis Emilios K., Horkay Ferenc, Maresca Julia, Kachar Bechara, Chadwick Richard S., *Determination of Elastic Moduli of Thin Layers of Soft Material Using the Atomic Force Microscope.* Biophysical Journal, 2002. **82**(5): p. 2798-2810.

[240] Long Rong, Hall Matthew S, Wu Mingming, Hui Chung-Yuen, *Effects of Gel Thickness on Microscopic Indentation Measurements of Gel Modulus.* Biophysical Journal, 2011. **101**(3): p. 643-650.

[241] Boughner D. R., Haldenby M., Hui A. J., Dunmore-Buyze J., Talman E. A., Wan W. K., *The pericardial bioprosthesis: altered tissue shear properties following glutaraldehyde fixation.* The Journal of heart valve disease, 2000. **9**(6): p. 752-760.

[242] Wan W. K., Campbell G., Zhang Z. F., Hui A. J., Boughner D. R., *Optimizing the tensile properties of polyvinyl alcohol hydrogel for the construction of a bioprosthetic heart valve stent.* Journal of Biomedical Materials Research, 2002. **63**(6): p. 854-861.

[243] Kanca Yusuf, Milner Piers, Dini Daniele, Amis Andrew A., *Tribological properties of PVA/PVP blend hydrogels against articular cartilage.* Journal of the Mechanical Behavior of Biomedical Materials, 2018. **78**: p. 36-45.

[244] Kazunobu Arakaki, Nobuto Kitamura, Hiroyuki Fujiki,Takayuki Kurokawa, Mikio Iwamoto, Masaru Ueno, Fuminori Kanaya, Yoshihito Osada, Jian Ping Gong, Kazun ori Yasuda, *Artificial cartilage made from a novel double-networkhydrogel: In vivo effects on the normal cartilageand ex vivo evaluation of the friction property.* Journal of Biomedical Materials Research - Part A, 2009. **93**(3): p. 8.

[245] Esteki Mohammad Hadi, Alemrajabi Ali Akbar, Hall Chloe M., Sheridan Graham K., Azadi Mojtaba, Moeendarbary Emad, *A new framework for characterization of poroelastic materials using indentation.* Acta Biomaterialia, 2020. **102**: p. 138-148.

[246] Klein Andrea, Whitten Philip G., Resch Katharina, Pinter Gerald, *Nanocomposite hydrogels: Fracture toughness and energy dissipation mechanisms.* Journal of Polymer Science Part B: Polymer Physics, 2015. **53**(24): p. 1763-1773.

[247] Ganji Fariba, Vasheghani Farahani S., Vasheghani Faraahani E., *THEORETICAL DESCRIPTION OF HYDROGEL SWELLING: A REVIEW.* IRANIAN POLYMER JOURNAL (ENGLISH), 2010. **19**(5 (119)): p. 375-398.

[248] Guo Peng, Yuan Yasheng, Chi Fanglu, *Biomimetic alginate/polyacrylamide porous scaffold supports human mesenchymal stem cell proliferation and chondrogenesis.* Materials Science and Engineering: C, 2014. **42**: p. 622-628.

[249] Kamata Hiroyuki, Akagi Yuki, Kayasuga-Kariya Yuko, Chung Ung-il, Sakai Takamasa, *"Nonswellable" Hydrogel Without Mechanical Hysteresis.* Science, 2014. **343**(6173): p. 873.

[250] L., O.M., *Mechanical characterisation of hydrogel materials.* International Materials Reviews, 2014. **59**(1): p. 44-59.

[251] Rodts T., Schmid S. R., Selles M. A., Pasang T., and S.-C. S., *Selective laser fiber welding on woven polymer fabrics for biomedical applications.* Materials Science and Engineering: C, 2019. **94**: p. 628-634.

[252] Lowman AM, *Smart pharmaceuticals*. 2008.

[253] Yoshida Ryo, Okano Teruo, *Stimuli-Responsive Hydrogels and Their Application to Functional Materials*, in *Biomedical Applications of Hydrogels Handbook*, R.M. Ottenbrite, K. Park, and T. Okano, Editors. 2010, Springer New York: New York, NY. p. 19-43.

[254] Bajpai S K, *Swelling Studies on Hydrogel Networks — A Review.* NISCAIR-CSIR, India, 2001(Jun-2001): p. 451-462.

[255] N. Seddiki, A. Djamel, *Synthesis, characterization and rheological behavior of pH sensitive poly(acrylamide-co-acrylic acid) hydrogels.* Arabian Journal of Chemistry, 2017. **10**(4): p. 539-547.

[256] K. Arakaki, N. Kitamura, H. Fujiki,T. Kurokawa, M. Iwamoto, M. Ueno, F. Kanaya, Y. Osada, J.P. Gong, K.O. Yasuda, *Artificial cartilage made from a novel double-networkhydrogel: In vivo effects on the normal cartilageand ex vivo evaluation of the friction property.* Journal of Biomedical Materials Research - Part A, 2009. **93**(3): p. 8.

[257] M. Arjmandi, M. Ramezani, *Mechanical and tribological assessment of silica nanoparticle-alginate-polyacrylamide nanocomposite hydrogels as a cartilage replacement.* Journal of the Mechanical Behavior of Biomedical Materials, 2019. **95**: p. 196-204.

[258] Oinas J., Ronkainen A. P., Rieppo L., Finnilä M. A. J., Iivarinen J. T., van Weeren P. R., Helminen H. J., Brama P. A. J., Korhonen R. K., Saarakkala S., *Composition, structure and tensile biomechanical properties of equine articular cartilage during growth and maturation.* Scientific Reports, 2018. **8**(1): p. 11357.

[259] Cameron Andrew R., Frith Jessica E., Cooper-White Justin J., *The influence of substrate creep on mesenchymal stem cell behaviour and phenotype.* Biomaterials, 2011. **32**(26): p. 5979-5993.

[260] M.M. Fitzgerald, K. Bootsma, J. A. Berberich, J. L. Sparks, *Tunable Stress Relaxation Behavior of an Alginate-Polyacrylamide Hydrogel: Comparison with Muscle Tissue.* Biomacromolecules, 2015. **16**(5): p. 1497-1505.

[261] Zhongliang Hu, Maje Haruna, Hui Gao, Ehsan Nourafkan, Dongsheng Wen, *Rheological Properties of Partially Hydrolyzed Polyacrylamide Seeded by Nanoparticles.* Industrial & Engineering Chemistry Research, 2017. **56**(12): p. 3456-3463.

[262] R. Zhang, P. Lin, W. Yang, M. Cai, B. Yu, F. Zhou, *Simultaneous superior lubrication and high load bearing by the dynamic weak interaction of a lubricant with mechanically strong bilayer porous hydrogels.* Polymer Chemistry, 2017. **8**(46): p. 7102-7107.

[263] Eisenberg Solomon R., Grodzinsky Alan J., *Swelling of articular cartilage and other connective tissues: Electromechanochemical forces.* Journal of Orthopaedic Research, 1985. **3**(2): p. 148-159.

[264] Zohreh Arabshahi, Isaac Oluwaseun Afara, Hayley Ruscoe Moody, Karsten Schrobback, Jamal Kashani, adine Fischer, dekunle Oloyede, Travis Jacob Klein, *A new mechanical indentation framework for functional assessment of articular cartilage.* Journal of the Mechanical Behavior of Biomedical Materials, 2018. **81**: p. 83-94.

[265] Manli Yang, Jinsheng Shi, Yanzhi Xia, *Effect of SiO2, PVA and glycerol concentrations on chemical and mechanical properties of alginate-based films.* International Journal of Biological Macromolecules, 2018. **107**: p. 2686-2694.

[266] Jiho Kim, Alison C. Dunn, *Soft hydrated sliding interfaces as complex fluids.* Soft Matter, 2016. **12**: p. 6536-6546.

[267] Dehghani E. S., Ramakrishna S. N., Spencer N. D., Benetti E. M., *Controlled Crosslinking Is a Tool To Precisely Modulate the Nanomechanical and Nanotribological Properties of Polymer Brushes.* Macromolecules, 2017. **50**(7): p. 2932-2941.

[268] Bhushan Bharat, *Nanotribology and nanomechanics.* Wear, 2005. **259**(7): p. 1507-1531.

[269] Nam Sungmin, Lee Joanna, Brownfield Doug G, Chaudhuri Ovijit, *Viscoplasticity Enables Mechanical Remodeling of Matrix by Cells.* Biophysical Journal, 2016. **111**(10): p. 2296-2308.

[270] Bonyadi Shabnam Z., Atten Michael, Dunn Alison C., *Self-regenerating compliance and lubrication of polyacrylamide hydrogels.* Soft Matter, 2019. **15**(43): p. 8728-8740.

[271] Liu Junjie, Yang Canhui, Yin Tenghao, Wang Zhengjin, Qu Shaoxing, Suo Zhigang, *Polyacrylamide hydrogels. II. elastic dissipater.* Journal of the Mechanics and Physics of Solids, 2019. **133**: p. 103737.

[272] Bavaresco V. P., Zavaglia C. A. C., Reis M. C., Gomes J. R., *Study on the tribological properties of pHEMA hydrogels for use in artificial articular cartilage.* Wear, 2008. **265**(3): p. 269-277.

[273] Gombert Yvonne, Simič Rok, Roncoroni Fabrice, Dübner Matthias, Geue Thomas, Spencer Nicholas D., *Structuring Hydrogel Surfaces for Tribology.* Advanced Materials Interfaces, 2019. **6**(22): p. 1901320.

[274] Affatato Saverio, Trucco Diego, Taddei Paola,Vannozzi Lorenzo, Ricotti Leonardo, Nessim Gilbert Daniel, Lisignoli Gina, *Wear Behavior Characterization of Hydrogels Constructs for Cartilage Tissue Replacement.* Materials, 2021. **14**(2): p. 428.

[275] Jianping Gong, Yoshihito Osada, *Gel friction: A model based on surface repulsion and adsorption.* The Journal of Chemical Physics, 1998. **109**(18): p. 8062-8068.

[276] Korres S., Sorochynska L., Grishchuk S., Karger-Kocsis J., *Swelling, compression and tribological behaviors of bentonite-modified polyacrylate-type hydrogels.* Journal of Applied Polymer Science, 2011. **119**(2): p. 1122-1134.

[277] Ohsedo Yutaka, Takashina Rikiya, Gong Jian Ping, Osada Yoshihito, *Surface Friction of Hydrogels with Well-Defined Polyelectrolyte Brushes.* Langmuir, 2004. **20**(16): p. 6549-6555.

[278] Ab Rahman Ismail, Padavettan Vejayakumaran, *Synthesis of Silica Nanoparticles by Sol-Gel: Size-Dependent Properties, Surface Modification, and Applications in Silica-Polymer Nanocomposites—A Review.* Journal of Nanomaterial, 2012. **2012**.

[279] Kenneth Langstreth Johnson, Kevin Kendall, A. D. Roberts, *Surface energy and the contact of elastic solids.* Proceedings of the royal society A, 1971.

[280] Yang Jun, Zhao Jingjing, *Preparation and mechanical properties of silica nanoparticles reinforced composite hydrogels.* Materials Letters, 2014. **120**: p. 36-38.

[281] Yang Jun, Wang Xi-Ping, Xie Xu-Ming, *In situ synthesis of poly(acrylic acid) physical hydrogels from silica nanoparticles.* Soft Matter, 2012. **8**(4): p. 1058-1063.